SIMULATION AND EXPERIMENTAL INVESTIGATION ON OPTIMUM APPLICATION OF MULTI-FUNCTIONAL SOLAR ASSISTED AIR SOURCE HEAT PUMP SYSTEMS

LI HONG

Ph.D

The Hong Kong

Polytechnic University

2010

The Hong Kong Polytechnic University

Department of Building Services Engineering

Simulation and Experimental Investigation on Optimum Application of Multi-functional Solar Assisted Air Source Heat Pump Systems

Li Hong

A thesis submitted in partial fulfilment of the requirements for the Degree of Doctor of Philosophy

December 2009

CERTIFICATE OF ORIGINALITY

I hereby declare that this thesis is my own work and that, to the best of my knowledge and belief, it reproduces no material previously published or written, nor material that has been accepted for the award of any other degree or diploma, except where due acknowledgement has been made in the text.

I also declare that the intellectual content of this thesis is the product of my own work, even though I may have received assistance from others on style, presentation and language expression.

_____ (Signed)

_____Li Hong_____ (Name of student)

Department of Building Services Engineering

The Hong Kong Polytechnic University

Hong Kong, China

December 2009

ABSTRACT

Abstract of thesis entitled: Simulation and Experimental Investigation on Optimum Application of Multi-functional Solar Assisted Air Source Heat Pump Systems

Submitted by: Li Hong

For the degree of: Doctor of Philosophy
at The Hong Kong Polytechnic University in Dec. 2009.

This thesis proposed the multi-functional solar assisted air source heat pump (MSA-ASHP) system for improving the energy performance of the traditional solar assisted heat pump technology in cooling-dominated buildings in sub-tropical areas like Hong Kong.

Firstly, the detailed mathematical models of the MSA-ASHP system are developed and a comprehensive simulation program of the proposed system is built. A number of cases were simulated, which shows that the MSA-ASHP system can provide a much better system performance than traditional air conditioners and water heaters, especially in the air conditioning and water heating (AC/WH) mode.

The simulation model of the MSA-ASHP system was extensively validated by experiments, covering all three operation modes. The investigation results demonstrate that the mathematical model is accurate to within 10% of the experimental data.

Based on experimental data, an exergy analysis of the MSA-ASHP system was carried out. It is found that the greatest irreversibility occurs in the solar collector, followed by the evaporator, the compressor, the desuperheater, the condenser and the

thermostatic expansion valve. The comparison analysis among the four different domestic hot water heating systems shows that the MSA-ASHP system offers the highest energy and exergy efficiencies.

Finally, the annual performance of the MSA-ASHP system was analyzed. The monthly solar fraction ranges between 39.4% and 77.4%. The monthly average system coefficient of performance (COP) value is 3.0 throughout a year. An annual energy saving of 54.9% would be achieved when the MSA-ASHP system is adopted instead of the electric water heater plus a conventional air conditioner. The life cycle saving (LCS) analysis for using the MSA-ASHP system in Hong Kong is also conducted.

In summary, the simulation model developed for the MSA-ASHP system can provide a useful and effective tool to investigate system performance in different operating modes. The simulation and experimental results demonstrate that the MSA-ASHP system can overcome the mentioned limitations and problems in subtropical areas. Besides, the system performance is improved significantly. Based on the substantial investigation results, it is feasible and desirable to apply the MSA-ASHP system to the cooling dominated buildings in Hong Kong and other subtropical areas.

Keywords: multi-functional solar assisted air source heat pump systems, air-conditioning, hot water production, simulation, energy and exergy analysis, control strategy

PUBLICATIONS DURING PHD STUDY

Journal papers during PhD study:

Li H, Yang HX. Potential Application of Solar Thermal Systems for Hot Water Production in Hong Kong. ***Applied Energy***. 2009; 86: 175-180.

Li H, Yang HX. Study on Performance of Solar Assisted Air Source Heat Pump Systems for Hot Water Production in Hong Kong. ***Applied Energy***. In press.

Li H, Yang HX. Energy and Exergy Analysis of Multi-functional Solar Assisted Heat Pump System. ***International Journal of Low Carbon Technologies***. Accepted.

Li H, Yang HX. Study on Operating Performance of a Multi-functional Solar Assisted Heat Pump System (Submitted to Energy and Buildings).

Li H, Yang HX. Investigation on Alternative Refrigerants to R22 for Direct Expansion Solar Assisted Heat Pump Systems (Submitted to International Journal of Energy Research).

Book chapters during PhD study:

Chapter 9 of the book: Application of Solar Energy Technologies in Buildings (in Chinese) published by China Construction Industry Press, ISBN 978-7-112-10377-5, Beijing, China, Jan 2009.

Conference papers during PhD study:

Li H, Yang HX. Potential Application of Solar Assisted Heat Pump Systems for Hot Water Production in Hong Kong. ***3rd International Green Energy Conference***. Västerås, Sweden. 2007.

Li H, Yang HX. Dynamic Performance Study on the Solar Collector/Evaporator of Direct Expansion Solar Assisted Heat Pump Systems. ***ISES Solar World Congress 2007***. Beijing, China. 2007.

Li H, Yang HX. Study on Performance of Solar Assisted Air Source Heat Pump Systems. ***4th International Green Energy Conference***. Beijing, China. 2008.

Li H, Yang HX. Energy and Exergy Analysis of Multi-functional Solar Assisted Heat Pump System. ***8th International Conference on Sustainable Energy and Technologies.*** Aachen, Germany. 2009.

Li H, Yang HX. Experimental Study on a Novel Multi-functional Solar Assisted Heat Pump System. ***International Conference on Applied Energy***. Singapore. 2010.

ACKNOWLEDGEMENTS

This thesis would not have been possible without the help and support from those who are gratefully acknowledged here.

First and foremost, I would like to express my deepest appreciation to my chief supervisor, Prof. Yang Hongxing, for his invaluable help, patient guidance, constructive advices, as well as continuous encouragement throughout the research.

I would also like to acknowledge my former supervisor, Prof. John D. Gilleard, for initiating this study and for his continuous support.

My sincere gratitude is devoted to Prof. Fang Zhaohong who helped me a lot and kept an eye on the process of my work.

Special thanks to the lab technicians who gave me great assistance and useful suggestions for setting up the experimental rig.

I am grateful for every expression of kindness, support, and encouragement from my colleagues in the Renewable Energy Research Group.

My heartfelt gratitude goes to my family for their endless support, love, encouragement and everything. This thesis is dedicated to all of them.

Finally, I want to thank everyone who directly or indirectly gave help and support to this thesis.

TABLE OF CONTENTS

LIST OF FIGURES

LIST OF TABLES

NOMENCLATURE

Symbols	Description	Unit
A	Area	m^2
A_0~A_{22}	Coefficients for water thermodynamic properties	
a_1~a_{12}	Coefficients for water thermodynamic properties	
B_r	Integrated coefficient of refrigerant thermophysical property	
B_0	Refrigerant boiling number	
c	Clearance volumetric ratio of compressor	
C	Initial extra expenditure	HK$
C_0	Refrigerant convection number	
c_p	Specific heat of water	J/(kg·K)
C_s	Initial cost	HK$
d	Diameter	m
d_e	Equivalent diameter	m
e	Inflation rate	
E_c	Energy consumption per year	MJ
$\dot{E}x$	Rate of exergy	kW
f	Solar fraction	
F_R	Heat removal factor of solar collector	
$F_R^{'}$	Collector-heat exchanger efficiency factor	
G_r	Mass velocity per unit area	kg/(s·m^2)

h	Enthalpy	J/kg
H	Refrigerant enthalpy	J/kg
I_d	Diffuse horiztontal radiation intensity	W/m^2
I_g	Global horizontal radiation intensity	W/m^2
I_T	Solar radiation intensity on tilted surface	W/m^2
k	Thermal conductivity	W/(m·K)
L	Length	m
m	Mass flow rate	kg/s
M	Refrigerant mass	kg
n	Isentropic exponent	
N	Number	
N_p	Payback period	year
P	Pressure	Pa
q_{Ls}	Load met by solar energy	W
q_s	Useful solar heat gain	W
q_{stl}	Storage heat loss of preheating solar tank	W
q_{evp}	Heat transferred in evaporator of an element	J
q_a	Heat transferred on air side of each element	J
Q	Total heat transferred in heat exchanger	J
R_b	Tilt factor	
Re	Reynolds number	
$s1$	Distance between fins	m
$s2$	Distance between tubes in air flow direction	m

T	Temperature	K
T_a	Ambient air temperature	℃
T_R	Cold water temperature	℃
T_{st}	Hot water temperature in preheating solar tank	℃
U	Overall heat transfer coefficient	W/(m^2·K)
V	Volume	m^3
W	Compressor power input	W
x	Degree of dryness	
X_{tt}	Coefficient	

Greek

α	Heat transfer coefficient	W/(m^2·K)
β	Tilt angle of solar collector	°
ε	Exergy efficiency	
ε_R	Correction factor	
ε_v	Void fraction	
η_v	Volumetric efficiency of compressor	
λ_l	Leakage coefficient of compressor	
λ_p	Pressure loss coefficient of compressor	
λ_T	Temperature coefficient of compressor	
μ	Dynamic viscosity	Pa·s
ν_{in}	Refrigerant specific volume at inlet of the compressor	m^3/kg

ρ	Density	kg/m^3
ρ_g	Ground reflectance	
$\tau\alpha$	Product of transmittance and absorptance	
ξ	Coefficient of heat loss	
ψ	Specific stream exergy of a fluid in a steady-flow process	J/kg

Subscript

com	Compressor
con	Condenser
des	Desuperheater
evp	Evaporator
in	Inlet
l	Liquid
L	Load
out	Outlet
r	Refrigerant
sub	Subcool
sup	Superheat
v	Vapor
w	Water

Abbreviation

AC	Air conditioning

AC/WH	Air conditioning and water heating
ASHP	Air-source heat pump
CDF	Cumulative distribution function
COP	Coefficient of performance
DHW	Domestic hot water
DX-SAHP	Direct expanded solar assisted heat pump
EER	Energy efficiency ratio
EWY	Example weather year
GWP	Global warming potential
LCS	Life cycle saving
LMTD	Log mean temperature difference
MSA-ASHP	Multi-functional solar assisted air source heat pump
SAHP	Solar assisted heat pump
SA-ASHP	Solar assisted air source heat pump
SA-WSHP	Solar assisted water source heat pump
SWH	Solar water heating
TEV	Thermostatic expansion valve
TEWI	Total equivalent warming impact
TMM	Typical meteorological month
TMY	Typical meteorological year
TRY	Test reference year
WH	Water heating
WYEC	Weather year for energy calculations

WYSS Weather year for solar systems

CHAPTER 1 INTRODUCTION

1.1 Solar Assisted Heat Pump Systems

Hot water supply is a necessity in most of residential, commercial and industrial buildings. On the other hand, residential air conditioners are becoming popular. Hot water is needed while air-conditioning is provided for a house, a flat or a building. For a residential flat of a high-rise building in an urban area, a number of room air-conditioners and electrical or gas-fired water heaters are usually needed for catering for space cooling and domestic hot water supply, respectively. In developed countries, energy consumption of domestic hot water is secondary after that of domestic heating and air-conditioning (Meyer, 1999) for residential buildings. Water heating accounts for 17% of all residential building energy use in the United States, making it the third largest use of energy in homes (Hepbasli and Kalinci, 2008). In China, a large percentage of building energy use was for domestic hot water heating, with ~10% to 40% in commercial buildings and ~20% to 30% in residential buildings (Xu et al., 2006). In Hong Kong, a large amount of hot water is required for both residential and commercial buildings. As a small territory with no indigenous energy sources, fossil fuels are the major energy sources for hot water production. According to a report of the "Hong Kong Energy End-use Data" conducted by the Electrical and Mechanical Services Department (2006) of the Hong Kong SAR Government, about 23% of the total energy end-use in residential buildings was consumed to heat domestic hot water (DHW) and 22% was used for space air-conditioning in the year of 2004. With the

deterioration of energy crisis and environment pollution, public awareness of energy efficiency and environmental protection has become more prominent recently. There is also a growing, government-led trend of applying renewable energy resources in Hong Kong. One area of interests lies in the wider use of solar energy systems.

Solar water heating (SWH) systems have been applied in a number of public facilities in Hong Kong, such as the installation of a 313 m^2 solar collector for a swimming pool complex, 882 m^2 for a central slaughter house, and 135 m^2 for a fire station and ambulance department. So far in these installations, conventional SWH systems are mainly adopted. However, high-rise buildings are found everywhere in the urban districts in Hong Kong, which means that there is space constraint for installing enough solar collector arrays to satisfy customers' requirement. For such a case, a solar assisted heat pump (SAHP) system might be a better solution instead of a conventional SWH system (Li and Yang, 2009).

A SAHP system combines the heat pump technology and solar thermal energy technology in mutual beneficial ways. This combination, to some extent, improves the coefficient of performance (COP) of the heat pump unit and reduces the consumption of fossil energy resource for hot water supply and cooling provision. According to different heat transfer media filled in the solar collector, the SAHP systems can be divided into the direct expanded solar assisted heat pump (DX-SAHP) system and the indirect expanded SAHP system. In the DX-SAHP system, refrigerant works as the heat transfer medium. For the indirect expanded SAHP system, which includes the solar assisted air source heat pump (SA-ASHP) system, the solar assisted water source heat pump (SA-

WSHP) system and the hybrid SAHP system, the heat transfer medium is usually water, air or antifreezing solutions, etc.

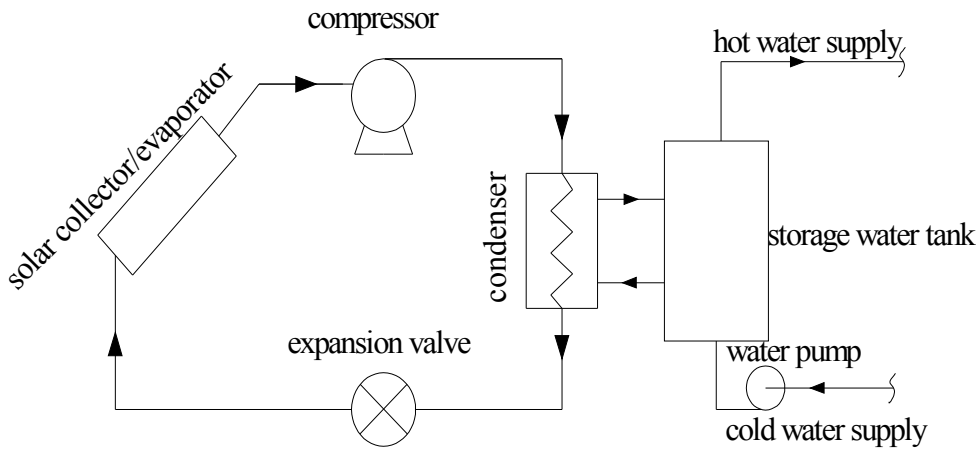

Figure 1.1 Schematic diagram of the DX-SAHP system

Figure 1.1 shows the schematic diagram of a DX-SAHP system. This system mainly consists of a flat plate solar collector which also acts as an evaporator, a compressor, a condenser, an expansion valve and a storage water tank. From the thermodynamic perspective, firstly, the liquid refrigerant is directly evaporated into vapor inside the solar collector/evaporator through the absorbed heat from the sun and/or ambient air. The working vapor is then drawn into the compressor, where it is compressed into high-pressure and high temperature vapor. After compression, the high-pressure vapor exchanges heat with water in the condenser. The condensed working fluid is then passing through an expansion valve where the pressure is reduced back to the evaporating pressure. The operating cycle is completed when the low-pressure liquid working fluid flows into the solar collector/evaporator again. The DX-SAHP system has the same operating principle as an air source heat pump system. The only difference is that this kind of system uses the solar energy as its major heat source, while air acts as

its supplementary energy source. As described above, the solar collector also works as the evaporator. Thus, the structure of the solar collector/evaporator should be very different from that of the solar collectors only used in conventional SWH systems, which means that it is necessary to redesign the configuration of the solar collector/evaporator in order to obtain comfortable system performance. At present, there is no uniform commercial product on market. Besides, the leakage problem of the refrigerant in the solar collector/evaporator restricts its application for relative small scale projects.

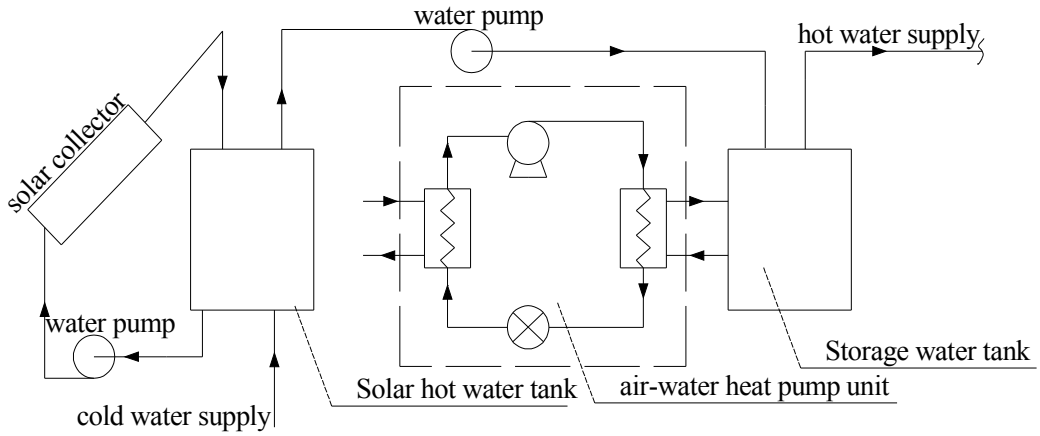

Figure 1.2 Schematic diagram of the SA-ASHP system

The schematic diagram of a SA-ASHP system is shown in Figure 1.2. It is composed of the solar collector loop and the heat pump unit which are connected in parallel. When solar radiation is strong, the solar collector loop itself can meet the hot water heating load. While on cloudy days or at night, the solar collector circle cannot supply enough hot water, the air source heat pump system starts to operate. It is obvious that this kind of system draws energy both from solar radiation and outdoor atmosphere.

As seen from Figure 1.3, a SA-WSHP system also contains two cycling loops – a flat plate solar collector loop and a water source heat pump loop. They are connected in series as distinct from the SA-ASHP system. In this system, the circulating water is heated in the solar collector, rejects part of its heat to the water in the solar hot water tank, and then flows into the evaporator for heat exchange with the working fluid in the heat pump loop and finally returns to the solar collector. The heated working fluid in the heat pump loop evaporates and experiences the same cycle as that in the DX-SAHP system. When available solar radiation is not strong enough, the circulating water in the solar collector loop absorbs heat from water in the storage tank which works as the lower temperature heat source of the heat pump unit for a complete working cycle. In this system, the heat pump draws energy only from solar thermal storage. The thermal performance of the WSHP unit is improved since the solar collector loop ensures a relatively higher temperature heat source as compared with that of a conventional WSHP system.

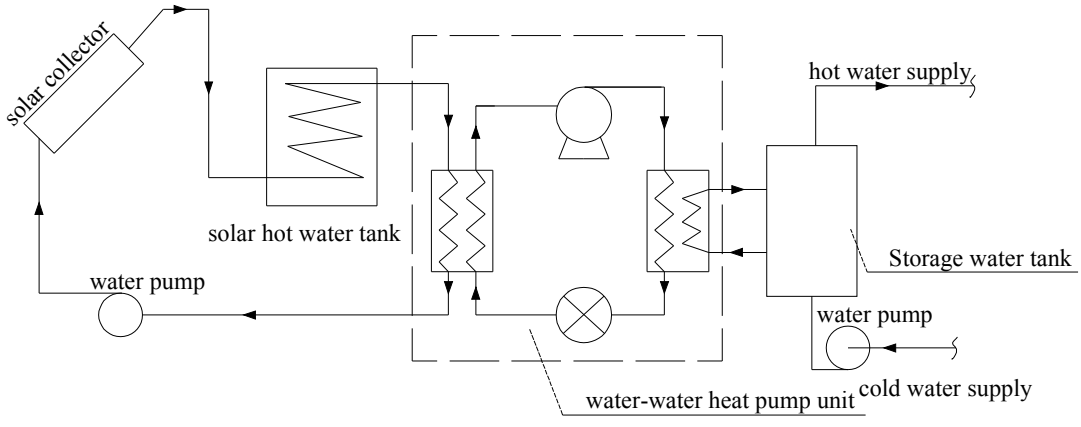

Figure 1.3 Schematic diagram of the SA-WSHP system

As for a hybrid SAHP system (i.e. the dual source SAHP system), the system combines the SA-ASHP system and the SA-WSHP system in which the heat pump can draw energy from either the thermal storage or the atmosphere. Generally, two evaporators are adopted in this kind of the SAHP system. One is the water-to-refrigerant evaporator and the other is the air-to-refrigerant heat exchanger. Due to the complicated configuration, the system's initial cost would be the highest and its control is difficult to ensure comfortable performance.

1.2 Multi-functional Solar Assisted Air Source Heat Pump System

For a subtropical region like Hong Kong, almost all residential families use room air conditioners merely for space cooling in summer. When it comes to the domestic hot water supply, the use of heat pump unit is not popular because of the relatively short and mild winter. Instead, electric heaters or gas-fired water heaters are used throughout a year for hot water supply.

Under such conditions, condensation heat from air conditioners has to directly be discharged to the environment. This not only engenders energy wasting, but yields thermal pollution to the ambient environment. For high-rise buildings in Hong Kong, the building re-entrant, an open space where kitchens receive daylight and ventilating air, is a popular place to accommodate the outdoor units of split-type air conditioners. The presence of these air cooled condensing units, however, introduces a thermal problem: the thermal buoyance as a result of heat dissipation leads to the development of a rising air plume. Inadequate air exchange at this recessed space elevates the ambient temperature, and the insufficient cooling significantly affects the condensers'

performance, especially for those at the upper floor levels. The result could be an overall degradation of the capacity and the efficiency of the air conditioners. At the same time, the air conditioner is used only in summer for cooling and remains idle in the rest of the year. The utilization rate of the split-type air-conditioners is very low.

On the other hand, electric water heaters or gas-fired water heaters for hot water supply consume much more energy than heat pumps. A gas-fired water heater also depends on the stability of water-pressure for its smooth operation. Besides, the system has the potential danger in life safety caused by the possible leakage of fuel gas or combustion products. In addition, a family has to buy both air conditioners for space cooling and water heaters for hot water production, which may not be economical in terms of cost and space.

In order to overcome the mentioned problems and limitations, a novel multi-functional air source heat pump (ASHP) system is proposed in this study. According to the customers' different requirement, the multi-functional ASHP system may work in three modes, i.e. the air conditioning and water heating (AC/WH) mode, the only air conditioning (AC) mode and the only water heating (WH) mode. Therefore, this kind of multi-functional ASHP system can simultaneously meet the cooling load and the hot water heating load as well.

In addition, the multi-functional ASHP system is combined with the solar thermal system which is called the multi-functional solar assisted ASHP (MSA-ASHP) system. As shown in Figure 1.4, this system consists of two cycling loops, i.e. the solar collector loop and the multi-functional ASHP circuit, which are coupled together with a storage

tank for hot water supply. The studied system is designed for multi-tasks and for year round services.

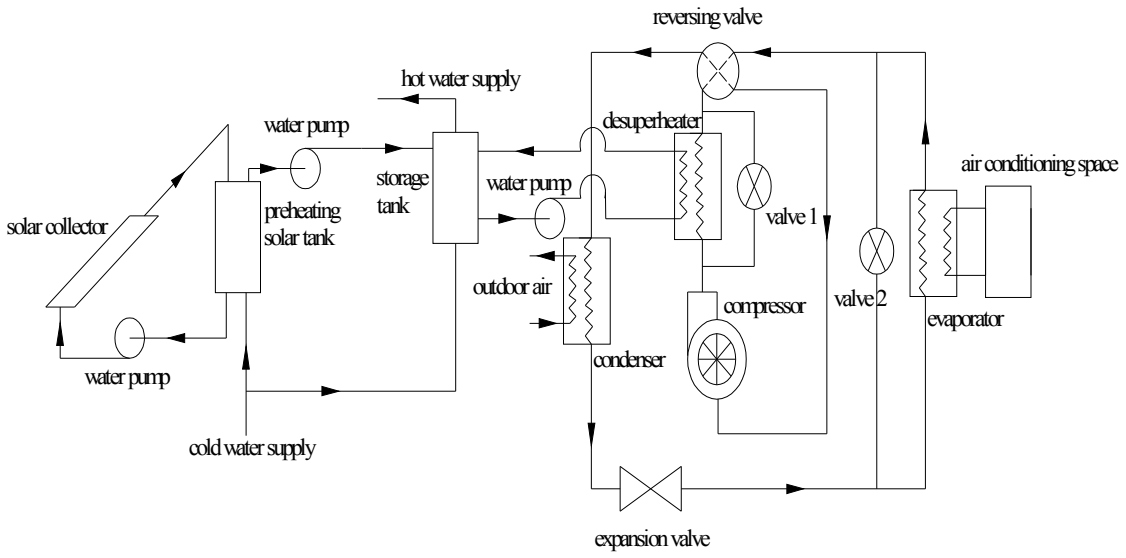

Figure 1.4 The MSA-ASHP system in the AC/WH mode

In summer, when solar radiation is not strong enough, the system mainly operates in the AC/WH mode. The superheated refrigerant vapor in the desuperheater sequentially heats the hot water to the required level. On sunny days, the required hot water temperature can be obtained only through the solar collector loop. In such case, the bypass valve 1 is opened, and the system switches to the only AC mode.

In mild seasons, air conditioning may not be necessary in a subtropical area. Meanwhile, solar radiation may not be strong enough so that the solar collector loop cannot meet the required hot water heating load by itself. Therefore, under such weather conditions, the proposed system works in the only WH mode, i.e. the multi-functional ASHP unit becomes an air source heat pump water heater. In such a case, valve 2 is

switched on and the indoor heat exchanger does not work while the outdoor air-to-refrigerant heat exchanger works as evaporator to absorb heat from ambient air.

As described above, generally, the MSA-ASHP system operates in three different modes including the AC/WH mode, the only AC mode and the only WH mode. Space heating load is sometimes required under subtropical weather conditions. Under such conditions, the MSA-ASHP system can also work in the space heating with domestic water heating mode. Sine the space heating load is insignificant in subtropical areas, the space heating function of the MSA-ASHP system is not discussed in this study.

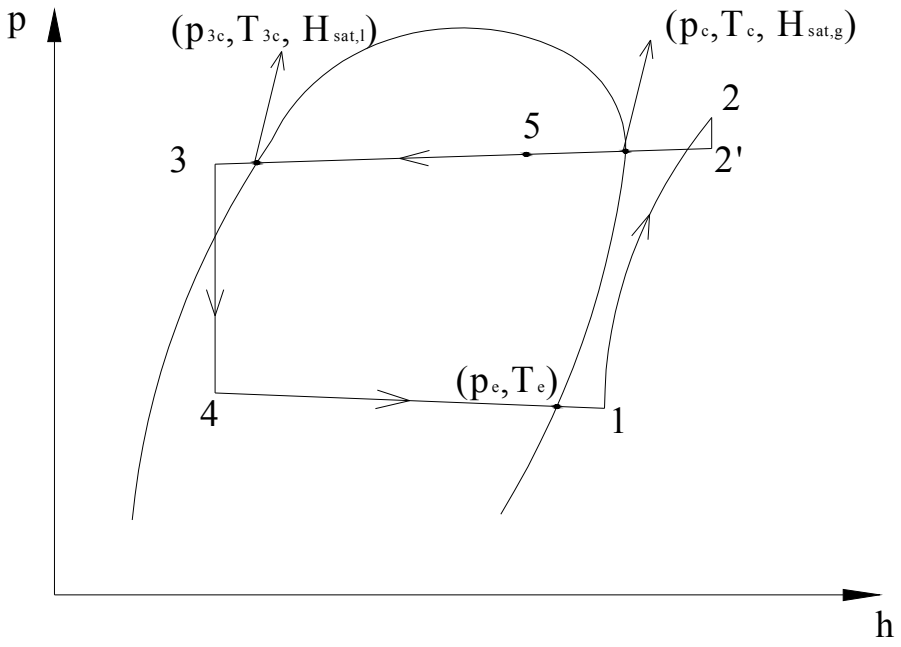

Figure 1.5 Refrigerant cycle in a pressure-enthalpy diagram

The corresponding refrigerant cycle is described in a pressure-enthalpy diagram as shown in Figure 1.5. The operating cycle can be represented by 5 refrigerant states. State

1 stands for the inlet state of the compressor; point 2 means its discharge state; point 2' is the inlet state of the desuperheater; point 5 is the inlet state of the air-cooled condenser which is also the outlet state of the desuperheater; point 3 is the outlet state of the air-cooled condenser, i.e. the inlet state of the expansion valve and point 4 is the inlet state of the evaporator.

As described above, the MSA-ASHP system utilizes solar energy resource for heating and cooling, which is clean and renewable. Besides, the system combines air conditioners and the water heaters into one product. In this way, the capital cost is reduced, the equipment is utilized completely throughout the year and the system performance is improved. As a result, the consumption of fossil fuel will be reduced, which means less greenhouse gases will be emitted to the environment.

1.3 Aims and Objectives

As it is known that the SAHP system combines the SWH technology and the heat pump system. Numerous studies have been conducted on the SWH systems, mono-functional heat pump systems, multi-functional heat pump systems, and their combination (i.e. the SAHP systems). At present, most of the SAHP systems are the combination of the SWH system with the mono-functional heat pump system. However, only a few researchers (Yang, 2007) focus on the combination of the SWH system with the multi-functional heat pump system. In this research, a novel SAHP system, i.e. the MSA-ASHP system, is proposed to replace the separate systems for air conditioning and water heating purposes in subtropical areas like Hong Kong. The main objective of this thesis is to develop an overall simulation model of the novel MSA-ASHP system to

analyze its operating performance and economic feasibility from energetic and exergetic perspectives. Not only the system components' models but also the economic evaluation of the life cycle savings (LCS) is to be proposed for system configurations evaluations in this study. In addition, a sample experimental system will be developed for validating the developed mathematical models and the simulation results. The specific objectives of this thesis are summarized as follows:

a) Development of the mathematical model of each component of the MSA-ASHP system will be the basic work for the estimation of the system performance. On the basis of the laws of energy conservation, mass balance and pressure balance as well as heat transfer correlations, a quasi-steady state model of the multi-functional ASHP system will be developed. For the solar collector loop, steady state modeling is also used except for the storage tank where dynamic modelling is adopted. Accordingly, a comprehensive simulation program of the proposed system is developed.

b) An experimental setup will be built for the efficiency test of the solar collector loop. The correlation between the solar collector efficiency and the major operating conditions will be analyzed. In addition, a prototype of the MSA-ASHP system will be set up. Experiments will be conducted to validate the simulation model and investigate the operating performance of the MSA-ASHP system in different operation modes. The judgment parameters for switching operating modes will be selected. Accordingly, the appropriate control strategy will be recommended for operating the MSA-ASHP system.

c) The comprehensive simulation model of the MSA-ASHP system will be validated under various operating conditions based on the collected experimental data. The operating performance of the MSA-ASHP system will be further discussed.

d) The energetic and exergetic analysis of the MSA-ASHP system will be conducted in all operation modes based on the recorded experimental data and the simulation results. Appropriate exergetic equations will be derived for the whole system and its each component. The exergetic results will reveal the most inefficient part of the system and point out which component has the highest improvement potential. Besides, the energy and exergy comparisons will be carried out among different hot water heating systems to better investigate the performance of the proposed MSA-ASHP system.

e) For evaluation of the long-term energy performance of the MSA-ASHP system, a straightforward method (i.e. weather year for solar systems, WYSS) will be proposed for the selection of typical meteorological year (TMY) weather conditions from a multi-year record. Based on the selected TMY, the annual monthly performance of the MSA-ASHP system will be analyzed. In addition, an economic feasibility analysis will be implemented for using the proposed system in Hong Kong.

1.4 Organization of the Thesis

This thesis is organized into 8 chapters. An introduction is made on the SAHP systems in the first chapter. The application limitations and problems of the SAHP

systems are subsequently discussed. Then, a novel MSA-ASHP system is proposed to overcome the mentioned problems in cooling-dominated buildings of subtropical areas. The detailed aims and objectives of this thesis are also proposed in this chapter.

A literature review about the SAHP system and its subsets (i.e. the SWH system and the multi-functional heat pump system) is presented in Chapter 2. Various studies about the application potential of the SWH systems are introduced. The application potential of different solar thermal systems including the SWH system and the SAHP systems for hot water production in Hong Kong is evaluated, considering both economic characteristics and global warming impacts. This is followed by reviewing the performance prediction methods for the SWH system, the monofunctional SAHP systems and the multi-functional heat pump systems.

In Chapter 3, the detailed mathematical models for the components of the MSA-ASHP system are developed. The systematic simulation model for the whole system is obtained through coupling components' model based on the principles of mass balance, pressure balance and energy balance. The operating performance of the MSA-ASHP system under various operating modes is predicted and discussed using the simulation model.

Chapter 4 describes a sample MSA-ASHP system for the validation of the simulation model and further investigation of the system performance. An experimental rig is built to do various tests and record the measured data. At the end of this chapter, an uncertainty analysis of the experimental data is conducted.

In Chapter 5, based on the experimental data under different weather conditions, the system simulation model is fully verified. All operating modes which are commonly used in practice are analyzed based on a sequence of experiments.

In Chapter 6, an exergy analysis is carried out based on the experimental data and the simulation model developed in Chapter 3. The exergy efficiency of the MSA-ASHP system in AC/WH mode is analyzed in details. Consequently, components with the greatest irreversibility and the highest improvement potential are pointed out, which are valuable information for the practical design of the MSA-ASHP system.

The typical meteorological year for the MSA-ASHP system is developed in Chapter 7. A new method is adopted during the TMY selection procedure. The annual monthly performance of the MSA-ASHP system is evaluated and discussed using the TMY data. A simple economic analysis is conducted for the proposed system.

Finally, Chapter 8 summarizes the main conclusions and achievements of this thesis and gives recommendations for the future work.

CHAPTER 2 LITERATURE REVIEW

2.1 Introduction

The depletion of conventional energy sources and its likely adverse impact on environment have created growing interest for the application of renewable energy sources such as geothermal, wind, solar and marine energy etc. For space heating and domestic water heating applications, more consideration is given to application of solar water heating (SWH) systems. At the beginning, conventional SWH systems were mainly used. Later, when the heat pump technology became popular, the combination of conventional SWH systems with heat pumps was proposed and developed. This SAHP provides a real capability of upgrading low-grade energy sources from the surroundings as well as using solar energy (Charters and Taylor, 1976; Charters et al., 1980; Charters and Lu Aye, 1999).

The concept of the SAHP system was firstly proposed by Sporn and Ambrose (1955) in West Virginia. Since then, numerous theoretical and experimental studies have been conducted. On one hand, significant interests are shown in studying the application of the direct expanded SAHP (DX-SAHP) systems. On the other hand, there have been a lot of studies focusing on the indirect expanded SAHP systems. In order to overcome the discharged heat pollution problem of traditional air conditioners in cooling-dominated buildings and to increase the utilization efficiency of equipment, the multi-functional heat pump technology was developed in this study. This chapter presents a detailed literature review about the performance prediction of the SAHP system and its subsets

including the conventional SWH system, the monofunctional SAHP system and the multi-functional heat pump technology.

2.2 Investigation on Potential of the SWH Applications

The application of the SWH systems for a particular location depends heavily on location of the site, the available solar radiation and the local price paid for electricity to drive or boost the system chosen. For different districts and locations, climatic conditions, including solar irradiance, variations in wind speed, ambient air temperature, and so forth, are always changing. In order to efficiently utilize solar thermal energy, an analysis of the application potential of the SWH systems in different sites should be made at the stage of inception.

The possibilities of using the SWH systems in many districts or countries (such as Australia, India, Turkey etc.) were studied (Aye et al. 2002; Sen and Sahin, 2001; Rylatt et al. 2001; Sozen et al. 2005; Chandrasekar and Kandpal, 2004; Voinvontas et al. 1998; Pillai et al. 2007) and different SWH systems are proved to be very practical and viable in those areas.

2.2.1 Application potential of conventional SWH systems in Hong Kong

Considerable studies have been conducted on the solar thermal energy technology for hot water production in Hong Kong. Ji et al. (2003) analyzed the annual performance of facade-integrated hybrid photovoltaic/thermal collector system for use in residential buildings of Hong Kong. Chow et al. (2006) estimated the potential application of a centralized solar water-heating system for a high-rise residential

building in Hong Kong. Chow et al. (2007) further conducted an experimental study of a centralized photovoltaic and hot water collector wall system which can serve as a water pre-heating system. Through modeling and experimental analysis, all of these researches show that there is a good application potential of solar thermal energy for hot water production in this territory.

However, most researches, until now, mainly focus on the application of the conventional SWH systems. Little systematic research is conducted on the application of different solar thermal systems, especially the SAHP systems, under the moderate weather conditions. Therefore, it is necessary to evaluate the application potential of different kinds of SWH systems for hot water production in moderate climates such as Hong Kong. Considering both economic characteristics and global warming impacts, in the following section, the application potential of various SAHP systems is discussed under Hong Kong weather conditions.

2.2.2 Application potential of SAHP systems in Hong Kong

In recent years, the depletion of conventional energy sources and their likely adverse impact on environment have created growing interest for application of renewable energy sources. In Hong Kong, there is also a growing government-led trend to use renewable energy resources and one area of interest lies in the use of solar thermal energy for hot water supply. Till now, as described in Chapter 1, a number of solar thermal systems using sunlight to heat water directly or indirectly have been installed in both governmental and residential premises.

On the other hand, the utilization of heat pump technology has been accepted world widely considering its energy-saving and environmental protection benefits. In Hong Kong, Chan and Lam (2003) presented the thermal performance, energy-saving, indirect emissions and financial feasibility of using heat pumps for hotel outdoor swimming pools. It was found that the average COP was ideal and the saving in energy was substantial.

At present, the energy sources commonly used for hot water production are towngas and electricity (EMSD, 2007) in Hong Kong. Thus, the following comparisons are made among four kinds of different water heating systems i.e. the electric water heater, the towngas water heater, the conventional SWH systems and various SAHP systems.

2.2.2.1 Case study

A case study is carried out for economic comparisons of different water heating systems. It is assumed that all the systems studied have the same heating capacity and are designed to supply hot water for one room with two persons in a hotel. According to CIBSE GUIDE (1986), the heating load should be able to heat 280 liter water from 20℃ to 55℃. The initial temperature of water is set as 20℃ because the average dry bulb air temperature is about 20℃ from February to May, a period during which the lowest solar radiation occurs. If the heating load during this period could be guaranteed, the system can then satisfy the hot water requirement a year round. In order to use the same basis for comparisons, the solar collector area of 6 m^2 is adopted and the efficiency of solar collector loop is set as 0.4 for all the solar thermal systems.

2.2.2.2 Methodology of the case study

A simple evaluation procedure is developed for the case study and the calculation is based on the savings compared to the use of an electric water heater. Details of the evaluation procedure are described as follows.

Firstly, the annual heating load is estimated by the following equation:

$$Q = 365mc\Delta t \tag{2.1}$$

where Q is the required heating load per year; m is the mass of hot water required per day; c is the specific heat of water; and Δt is the water temperature difference between the inlet and the outlet temperatures.

Secondly, the useful solar thermal energy collected by the solar collectors is calculated by:

$$Q_u = A_c I_t \eta_{coll} \tag{2.2}$$

where Q_u is the useful solar thermal energy per year; A_c is the area of solar collector; I_t is the maximum annual solar radiation received by the solar collector; and η_{coll} is the efficiency of the solar collector loop.

The conventional energy consumption is then evaluated:

$$E_c = (Q - Q_u)/\eta \tag{2.3}$$

Where E_c is the conventional energy consumption per year and η is the system efficiency.

Based on the aforementioned calculation, the annual operating cost and the annual cost savings compared to the electric water heater system can be estimated accordingly.

Finally, the solar fraction and the simple payback period are defined by Equation (2.4) and Equation (2.5).

$$solar\ fraction = \frac{Q_u}{Q_u + E_c} \times 100\% \tag{2.4}$$

$$simple\ payback\ period = \frac{initial\ \mathrm{cos}t}{\mathrm{cos}t\ saving\ per\ year} \tag{2.5}$$

The initial cost includes the cost of the major equipment shown in the schematic diagrams in Chapter 1. The average price of the equipment with medium quality in the market is adopted for the initial cost calculation.

In the case study, the solar collector surface is tilted at 19.4° due south in order to receive the maximum solar radiation throughout a year in Hong Kong (Fung and Yang, 2005). The typical example year of 1989 for solar energy application is utilized for calculating the solar radiation exposed on the solar collector surface because the weather in this year has been found to be the most representative based on a statistical analysis on weather data of Hong Kong from 1971 to 1991 (Yang and Lu, 2004). Based on the above assumptions, the maximum annual solar radiation received by the surface of solar

collector is 4910.7 MJ/m^2 (Fung and Yang, 2005). The economic comparison is based on the energy price of 2004 in Hong Kong. The average tariff of electricity and gas were about HK$1 per kWh and HK$0.21 per MJ (Fung et al., 2006). The theoretical calorific value of electricity is adopted as 3.6 MJ/kWh.

2.2.2.3 Economic results and discussions

The economic comparisons between different water heating systems are performed by means of the aforementioned calculation method. The results are summarized in Table 2.1. The results show that the solar thermal systems, especially the SA-ASHP system, have great potential of saving energy. As a result, their payback periods are much shorter than the towngas water heater compared with the base case: the electric water heater. Among the solar thermal systems, the conventional SWH system exhibits the shortest payback period. Although the SA-ASHP system has the highest annual cost saving, its payback period is longer than the conventional SWH system because of higher initial cost. Also, the payback periods of other SAHP systems are much longer than the conventional SWH system even though they have similar annual cost savings.

Table 2.1 indicates that different solar thermal systems have different solar fractions. Since solar fraction, which can determine to a large extent the system annual cost saving, is affected by solar collector area, the impacts of solar collector area change on the solar thermal system performance are analyzed. According to the study results (Kuang et al., 2003), it is assumed that the COP of the DX-SAHP system increases by 10% as 1 m^2 of solar collector is added. For the SA-WSHP system, the COP increases by 15% for the increment of 1 m^2 solar collector. In addition, other basic data remains unchanged.

Table 2.1 Economic comparison among different water heating systems

Item	Towngas water heater	Electricity boosted SWH	Towngas boosted SWH	SA-ASHP	DX-SAHP	SA-WSHP
η	0.85	0.95	0.85	COP=3	COP=4	COP=4
E_c (MJ/year)	17675	3405	3809	1079	3756	3756
Initial cost (HK$)	3700	10980	12940	16800	14700	21500
Operating cost (HK$/year)	3712	946	800	300	1043	1043
Cost saving per year (HK$)	461	3227	3373	3873	3130	3130
Solar fraction (%)		77.6%	75.6%	91.6%	75.8%	75.8%
Payback period (year)	8	3.4	3.8	4.3	4.7	6.9

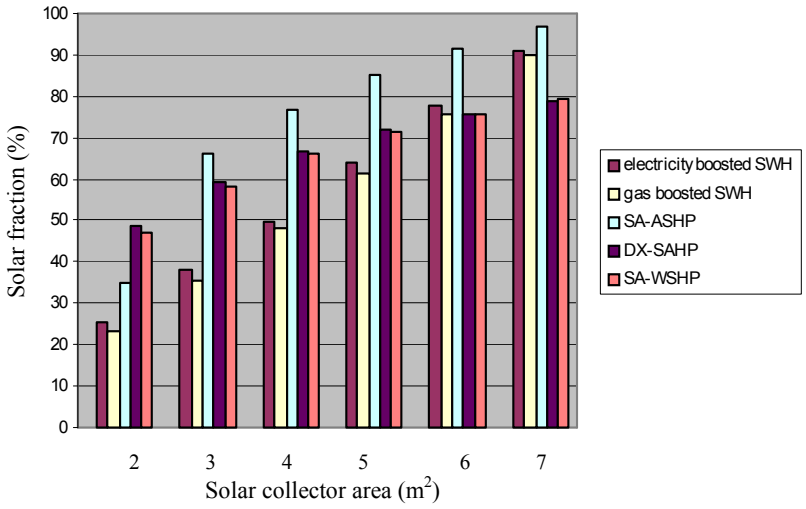

Figure 2.1 Effect of the solar collector area on solar fraction

Figure 2.1 shows that solar fraction is increased obviously with the increment of the solar collector area. It is clear that the solar fractions of conventional SWH systems are

much lower than the SAHP systems when the solar collector area is less than 4 m^2. Conversely, while the solar collector area is larger than 4 m^2 which also means solar fractions of conventional SWH systems are above 50%, the solar fractions of the conventional SWH systems are comparable with those of the SAHP systems.

Figure 2.2 presents the cost saving variations of different water heating systems as the solar collector area changes. The cost saving of each system grows evidently as the solar collector area increases, especially for conventional SWH systems. Meanwhile, the conventional SWH system offers similar energy saving compared with the SAHP systems when the solar collector area is greater than 4 m^2.

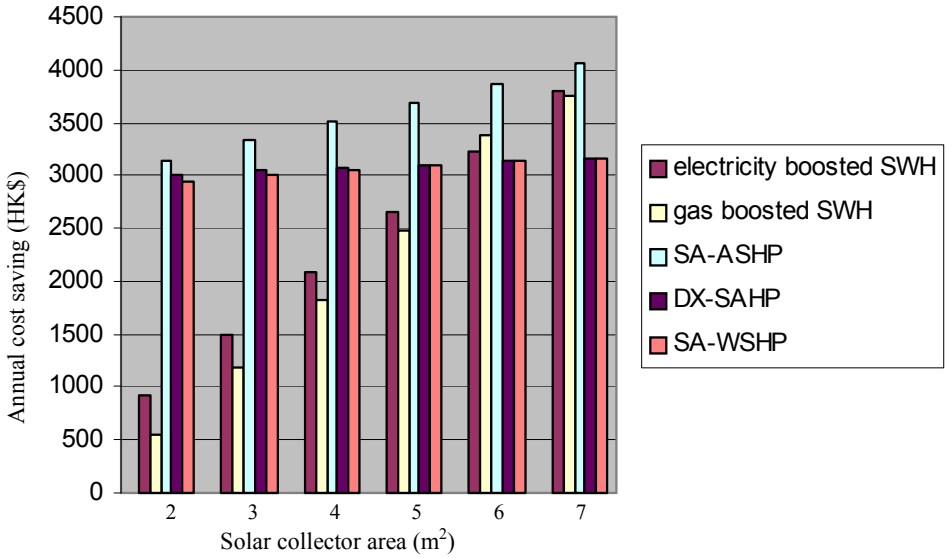

Figure 2.2 Effect of the solar collector area on annual cost saving

The influences of the solar collector area on the payback periods are also analyzed, as shown in Figure 2.3. It can be noticed that the payback period of the

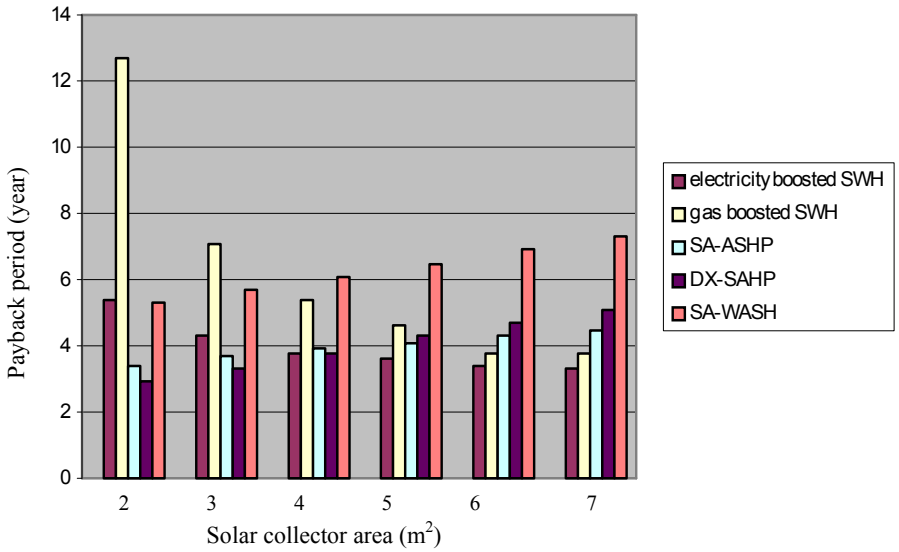

Figure 2.3 Effect of the solar collector area on payback period

conventional SWH system decreases sharply with the increment of the solar collector area, especially the towngas boosted SWH system. On the contrary, the SAHP systems' payback periods increase since their initial costs grow faster than the corresponding annual cost savings. It is found that the conventional SWH systems have shorter payback periods than the SAHP systems when the solar collector area is larger than 4 m^2.

The analysis demonstrates that the conventional SWH systems are comparable with the SAHP systems in terms of solar fractions, annual cost savings and payback periods when their solar collector areas are large enough to ensure that a solar fraction is higher than 50%.

2.2.2.4 Global Warming Impact Analysis

In Hong Kong, carbon dioxide is the dominated greenhouse gas released from fossil fuel consumption, making up 86% of the total greenhouse gases (carbon dioxide-

equivalent) emissions in 2004 (Environmental Protection Department, 2007). Therefore, it is reasonable to assess different hot water systems' global warming impacts through evaluating the amount of CO_2 produced by these hot water systems during their lifecycles.

For the SAHP systems, both their direct and indirect effects on greenhouse gas emissions should be considered. The direct component relates to the release of refrigerants (R22), and the indirect one is the carbon dioxide production in powering the equipment. An indicator of the combined effects is the total equivalent warming impact (TEWI), which is defined by equation (2.6) and Equation (2.7) (Florides et al., 2002):

$$direct\ \ effect(kg\ CO_2) = [(make-up\ rate \times service\ life) + end-of-life\ loss] \times change \times GWP \quad (2.6)$$

The make-up rate is the refrigerant lost per year in percentage; the service life is the number of years that the system is utilized (years); the end-of-life loss is the percentage of the lost refrigerant when the lifetime ends; the charge is the initial charge of refrigerant in the system (kg) and *GWP* is the global warming potential of gas. The *GWP* actually varies depending on the time frame considered, but usually a 100-year integrated time horizon is used. For R22, the *GWP* is 1700.

$$indirect\ \ effect(kg\ CO_2) = operation\ \ power \times service\ life \times emitted CO_2 \quad (2.7)$$

The operation power is the power required by the system per year (kWh/year); the emitted CO_2 is the amount of CO_2 emitted from the power plant per unit power generated (kg/kWh).

For other hot water systems, since no refrigerants are used, the indirect effect is only calculated.

In the case study, the make-up rate, the end-of-life loss and the initial charge of refrigerant of the SAHP systems are set as 3%, 20% and 2 kg, respectively. All these data are assumed according to the average figures from manufacturers' specifications. In addition, it is assumed that all the systems considered have the same service life of 10 years. In Hong Kong, the average CO_2 emission per unit power production in recent years is 0.54 kg/kWh (Lancaster and Richard, 2007) and the average CO_2 emission of towngas is 0.01444 kg/MJ (Hong Kong and China Gas Company Limited, 2007). Based on the calculation method and basic data assumed, the results for TEWI are shown in Table 2.2.

Table 2.2 TEWI of different water heating systems

Hot water system	Electric water heater	Towngas water heater	Electricity boosted SWH	Towngas boosted SWH	SA-ASHP	DX-SAHP	SA-WSHP
TEWI (kg CO_2)	22535	2552	5108	550	3320	7332	7332

From Table 2.2, it is found that the towngas boosted SWH system has the lowest value of TEWI, which means the least global warming impact is caused. Compared with the towngas heater, about 80% of CO_2 emission can be reduced from this towngas boosted SWH system. It is also found that the TEWI of the electric water heater system would be 4.4 times greater than that of the electricity boosted SWH system, 6.8 times than the SA-ASHP system, and 3.1 times than the DX-SAHP system and the SA-WSHP

system. These results prove that solar thermal systems have great potential in reduction of greenhouse gas emission.

In order to offer a comprehensive comparison, the sensitivity of TEWI reacting to the solar collector area is analyzed. The result is shown in Figure 2.4. It is obvious that the towngas boosted SWH system has the greatest potential in reducing greenhouse gas emission under any design condition. For the electricity boosted SWH system, it has the comparative TEWI with SAHP systems if the solar collector area is larger than 4 m^2. Among the SAHP systems, the SA-ASHP system has evident advantage with respect to the global warming impact. In conclusion, the TEWI of the electricity boosted SWH system is sensitive to the solar collector area and decreases sharply with the increment of the solar collector area. As for SAHP systems, the SA-ASHP system is more sensitive than other systems.

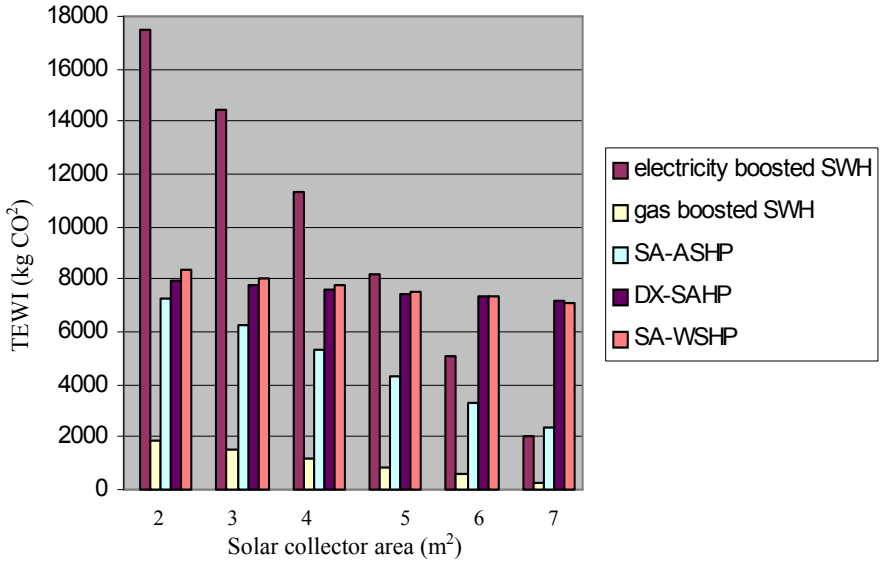

Figure 2.4 Effect of the solar collector area on TEWI

The economic comparison results show that a solar thermal system has greater economic benefits than an electric water heater and a towngas water heater. Accordingly, its payback period is much shorter than a towngas water heater. Further analysis demonstrates that the solar fraction of a conventional SWH system is much lower than a SAHP system when the solar collector area is less than 4 m^2. Conversely, while the solar collector area is larger than 4 m^2 which means the solar fraction of a conventional SWH system is above 50%, both the cost saving and payback period of a conventional SWH system are comparable with that of a SAHP system.

From analysis on the sensitivity of TEWI of different solar thermal systems, it is concluded that the towngas boosted SWH system has the greatest potential in reducing greenhouse gas emission under any design conditions. While the electricity boosted SWH system has the comparative TEWI with the SAHP systems if its solar collector area is larger than 4 m^2. As for the SAHP systems, the SA-ASHP system has evident advantage considering its global warming impact.

All investigation results demonstrate that solar thermal systems have greater application potential under Hong Kong weather conditions. In order to utilize solar thermal energy more efficiently, the system selection should depend on the available space for solar collector arrangement. If there is enough space to ensure that the solar fractions of the conventional SWH systems are above 50%, the conventional SWH systems, especially the towngas boosted SWH system, are preferred compared with SAHP systems. Otherwise, SAHP systems are proposed, especially the SA-ASHP system. In Hong Kong, the limited space has significant impact for the installation of the

solar collector loop. Therefore, for most occasions, the SAHP system is a better choice rather than the conventional SWH systems for hot water production.

2.3 Performance Study on the Conventional SWH Systems

A number of methods are available for the theoretical evaluation of the long term performance of the conventional SWH systems. These methods can be broadly classified into two categories, namely, correlation based methods and simulation based methods. Methods based on utilizability (Duffie and Beckman, 1991), F-chart (Klein et al. 1976), $\bar{\phi}-F$ chart (Klein and Beckman, 1979) etc. are prominent examples of correlation based methods. Different simulation programs such as TRNSYS (Klein et al. 1975), SOLCHIPS (Lund, 1989; Lund and Peltola, 1992), etc. have been used to design the conventional SWH systems through detailed simulation approach.

The use of correlation based methods (i.e. simplified calculation methods) has maintained its popularity and usefulness, and recently a few more developments have been added to this line of approach (Brinkworht, 2001; Joudi and Abdul-Ghafour, 2003a,b; Colle and Vidal, 2004). By identifying the most important parameters governing system performance, these methods are most useful for system design, as they provide a means of evaluating the effect of changing system parameters during the design process. This is not easy with detailed simulations, as the change in some input variables does not necessary have a significant effect in system long term performance and does not show the "complete picture" – note that a large number of individual input variables are present in solar thermal system simulation. Therefore, in this research, the

F-chart method, one of the correlation based methods, is adopted for the performance prediction of the solar collector loop.

Historically, the F-chart method is the first simplified method (Klein et al. 1976). It is developed for the design of active and passive solar heating systems, especially for the size and type of solar collectors supplying the domestic hot water and heating loads. Its accuracy has been verified comprehensively (Evans et al., 1985; Ammar et al., 1989; Minnerly et al., 1991; Barley and Winn, 1978; Drew and Selvage, 1979; Sfeir, 1980; Ajona and Gordon, 1987; Tsilingiris, 1996). It is worth noting that F-chart method is so widely used as a standard for assessing new methods.

The F-chart method is a correlation of the results of many hundreds of thermal performance simulations of solar heating systems. The resulting simulations give *f*, the fraction of the monthly heating load supplied by solar energy as a function of two dimensionless parameters, *X* (Collector Loss) and *Y* (Collector Gain). *X* is related to the ratio of collector losses to heating loads, and *Y* is related to the ratio of absorbed solar radiation to the heating loads. The two dimensionless groups are

$$X = F_R U_L \times \frac{F_R^{'}}{F_R} \times \left(T_{ref} - \bar{T}_a \right) \times \Delta t \times \frac{A_c}{L} \tag{2.8}$$

$$Y = F_R \left(\tau\alpha \right)_n \times \frac{F_R^{'}}{F_R} \times \frac{\overline{\tau\alpha}}{\left(\tau\alpha \right)_n} \times \overline{H}_T N \times \frac{A_c}{L} \tag{2.9}$$

where

A_c = Area of solar collector (m^2),

$F_R^{'}$ = Collector-heat exchanger efficiency factor (%),

F_R = Collector heat removal factor (%),

U_L = Collector overall energy loss coefficient (W/(m^{2}K))

Δt = Total number of seconds in the month,

$\overline{T}_a$ = Monthly average ambient temperature (℃),

L = Monthly total heating load for space heating and hot water (GJ)

$\overline{H}_T$ = Monthly averaged, daily radiation incident on collector surface per unit area (MJ/m^2),

N = Number of days in the month,

$\left(\overline{\tau\alpha}\right)$ = Monthly average transmittance-absorptance product (%),

$\left(\tau\alpha\right)_n$ = Normal transmittance-absorptance product (%),

T_{ref} = An empirically derived reference temperature (100℃)

The F-chart equations for the fraction *f* of the monthly space and water heating loads supplied by solar energy are given as follows:

$$f = 1.029Y - 0.065X - 0.245Y^2 + 0.0018X^2 + 0.0215Y^3 \tag{2.10}$$

2.4 Performance Study on Multi-functional Heat Pump Systems

The multi-functional heat pump system is the combination of an air-conditioning system and a heat pump water heater for space heating, water heating and space cooling services of buildings. In the combined system, only one set of key components (i.e. the

compressor, the heat exchangers, the four-way valve etc.) is used. Thus, the investment cost will be reduced obviously when compared with using two separate units. Besides, the new equipment can meet both cooling load and heating loads. This practical use of the waste heat of condensation not only improves the overall efficiency of the air conditioner, but also supplies "free" hot water and reduces the heat pollution to the surroundings.

Healy and Wetherington (1965) firstly demonstrated the potential for using heat from condensers as ''free'' energy for producing hot water in residential buildings. They found that it could save 70% energy for heating domestic hot water every year. In succession, Cook (1990), Ying (1989), Toh and Chan (1993) and Goldschmidt (1990) launched experiments and simulations on using condenser heat to heat hot water and proved its feasibility. They concluded that the modified system could provide domestic hot water without losing its cooling capacity. It was also found that the actual recovery was about 20% of the total discharged condensing heat and COP of the system was increased.

Olszeweki (1984) analyzed the economic feasibility of desuperheaters in heat pumps for supplying domestic hot water. The assessment indicated that this system was especially suitable for areas where cooling load was substantial and the price of electricity was high. However, its use has not by far been fully exploited. In China, there has not been found in open literatures on it until recent years. Ying et al. (2002) presented a new heat pump system with hot water supply. No further research has been found as yet. Shi et al. (2002) put forward an assumption on an inverter air cooled heat

pump with a water heater. They calculated the all-year-round operation energy consumption of the system, but this system was too complex to be realized in practice. Later, Tan and Deng (2002) developed a simulation research on utilizing condenser heat from a water chiller to generate hot water. The simulation results showed that the system could achieve high-energy efficiency. Ji et al. (2003) carried out experiment and simulation researches on energy performance of the air conditioner integrated a water heater, and found that the energy efficiency ratio (EER) of the unit was about 30% higher than that of the conventional unit. Jiang et al. (2006) did an experimental study on a modified air conditioner with a domestic hot water supply. The dynamic operation characteristics, hot water supply performance, energy efficiency and temperature distribution of hot water in the storage tank were tested in different operation condition by using the experimental rig. The investigation results show that the modified system not only has a better operation performance than the original unit, but also can provide a continuous hot water supply for householders.

2.5 Performance Prediction of the Multi-functional Heat Pump Unit

As aforementioned, the multi-functional heat pump systems have been the target of numerous researches. However, few standard simulation models of the multi-functional heat pump are found in open literatures that can evaluate its system performance under all possible operating conditions. Inversely, the simulation models of vapor-compression refrigeration and air conditioning systems, such as traditional heat pumps and chillers, have been the topic of numerous papers. These models can generally be classified in terms of the degree of complexity and empiricism. Hamilton and Miller (1990)

classified the available simulation methods into two groups: one is the equation-fit model (i.e. functional fit model), which treats the system as a black box and fit the system performance into a few functional equations using catalog data; the other is the deterministic model (i.e. first principle model), which are detailed models based on thermodynamic laws and fundamental heat and mass transfer relations to individual components.

Allen and Hamilton (1983) developed a typical equation-fit model of a reciprocating water chiller. The other models employing the equation-fit approach in the literature are much similar to this one. These models did not consider individual component models and eliminated the internal variables by utilizing the functional relationships among variables and existing typical water chiller performance data. Therefore, they are most suitable for users that only have access to catalog data. These models would not be useful for someone attempting to design a heat pump or chiller by modifying or replacing internal components. Especially troublesome for some applications, extrapolation of the model may lead to unrealistic results (Jin and Spitler, 2002).

The majority of the models differed from the equation-fit method are near to the deterministic model, although the detailed deterministic models often apply equation-fitting for some of the components. Fishcer and Rice (1983) developed an air-to-air heat pump model to predict the steady state performance of conventional, vapor compression heat pumps in both heating and cooling modes. This model is proposed as an analytical design tool for use by heat pump manufacturers, consulting engineers, research institutions and universities in studies directed toward the improvement of heat pump

efficiency. The compressor was modeled using the data "curve-fits" and "compressor maps" provided by the manufacturers. Modeling of the other components employed many fundamental correlations and detailed design data are required. Hence, this model may be useful in the heat pump design process.

2.6 Summary

This chapter mainly presents a literature review on the conventional SWH systems, the SAHP systems and the multi-functional heat pump systems considering several aspects.

First of all, a review of numerous studies about the application potential of the conventional SWH system has been made. With the commonly used hot water heater (i.e. the electric water heater) as the base case system, the application potential of different SAHP systems is then discussed considering both economic and environmental impacts.

The available methods for performance prediction of the conventional SWH systems have been reviewed. The F-chat method is proposed for the long term performance evaluation of the solar collector circuit in this research.

Finally, various performance studies and simulation models of the multi-functional heat pump systems have been reviewed. Compared with few theoretical studies on the multi-functional heat pump systems, two kinds of simulation models for conventional heat pump and water chillers have been developed.

It is found that although a large amount of work has been done on the conventional SWH systems and the multi-functional heat pump, only limited number of researchers focus on the performance evaluation of the combined system, i.e. the MSA-ASHP system, based on experiments. Therefore, in this thesis, a comprehensive simulation model of the MSA-ASHP system will be developed and the system performance will be evaluated and validated based on a practical system under various operating modes in subtropical areas, like Hong Kong.

CHAPTER 3 DEVELOPMENT OF SIMULATION MODEL OF THE MSA-ASHP SYSTEM

3.1 Introduction

The configuration and characteristics of the proposed MSA-ASHP system has been described in Chapter 1. In order to accurately investigate the operating performance of the MSA-ASHP system, an effective and practical simulation model is strongly desirable. The objective of this chapter is to develop a systematic simulation model for the MSA-ASHP system and to analyze its operating performance under various operating conditions based on the developed simulation model.

According to the literature review on heat pump models in Chapter 2, it can be found that, obviously, the equation-fit model is not helpful for the heat pump design process and modification of internal components. On the contrary, one of the primary advantages of the deterministic model is the convenience of designing an efficient and cost-effective heat pump unit by varying the design parameters of each component and conditions. Furthermore, it is able to simulate the system responses for a variety of external and internal conditions which may be beyond the range of catalog data.

It is worth noticing that the deterministic models include the dynamic and steady-state models. Generally, the dynamic model is used to analyze the dynamic behavior during the start-up or shutdown period of a system or to evaluate the operating performance of a complicated system with variable speed pumps or compressors. In the

MSA-ASHP system, both the compressor and water pumps operate with constant speed. For a heat pump system with constant speed water pumps and compressor, only a short time is needed to approach the stead-state operation. The steady-state deterministic model is therefore employed in this research to develop the simulation model of the multi-functional ASHP unit which incorporates laws of thermodynamics, fluid mechanics and heat transfer correlations into a network of simulation algorithms.

As shown in Figure 1.4, the MSA-ASHP system is mainly composed of a solar collector loop and a multi-functional ASHP unit. And the multi-functional ASHP unit consists of five subsets: a rolling piston compressor, evaporator, desuperheater, condenser and a thermostatic expansion valve. In this thesis, steady-state models are developed for each component of the MSA-ASHP system except for the storage water tank of the solar collector loop. On the basis of the energy balance, the pressure balance and mass balance, all the components' models are coupled together into an overall systematic model for the proposed MSA-ASHP system.

3.2 The Solar Collector Loop Module

Similar with most conventional SWH systems, the solar collector loop of the studied system has two main parts: a solar collector array and a storage tank. The corresponding models for these two components are developed one by one in this section.

3.2.1 Model of solar radiation on tilt surface

A solar collector is a special kind of heat exchanger that transforms solar radiant energy into heat. In the MSA-ASHP system, a flat plate solar collector is selected. This

kind of solar collector is usually designed for applications requiring energy delivery at moderate temperatures, up to perhaps 80℃. It absorbs both beam and diffuse solar radiation, does not require tracking of the sun, and requires little maintenance. It is the most commonly used solar collector.

In steady state, the performance of the solar collector array is described by an energy balance that indicates the distribution of incident solar energy into useful energy gain, thermal losses, and optical losses. Accordingly, the useful heat gain from the solar collector array (q_s), the heating load met by solar energy (q_{Ls}) and the storage heat loss (q_{stl}) are evaluated by the following equations.

$$q_s = A_c\left[I_T F_R(\tau\alpha) - F_R U_L\left(T_{st} - T_a\right)\right] \tag{3.1}$$

$$q_{Ls} = m_L C_p\left(T_{st} - T_R\right) \tag{3.2}$$

$$q_{stl} = U_{st} A_{st}\left(T_{st} - T_a\right) \tag{3.3}$$

where the incident solar radiation on a tilted surface (I_T) is calculated by:

$$I_T = \left(I_g - I_d\right)R_b + I_d\left(\frac{1+\cos\beta}{2}\right) + I_g\left(\frac{1-\cos\beta}{2}\right)\rho_g \tag{3.4}$$

In equation (3.4), to get I_T, the known values of the total horizontal and diffuse solar radiations, i.e. I_g and I_d, are necessary. The total horizontal solar radiation can be obtained from The Hong Kong Observatory. However, data on beam and diffuse solar

radiation are not available. Therefore, a correlation between horizontal diffuse and horizontal total solar radiation is required. A model which based on locally measured data was developed by Yik, Chung and Chan (1995) to simulate the relationship between horizontal diffuse radiation and horizontal total radiation for Hong Kong conditions. The co-relations are as follows:

$$\frac{I_d}{I_g} = 1 - 0.435 \cdot k_T \qquad For\ 0 \le k_T < 0.325 \tag{3.5}$$

$$\frac{I_d}{I_g} = 1.41 - 1.695 \cdot k_T \qquad For\ 0.325 \le k_T \le 0.679 \tag{3.6}$$

$$\frac{I_d}{I_g} = 0.259 \qquad For\ k_T > 0.679 \tag{3.7}$$

The above correlation involves the sky clearness, k_T, which is defined as the ratio of the total horizontal radiation (I_g) to the extraterrestrial radiation (I_0).

3.2.2 Water temperature in preheating solar tank

Based on the principle of energy balance, the water temperature in the unstratified preheating solar tank can be expressed as:

$$\left(\rho C_p V_{st}\right)\frac{dT_{st}}{dt} = q_s - q_{Ls} - q_{stl} \tag{3.8}$$

Combining equations (3.1), (3.2) and (3.3) with (3.8), the energy balance equation of the preheating solar tank can be expressed as:

$$\left(\rho C_p V_{st}\right)\frac{dT_{st}}{dt} = A_c\left[I_T F_R\left(\tau\alpha\right) - F_R U_L\left(T_{st} - T_a\right)\right] - m_L \cdot C_p\left(T_{st} - T_R\right) - U_{st} A_{st}\left(T_{st} - T_a\right) \tag{3.9}$$

The solar fraction of the solar collector loop is defined as:

$$f = \frac{q_s}{m_L C_p\left(T_L - T_R\right)} \times 100\% \tag{3.10}$$

3.3 Compressor Module

In the multi-functional ASHP unit, a rolling piston compressor is adopted. This kind of compressor uses a roller mounted on an eccentric shaft to compress vapor refrigerant entering the compression chamber through the suction inlet (as shown in Figure 3.1). When the rolling piston is in contact with the top of the cylindrical housing, the high pressure and temperature gas is squeezed out through the discharge valve. Rolling piston compressor has a high volumetric efficiency because of the small clearance volume and correspondingly low re-expansion losses inherent in its design. It is therefore used in household refrigerators, air conditioning units or unitary hermetic heat pump.

The compression and expansion processes in the compressor are assumed to be isentropic processes. The oil effects on refrigerant properties and compressor operations are neglected. Besides, it is assumed that the thermal properties of the refrigerant in the compressor are uniform at any time. Based on these assumptions, the lumped-parameter method is employed for the compressor model in view of the high speed of the compression process.

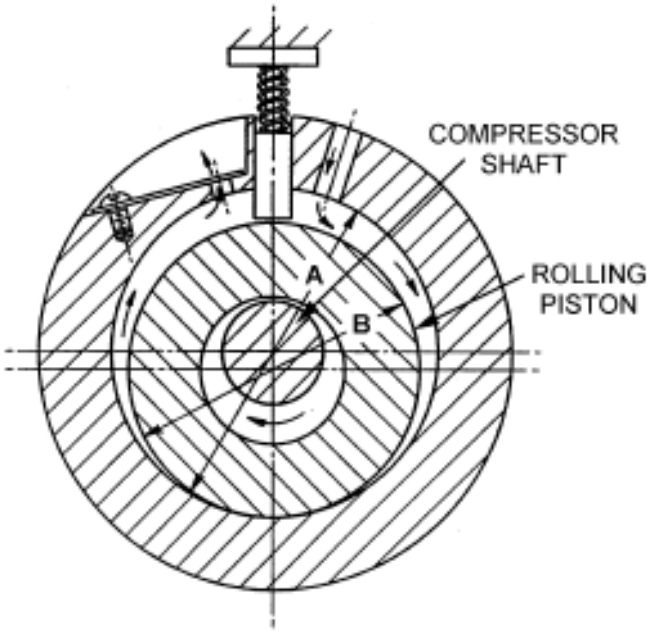

Figure 3.1 A rolling-piston rotary compressor (ASHRAE handbook 2000)

The refrigerant mass flow rate which is critical for the performance of the compressor can be evaluated by:

$$m_r = \lambda \frac{V_{th}}{v_{in}} \tag{3.11}$$

where, m_r = refrigerant mass flow rate, kg/s;

V_{th} = theoretical displacement volumetric flow rate, m^3/s;

v_{in} = specific volume at inlet of the compressor, m^3/kg;

λ = volumetric efficiency, which is given as:

$$\lambda = \lambda_v \cdot \lambda_p \cdot \lambda_T \cdot \lambda_l \tag{3.12}$$

The compressor volumetric efficiency can be estimated (Jordan and Priester, 1948) as:

$$\lambda_v = 1 + c - c\left(\frac{P_{out}}{P_{in}}\right)^{1/n} \tag{3.13}$$

where,

λ_p = pressure loss coefficient with a value of approximately 1 due to the absence of the suction valve;

λ_T = temperature coefficient with a range of 0.82-0.95;

λ_l = leakage coefficient with a range of 0.98-0.92;

c = clearance volumetric ratio of compressor;

n = re-expansion exponent, which is assumed to be isentropic exponent.

The compressor power input can be obtained as:

$$W = m_r \frac{P_{in} v_{in}}{\eta} \frac{n}{n-1}\left[\left(\frac{P_{out}}{P_{in}}\right)^{(n-1)/n} - 1\right] \tag{3.14}$$

where, η is the overall efficiency which should be calculated considering the indicated efficiency, the mechanical efficiency and the motor efficiency.

If the degree of superheating, the condensing and evaporation temperature are known, the refrigerant mass flow rate and the power input together with the inlet and outlet refrigerant thermal properties can be determined by the aforementioned equations.

The refrigerant thermodynamic parameters at the inlet and outlet of the compressor can be calculated based on the simplified model developed by Cleland (1986).

3.4 Evaporator Module

In the past decades, a great deal of research work on the modeling of heat exchangers has been completed in the open literature. Generally, the existing models fall into two broad classifications: zone-based (i.e. lumped-parameter) and distributed-parameter models (Bensafi et al. 1997). In the zone-based model, a heat exchanger is divided into several parts, depending on the number of the phases that the refrigerant exhibits throughout the heat exchanger (vapor, liquid and two-phase). Each zone is treated as a separate heat exchanger (Chi and Didion 1982). Doing in this way, the zone-based models are hardly used to evaluate the detailed variations of the refrigerant along its flow direction because of their oversimplifying assumptions. On the other hand, the distributed-parameter model divides the heat exchanger into a great number of small elements each of which can be solved using local values of thermal properties and heat transfer coefficients. Hence, it is more rigorous and accurate compared with the zone-based method. However, the distributed-parameter method is extremely time-consuming.

Considering the advantages and disadvantages of the aforementioned methods and the complicated structure of the MSA-ASHP system, a zone-based distributed-parameter model is employed here to analyze the performance of the heat exchangers in the MSA-ASHP system.

The evaporator changes as the MSA-ASHP system operates in different modes. In both the AC/WH mode and the only AC mode, the water-to-refrigerant indoor tube-in-

tube heat exchanger is used as the evaporator. When the system operates as the only WH mode, the air-to-refrigerant outdoor finned tube heat exchanger is adopted as the evaporator.

It is assumed that there exist two sections (i.e. the two-phase and superheat sections) in the evaporator. Each section is subdivided into a number of small elements. The lumped-parameter model and the log mean temperature difference (LMTD) are used to solve the heat transfer process in each element. The two working streams are taken as counter flow in both the AC/WH mode and the only AC mode. While in the only WH mode, the two fluids are in concurrent flow. The mathematical models of the two kinds of evaporators are described individually.

3.4.1 Model of the water-to-refrigerant evaporator

For each element, the energy balance between the refrigerant and water can be described by the following equation:

$$m_w c_p (t_{w,in} - t_{w,out}) = \xi_{evp} m_r (h_{r,out} - h_{r,in}) \tag{3.15}$$

where,

m_w = water mass flow rate, kg/s;

c_p = water heat capacity, kJ/(kg.K);

$t_{w,in}$ = inlet water temperature of an element, ℃;

$t_{w,out}$ = outlet water temperature of an element, ℃;

$h_{r,in}$ = inlet refrigerant enthalpy of an element, kJ/kg;

$h_{r,out}$ = outlet refrigerant enthalpy of an element, kJ/kg;

ξ_{evp} = coefficient of heat loss, which varies according to the evaporator configuration and the insulation, usually within a range of 0.8-1.

The heat transfer between the countercurrent flows in a given element can also be calculated by:

$$q_{evp} = U\Delta t_m A \tag{3.16}$$

The LMTD is defined as:

$$\Delta t_m = \frac{\left(t_{w,in} - t_{r,out}\right) - \left(t_{w,out} - t_{r,in}\right)}{\ln\left(\frac{t_{w,in} - t_{r,out}}{t_{w,out} - t_{r,in}}\right)} \tag{3.17}$$

where U is the overall heat transfer coefficient evaluated at the mean properties of the element, which can be calculated by:

$$U = \frac{1}{\frac{1}{\alpha_w} + \frac{d_o}{2k_p}\ln\left(\frac{d_o}{d_{in}}\right) + \frac{d_o}{\alpha_r d_{in}}} \tag{3.18}$$

where,

α_w = water heat transfer coefficient, (W/(m.^{2}K));

α_r = refrigerant heat transfer coefficient, (W/(m^2.K));

k_p = pipe wall thermal conductivity, (W/(m.K));

d_o = the outer diameter of the inner tube (m);

d_{in} = the inner diameter of the inner tube (m).

The water-side heat transfer coefficient (α_w) can be determined by the Dittus-Boelter correlation (Incropera and DeWitt, 1990):

$$\alpha_w = 0.023\,\mathrm{Re}_w^{0.8}\,\mathrm{Pr}_w^{0.4}\,k_w / d_e \cdot \varepsilon_R \tag{3.19}$$

where,

Re_w = the Reynolds number of water;

Pr_w = the Prandtl number of water;

k_w = water thermal conductivity, (W/(m.K));

d_e = equivalent diameter (m);

ε_R = correction factor for the tube rows.

In the superheated refrigerant region, heat transfer is dominated by the forced convective mechanism, which can also be approximately evaluated by the Dittus-Boelter correlation:

$$\alpha_r = 0.023\,\mathrm{Re}_r^{0.8}\,\mathrm{Pr}_r^{0.4}\,k_r / d_{in} \cdot \varepsilon_R \tag{3.20}$$

where, Re_r and Pr_r are the Reynolds and Prandtl numbers of the refrigerant, respectively.

k_r = thermal conductivity of the refrigerant, (W/(m.K)).

The heat transfer in the flow boiling area has been studied for decades. In the literature, there are over 30 saturated flow boiling correlations available. Generally, the flow boiling correlations can be classified into two categories. Under the first category, the correlations are developed by experimental investigators to represent their own data. After ascertaining the accuracy of the experiments conducted, these individual correlations may be used within the same range of parameters. The correlations under the second category are developed based on a larger number of data sets involving a number of fluids over a wide range of parameters. A general correlation proposed by Kandlikar (1990) is used here. This correlation can be widely used in a number of refrigerants, e.g. water, R11, R12, R22, R113, and R114, by incorporating a fluid-dependent parameter F_{fl}. The general correlation is expressed as a sum of the convective and nucleate boiling terms as follows:

$$\alpha_r = [C_1 (C_0)^{C_2} (25 Fr_{lo})^{C_5} + C_3 (B_0)^{C_4} F_{fl}] \alpha_l \qquad (3.21)$$

where,

α_l = single-phase liquid-only heat transfer coefficient, W/(m^2.K);

C_0 = refrigerant convection number;

B_0 = refrigerant boiling number;

Fr_{lo} = Froude number with all flow as liquid;

F_{fl} = fluid-dependent parameter.

Based on the energy balance of each element, the heat transfer area of a certain element under given conditions can be calculated as:

$$A_i = \frac{m_r \left(h_{r,out} - h_{r,in} \right)}{U \Delta t_m} \tag{3.22}$$

Thus, the total calculated area of the evaporator is a sum of areas of all the elements.

$$A_{evp,cal} = \sum A_i \tag{3.23}$$

3.4.2 Model of the air-to-refrigerant evaporator

The heat transfer on the air side of each element is expressed as:

$$\begin{aligned} q_a &= m_a \left(h_{a,in} - h_{a,out} \right) \\ &= \xi \alpha_{os} A_o (t_{am} - t_{wall}) \end{aligned} \tag{3.24}$$

The sensible heat transfer coefficient α_{os} is calculated as (Li et al., 1997):

$$\alpha_{os} = 0.982 \, Re_a^{0.424} \left(\frac{s1}{d_b} \right)^{-0.0887} \left(\frac{N \cdot s2}{d_b} \right)^{-0.159} \frac{k_a}{d_b} \tag{3.25}$$

where,

m_a = air mass flow rate, kg/s;

$h_{a,in}$ = inlet air enthalpy of an element, kJ/kg;

$h_{a,out}$ = outlet air enthalpy of an element, kJ/kg;

α_{os} = sensible heat transfer coefficient, W/(m^2.K);

A_o = surface area of outer tube, m^2;

t_{am} = average air temperature, ℃;

t_{wall} = temperature of tube wall, ℃;

ξ = coefficient of heat loss, within a range of 0.8-1;

Re_a = the Reynolds number of air;

sl = distance between fins, m;

$s2$ = distance between tubes in air flow direction, m;

d_b = diameter of the bottom finned tube, m;

N = number of tube column;

k_a = thermal conductivity of air, W/(m.K).

For the calculation of the heat transfer coefficient on refrigerant side, the same equations are adopted as those for the water-to-refrigerant evaporator.

3.4.3 Pressure drop prediction

In order to simplify the simulation procedure, the pressure drop in a single-phase section is negligible owing to its relatively short length. For each element, the pressure drop in a two-phase section can be estimated using the following equation (Ding and Zhang, 2001):

$$\Delta P = \frac{4L \cdot f \cdot Gr^2}{\rho_{in} d_{in}} + Gr^2 \left(\frac{1}{\rho_{out}} - \frac{1}{\rho_{in}} \right) \tag{3.26}$$

where,

L = length of an element, m;

f = fraction factor;

ρ_{in} = inlet refrigerant density, kg/m^3;

ρ_{out} = outlet refrigerant density, kg/m^3;

Gr = refrigerant mass flow rate per unit area, (kg/(m^2.s)).

3.4.4 Simulation algorithm

Based on the aforementioned equations, an iterative method is established to determine the outlet states of the water or air together with refrigerant in the evaporator for the given operating conditions.

For the modeling process, the input parameters include the detailed evaporator configuration, the water or air inlet temperature and flow rate, the inlet state of the refrigerant and its flow rate. The constraint condition of the model is that the calculated heat transfer area of the evaporator should equal the actual physical area. The detailed simulation procedure is summarized as follows.

1) Input the inlet variables of the two working fluids and assume the refrigerant outlet enthalpy and evaporation pressure drop.
2) Determine the two-phase and superheat regions respectively and divide them into a number of small elements.
3) Calculate the intermediate and outlet temperatures of the two working fluids.

4) Calculate the LMTD, the heat transfer coefficient of each working stream and the overall heat transfer coefficient.
5) Calculate the required heat transfer area corresponding to the heat transfer rate in each element.
6) Calculate the total pressure drop of the refrigerant in evaporator.
7) Update the guessed pressure drop until the difference between the calculated value and the guessed is within the acceptable error.
8) Determine the total required heat transfer area of the evaporator.
9) Update the guessed refrigerant outlet enthalpy and repeat steps above until the calculated area converges to the actual area within an allowable error.
10) Calculate the refrigerant mass in the evaporator.

3.5 Desuperheater Module

The desuperheater installed in the heat pump unit is for recovering the thermal energy at temperatures substantially above the condensing temperature (superheated vapor). Accordingly, the heat pollution to the ambient air is reduced. In the MSA-ASHP system, the desuperheater and the condenser are connected in series. In this way, the desuperheater is able to absorb all or part condensation heat to heat hot water. Actually, the desuperheater has the similar operating principle with the condenser.

In actual operation, the desuperheater cools the superheated vapor and condense part of the saturated refrigerant. Accordingly, the refrigerant in the desuperheater may have two states (superheat and two-phase) or one state (superheat) depending on its outlet

enthalpy. The steady state zone-based distributed-parameter method together with the LMTD method used in the evaporator model is also applied in the models of the desuperheater and condenser.

3.5.1 Calculation of heat transfer coefficient

The heat transfer coefficients of the water side and the superheated refrigerant region have the same characteristics and formulas as those of the water-to-refrigerant evaporator. As for the condensation heat transfer coefficient of the refrigerant side, an empirical correlation is given by Wu (1997):

$$h_r = 0.725 B_r d_{in}^{-0.25} (T_c - T_{wo})^{-0.25} \tag{3.27}$$

where, B_r is the integrated refrigerant thermophysical property related to the condensing temperature T_c; T_{wo} is the inner tube wall temperature, which can be calculated through the Newton iteration method.

3.5.2 Simulation algorithm

The simulation algorithm of the desuperheater is quite similar with that for the evaporator.

Firstly, the outlet enthalpy of the refrigerant is assumed. Based on this assumption, the desuperheater can be divided into one or two heat transfer zones. Each section is subdivided into several elements with equal enthalpy change or equal temperature change. Then, the heat transfer area can be calculated. Based on the iteration procedure,

finally, the appropriate value of the refrigerant enthalpy will be found. The detailed simulation flow chart is shown in Figure 3.2.

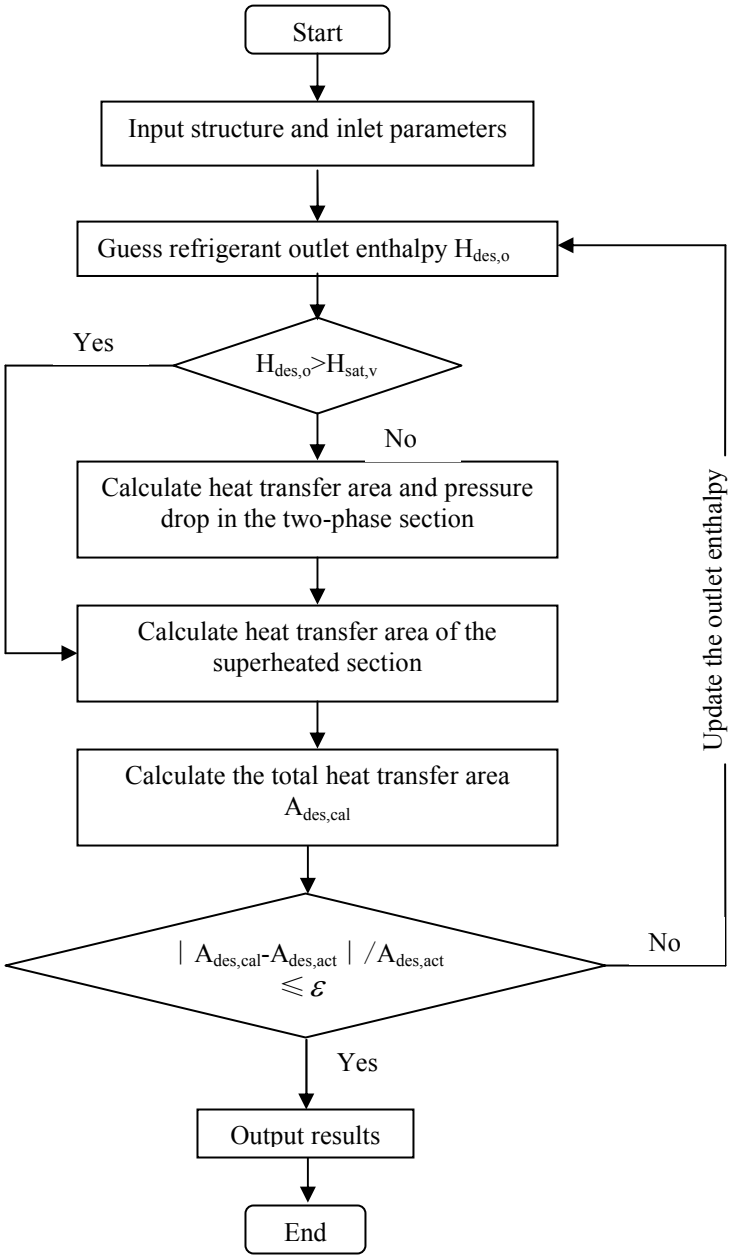

Figure 3.2 Flow chart for the simulation of the desuperheater

3.6 Condenser Module

Different heat exchangers work as the condenser when the MSA-ASHP system operates in different modes. In the AC/WH mode, the outdoor air-to-refrigerant finned-tube heat exchanger works as condenser while in the only WH mode, the water-to-refrigerant heat exchanger, which is the desuperheater in the AC/WH mode, becomes the condenser.

3.6.1 Calculation of heat transfer coefficient

In the condensation process, on the refrigerant side, there exist three possible heat transfer modes, i.e. superheated, two-phase and sub-cooled sections. The heat transfer coefficients in both the two-phase and the superheat regions can be estimated using the correlations employed in the desuperheater. For the sub-cooled area, the heat transfer coefficient of refrigerant is calculated in the same way as that used for the superheated refrigerant vapor.

For the air-to-refrigerant condenser, the air-side heat transfer coefficient is evaluated using the same method as that for the air-to-refrigerant evaporator. As for the water-side heat transfer coefficient of the water-to-refrigerant condenser, the same equation is employed as that for the water-to-refrigerant evaporator.

3.6.2 Simulation algorithm

During the simulation process of the condenser, firstly, the outlet refrigerant enthalpy should be assumed based on the flow pattern of working fluids. Besides, the pressure drop of the two-phase section should be guessed. The existing heat transfer

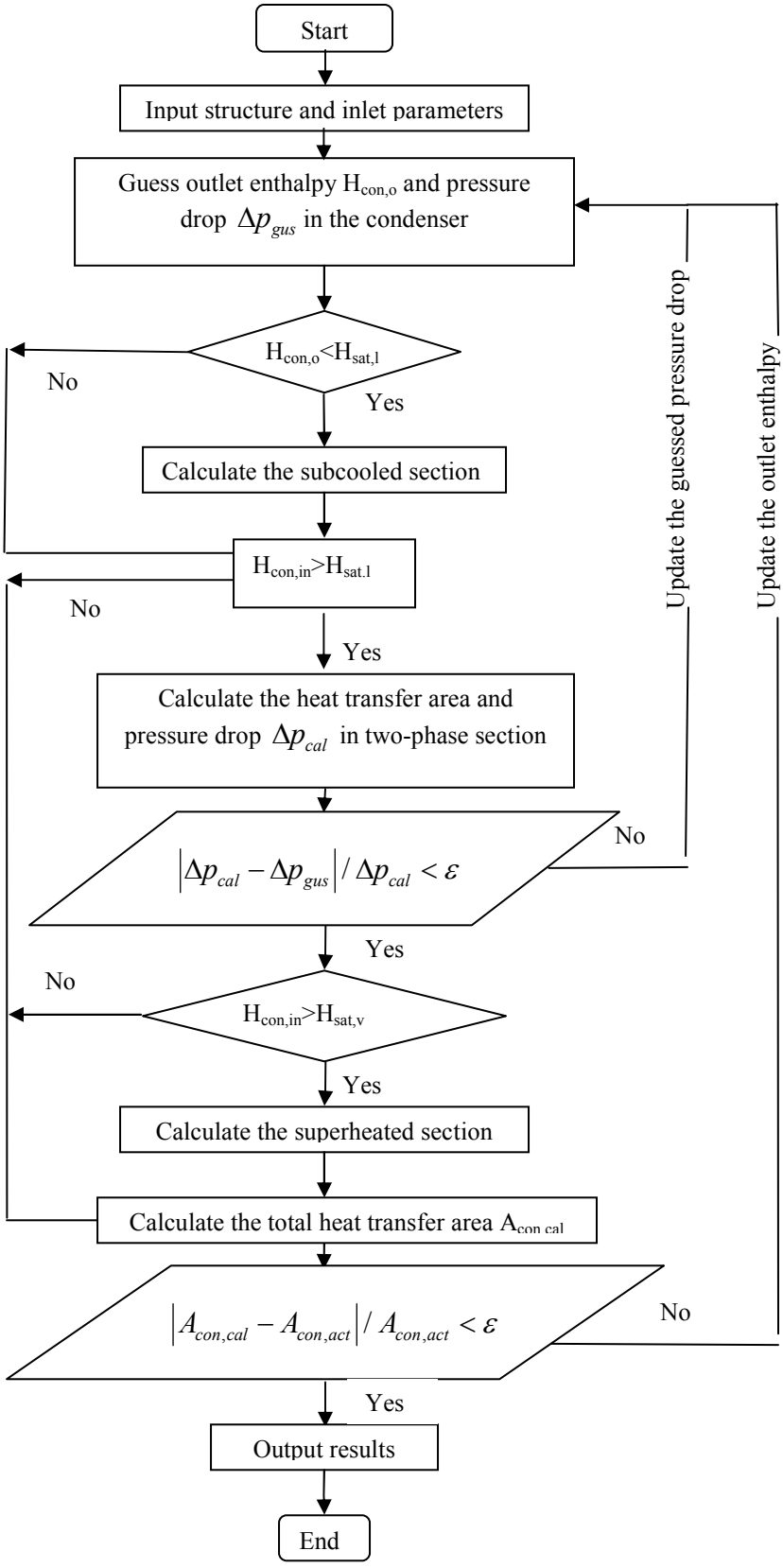

Figure 3.3 Flow chart for the simulation process of condenser

modes will be determined according to the outlet refrigerant enthalpy. Consequently, the total heat transfer area and the pressure drop can be calculated using the chosen formulas and given parameters. At last, based on the iteration process, the suitable value of the outlet refrigerant enthalpy and the corresponding pressure drop will be found. The flow chart for the whole simulation process is indicated in Figure 3.3.

3.7 Thermostatic Expansion Valve

In this research, a thermostatic expansion valve (TEV) is employed which is used to modify the flow of liquid refrigerant entering the evaporator. For simplicity, a constant degree of superheating and the refrigerant mass flow rate obtained in the compressor are directly used in the thermostatic expansion valve model. The thermal process in the expansion device is assumed to be adiabatic. Therefore, the following relationship can be used from the first law of thermodynamics:

$$H_{con,o} = H_{evp,in} \tag{3.28}$$

where $H_{con,o}$ is the outlet refrigerant enthalpy of the condenser and $H_{evp,in}$ represents the inlet refrigerant enthalpy of the evaporator.

3.8 Modeling of the Multi-functional ASHP Unit

With the above detailed mathematical models of each component of the MSA-ASHP system, based on the principles of the energy balance, the refrigerant mass balance and the pressure balance, the systematic model for the whole MSA-ASHP system is obtained.

The corresponding simulation algorithm is described and illustrated in the following section.

3.8.1 Refrigerant mass balance

Based on the principle of mass balance, the system refrigerant mass balance is expressed by the following equation:

$$M_{char} = M_{con} + M_{evp} + M_{com} + M_{des} + M_{pipe} \tag{3.29}$$

The refrigerant mass in the compressor can be calculated as:

$$M_{com} = \lambda V_{th} \rho_m \tag{3.30}$$

The detailed calculation procedure of the refrigerant mass with different phases is introduced in the following subsections.

3.8.1.1 Single-phase refrigerant mass

The refrigerant mass in a single-phase zone can be estimated by the mean density and internal volume.

For the subcooled zone,

$$M_{sub} = \int_0^{L_{sub}} A_{in} \rho_l dx \tag{3.31}$$

For the superheated zone,

$$M_{sup} = \int_{0}^{L_{sup}} A_{in}\rho_v dx \tag{3.32}$$

where, M is the refrigerant mass in the corresponding zone, kg; L is the length of the section; ρ is the refrigerant density, kg/m^3.

3.8.1.2 Two-phase refrigerant mass

In the two-phase zone, the mean density is estimated by the saturated liquid density, the saturated vapor density and the void fraction (ε_v) which is defined as the ratio of the cross-sectional area occupied by vapor to the total cross-sectional area.

The modified coefficient X_{tt} is employed for the calculation of the void fraction (Wallis; Domanski and Didion).

$$\begin{cases} \varepsilon_v = \left(1 + X_{tt}^{0.8}\right)^{-0.378} & \left(X_{tt} \le 10\right) \\ \varepsilon_v = 0.823 - 0.157 \ln X_{tt} & \left(X_{tt} > 10\right) \end{cases} \tag{3.33}$$

where X_{tt} is the square root ratio of the liquid-only pressure gradient to the vapor-only pressure gradient, which is calculated using the following equation (Lockhar and Martinelli, 1949):

$$X_{tt} = \left(\frac{1-x}{x}\right)^{0.9} \left[\left(\frac{\mu_l}{\mu_v}\right)^{0.2} \cdot \frac{\rho_v}{\rho_l}\right]^{0.5} \tag{3.34}$$

Based on the definition of the void fraction, the two-phase refrigerant mass can be consequently calculated through the following equation:

$$M_{tp} = \int_0^{L_{tp}} A\left[\left(1-\varepsilon_v\right)\rho_l + \varepsilon_v \rho_v\right] dx \tag{3.35}$$

where, M_{tp} is the two-phase refrigerant mass, kg; L_{tp} is the length of the two-phase zone, m.

3.8.2 Energy balance and definition of system performance

For the multi-functional ASHP unit under considered, according to the first-law thermodynamic, the amount of energy absorbed by the refrigerant in the evaporator and compressor theoretically equals the energy released from the refrigerant in the condenser and the desuperheater when the system operates in the AC/WH mode. Based on this theory, the energy balance can be given as follows：

$$Q_{des} + Q_{con} = W + Q_{evp} \tag{3.36}$$

where, Q_{des} = the heat absorbed by the water in the desuperheater, W;

Q_{con} = the heat released to the condenser, W;

W = the power consumption of the compressor, W;

Q_{evp} = the heat transfer rate in the evaporator, W.

The energy performance of a heat pump system can be evaluated by its coefficient of performance (COP), which can be defined according to its specific applications.

In the AC/WH mode and the only AC mode, the COP for air conditioning is given by:

$$COP_{AC} = \frac{Q_{evp}}{W} \tag{3.37}$$

and the overall COP is given by taking into account the free production of hot water in the desuperheater.

$$COP_{AC/WH} = \frac{Q_{evp} + Q_{des}}{W} \tag{3.38}$$

When the proposed system operates in the only WH mode, the definition of COP is expressed as:

$$COP_{WH} = \frac{Q_{con}}{W} \tag{3.39}$$

3.8.3 Simulation algorithm

It is known that the thermodynamic cycle of the heat pump is a closed loop, which makes it convenient to incorporate the component modules of the multi-functional ASHP unit into an overall systematic model. As shown in Figure 1.4, the solar collector loop and multi-functional ASHP system are connected by the storage tank. In this way, the hot water produced by the solar collector loop is supplied to the desuperheater or condenser of the multi-functional ASHP system. Therefore, the module of the solar

collector loop can be easily coupled together with the model for the multi-functional ASHP unit to get the entire systematic model for the whole MSA-ASHP system.

Using the mathematical model of the MSA-ASHP system, firstly, the states of the refrigerant, the outlet hot water properties and the discharged air states will be determined. The operating performance in different operating modes is then evaluated under the pre-specified working conditions.

For the simulation procedure of the heat pump unit, there are various control strategies. At present, controlling superheat degree is the most commonly used method (Krakow and Lin, 1987). In this research, this kind of control method is adopted here. The complete simulation procedure for the whole MSA-ASHP system is illustrated in Figure 3.4.

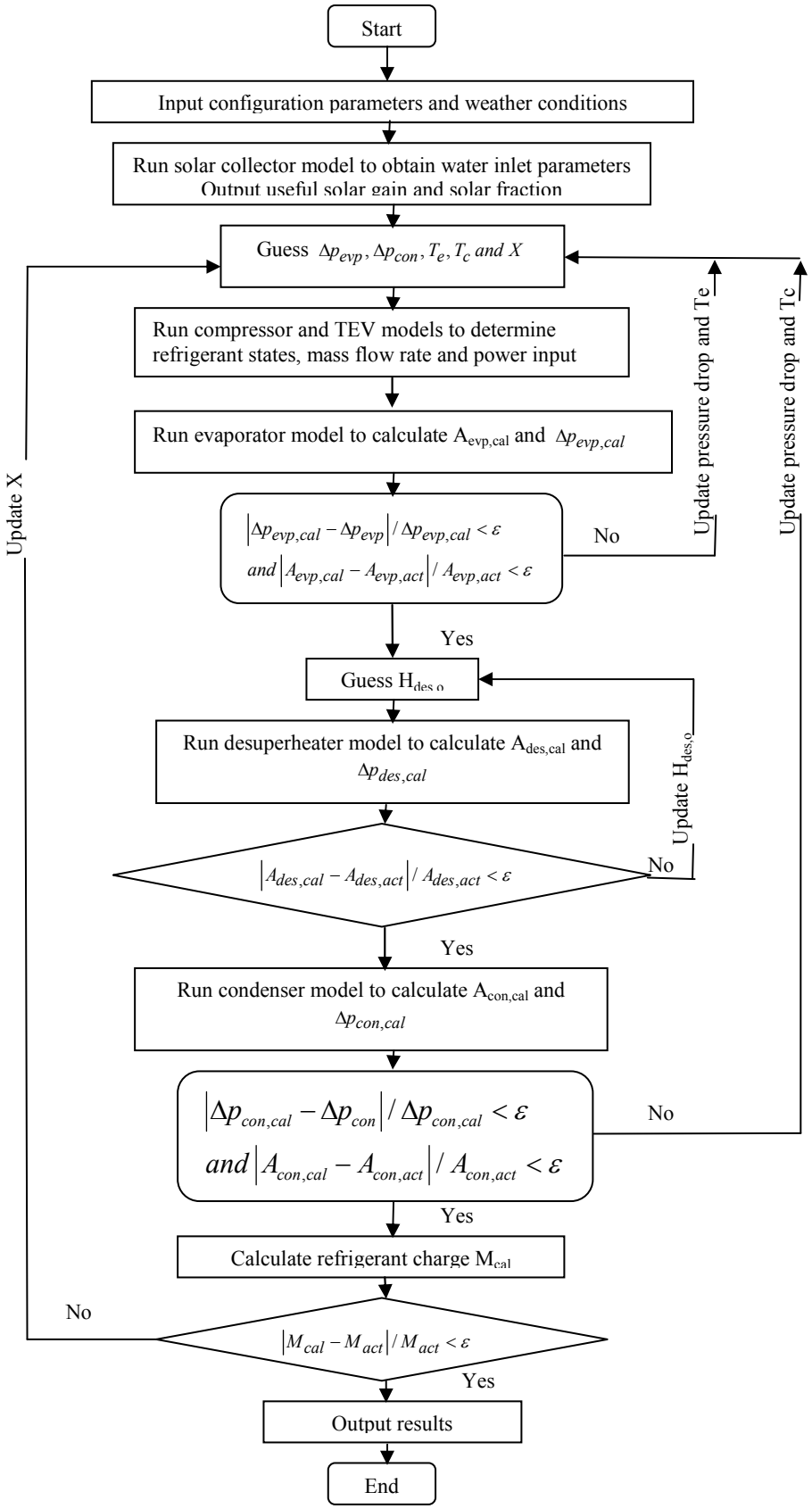

Figure 3.4 Flow chart of complete simulation for the MSA-ASHP system

3.9 Discussion on the Simulation Results

In this research, the simulation calculation is implemented by using FORTRAN language owing to its distinct advantage of the high speed of scientific computing over other compiling languages. Based on the simulation program, the system performance under various operating modes is discussed in this section. It should be noted that the space heating mode will not be discussed here since the operating principle and system performance are generally similar to those of the only WH mode. Besides, the possibility of operating in the space heating mode is quite little in cooling-dominated buildings in subtropical areas. Therefore, this section mainly focuses on three operating modes, i.e. the AC/WH mode, the only AC mode and the only WH mode.

The sample system built for the experimental validation in Chapter 4 is selected to be the basic case for the following analyses. The basic parameters in the simulation model including the structure parameters and installation specifications are shown in Table 4.2.

3.9.1 Performance of the solar collector loop

The measured horizontal solar radiation during one day (i.e. June 20th in 2009) of the experimental period is shown in Figure 3.5. Based on the mathematical model of the solar collector loop and the measured data, the hourly water temperature in the preheating solar tank and the solar fraction are found. The results are shown in Figure 3.6 and Figure 3.7.

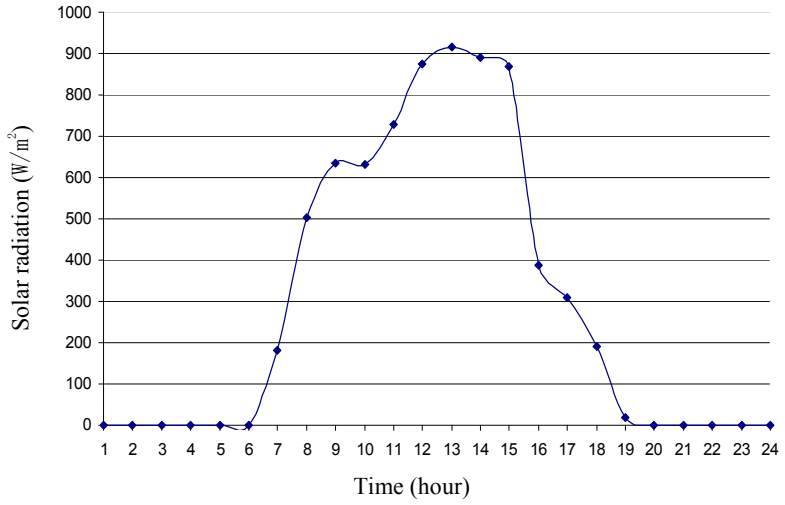

Figure 3.5 Measured hourly horizontal solar radiation

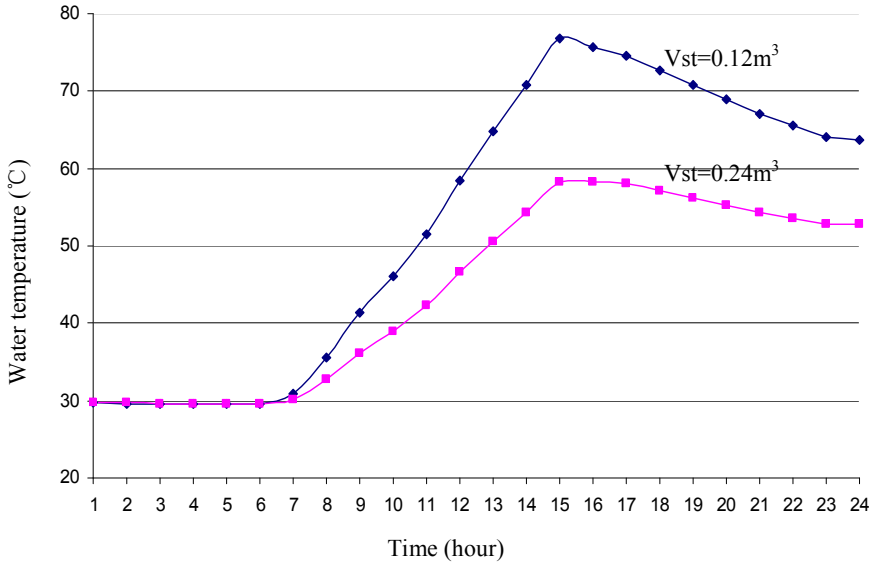

Figure 3.6 Hourly water temperature of preheating solar tank

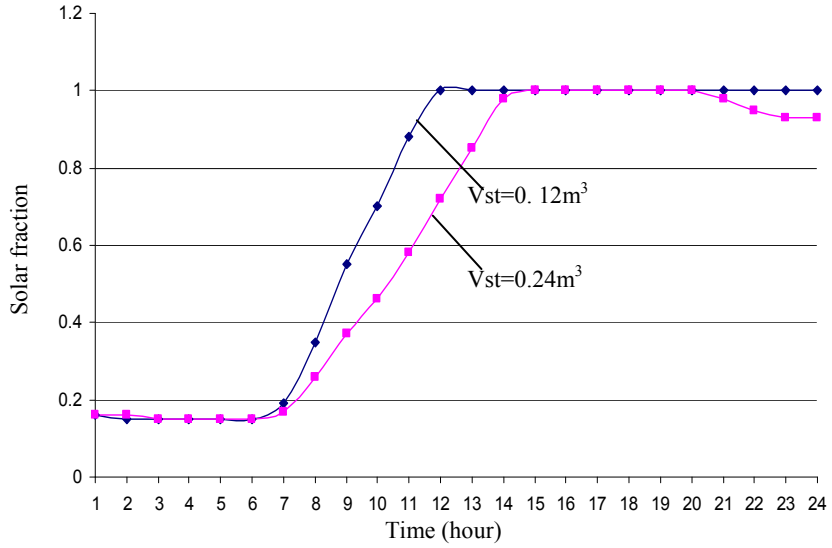

Figure 3.7 Hourly solar fraction on June 20th

It can be found that solar radiation has obvious effect on the water temperature and solar fraction especially when solar radiation gradually becomes stronger throughout a day. It can also be seen that a larger volume of the preheating solar tank results in a relatively lower water temperature and a smaller solar fraction. With a tank volume of $0.12m^3$, the required hot water temperature can be reached at 12:00; when the $0.24m^3$ tank is used, the water can be heated to the required level until 14:00.

3.9.2 Performance of the Multi-functional ASHP Unit

The system operating performance of the multi-functional ASHP unit under various working modes is discussed as follows. Prior to the analyses, the related operating parameters of the system are set as shown in Table 3.1.

Table 3.1 Operating parameters of the multi-functional ASHP unit

Parameter	Value
Air flow rate in condenser	0.25m^3/s
Water flow rate in evaporator	0.28kg/s
Water flow rate in desuperheater	0.28kg/s
Chilled water return temperature	12.5℃

3.9.2.1 Performance in the AC/WH mode

When the system operates in the AC/WH mode, it can supply both air conditioning load and hot water heating load. Depending on the specific requirement of the customer, the condensing heat could be absorbed partly or completely by the desuperheater to heat hot water. In this research, both conditions are considered.

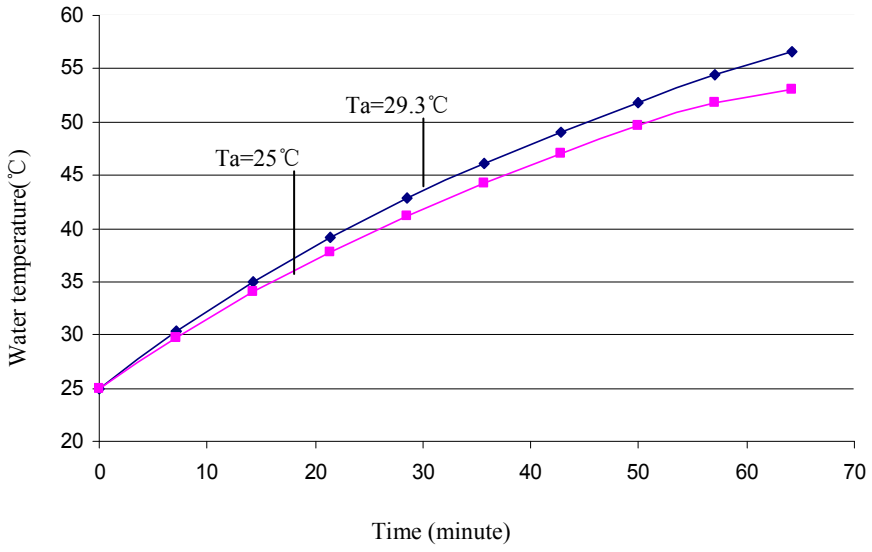

Figure 3.8 Outlet water temperature of desuperheater

The changing characteristic of the outlet water temperature from the desuperheater is indicated in Figure 3.8. It can be observed that the water temperature tends to rise rapidly at higher ambient temperature, which shows that the water heating capacity of the multi-functional heat pump will be higher under warmer ambient conditions. When the system operates in the AC/WH mode, a higher ambient air temperature leads to a smaller temperature difference between the air and the refrigerant, which decreases the heat dissipation of the outdoor air-to-refrigerant condenser. Therefore, the condensation heat discharged to hot water becomes larger and a higher water heating capacity is obtained.

In addition, it can be found that the increasing rate of water temperature decelerates throughout the heating period. At the same time, the water heating capacity drops significantly at an elevated water temperature as shown in Figure 3.9 and with operating time as shown in Figure 3.10. The reason is that the raised water temperature leads to higher condenser or desuperheater working temperatures and pressures as shown in Figure 3.11, which increases the outlet temperature of the compressor (Figure 3.12) so that more power input is consumed by the compressor (Figure 3.13) and the heat transfer rate of the condenser or the desuperheater deteriorates. As a result, the thermal performance of the system declines (Figure 3.14).

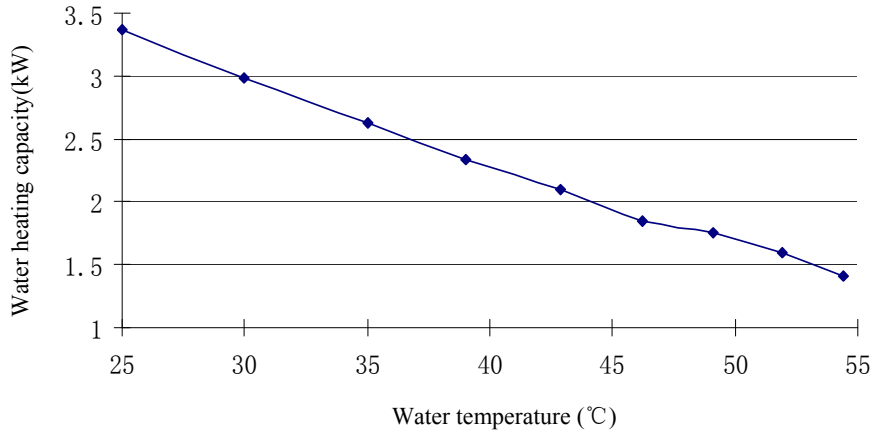

Figure 3.9 Effect of water temperature on water heating capacity

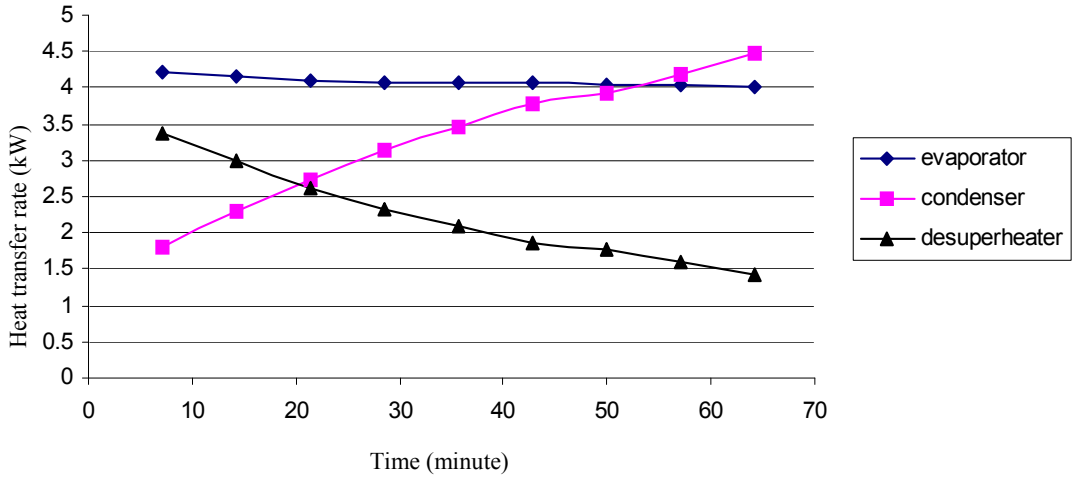

Figure 3.10 Heat transfer rates in the AC/WH mode

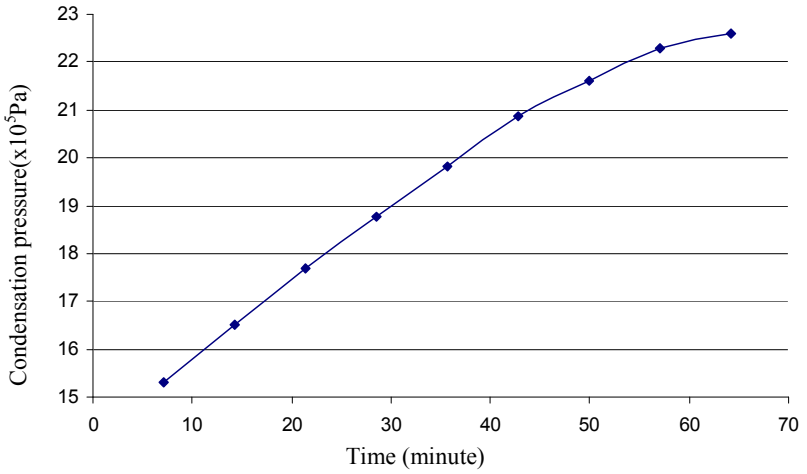

Figure 3.11 Condensation pressure in the AC/WH mode

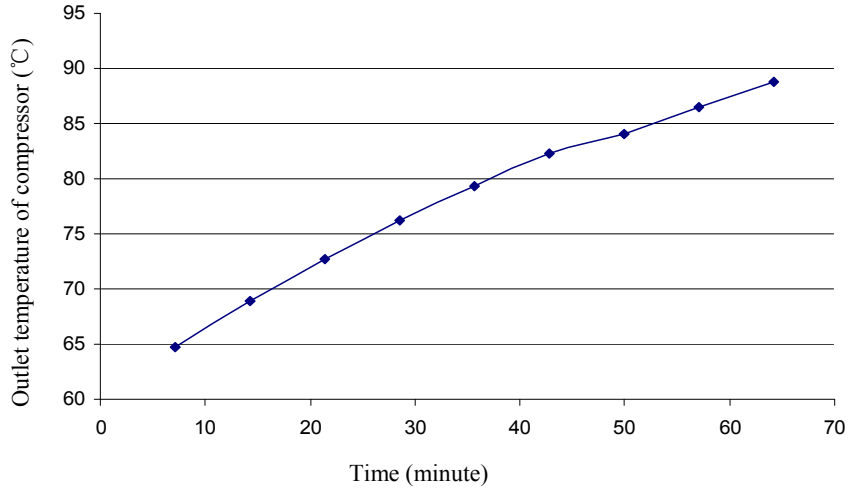

Figure 3.12 Outlet temperature of compressor in AC/WH mode

Figure 3.13 shows that the system performance is greatly improved when taking into account the free production of hot water. On an average basis, the $COP_{AC/WH}$ is 36.2% greater than the COP_{AC}. Furthermore, the $COP_{AC/WH}$ is 4.7% larger than the COP_{WH} when ambient air temperatures are 29.3℃ and 17.2℃, respectively. The results show that the $COP_{AC/WH}$ ranges from 3.3 to 6.37. Compared with a conventional air

conditioner, which has a COP around 2.4, the proposed system gives much better performance.

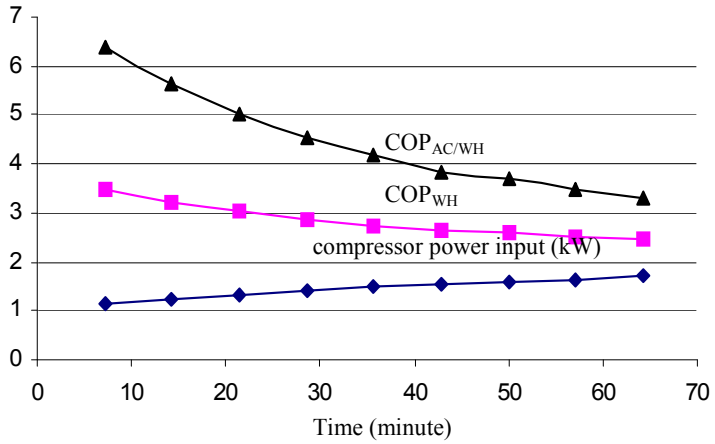

Figure 3.13 Thermal performance in the AC/WH mode

From Figure 3.14, it can also be found that the overall system performance (i.e. $COP_{AC/WH}$) is better when the ambient air temperature is relatively lower.

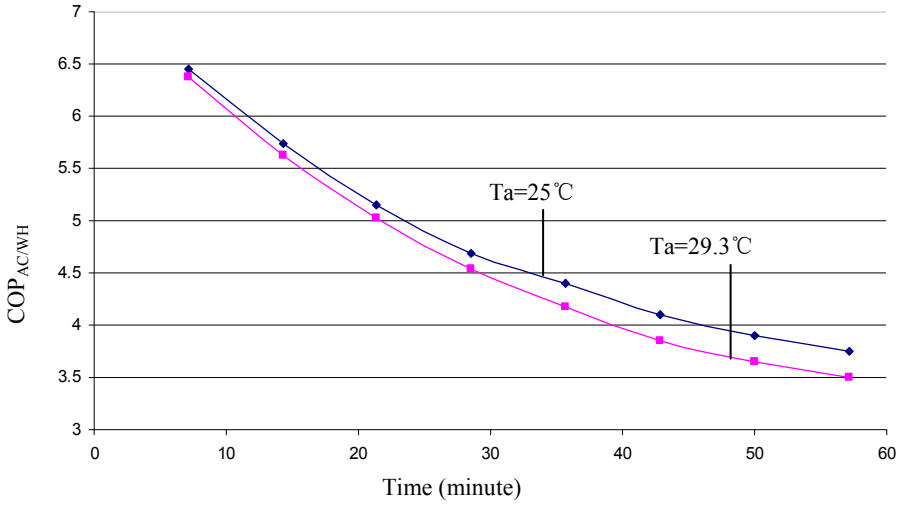

Figure 3.14 Effect of air temperature in AC/WH mode

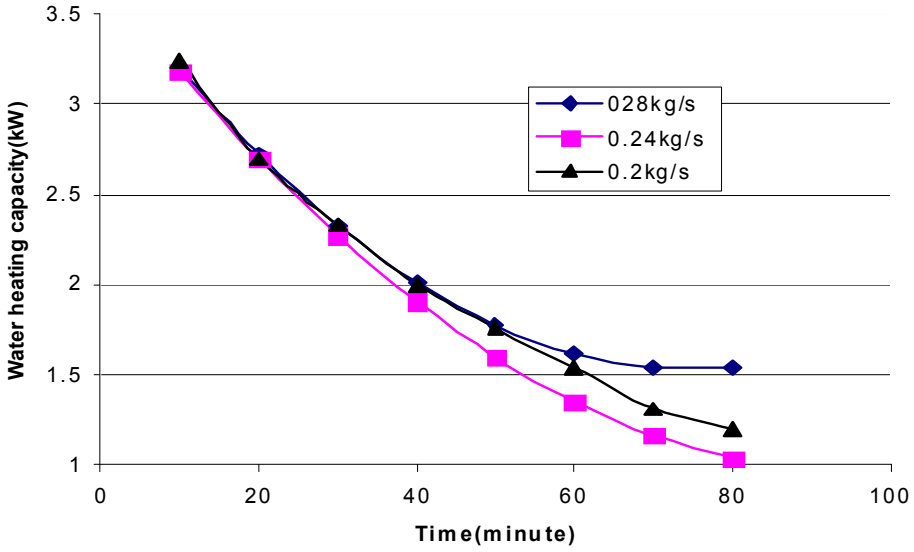

Figure 3.15 Effect of flow rate on water heating capacity in AC/WH mode

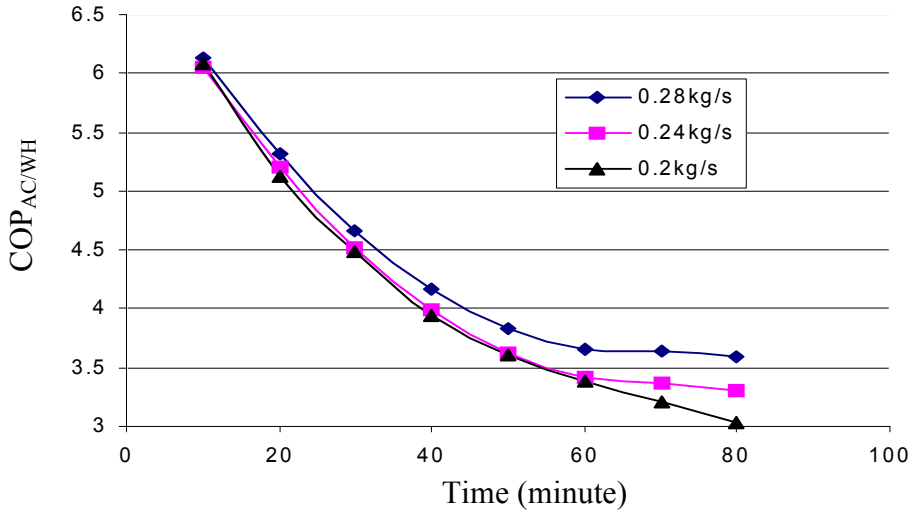

Figure 3.16 Effect of flow rate on system performance

The impact of the circulation flow rate from the storage tank to the desuperheater is shown in Figures 3.15 and 3.16. It can be found that, with the higher flow rate, a greater $COP_{AC/WH}$ is obtained. However, in this study, the power input consumed by the water pump is not considered. Therefore, it is not good for the improvement of the system thermal performance to increase the flow rate randomly. For the water heating capacity,

with the growth of the flow rate, it does not increase consistently, which further verifies that a larger flow rate is not always good for the thermal performance of the studied system. In other words, there exists an optimum flow rate for a specific system.

The inlet water temperature of the desuperheater is significantly critical for the system performance, especially in the AC/WH mode. The effects of the inlet water temperature of the desuperheater on the operating performance are analyzed and shown in Figures 3.17 and 3.18. From Figure 3.17, it is clear that, whereas the heat transfer rate of the desuperheater and the evaporator decreased, the power consumption of the compressor increased as the growth of the inlet water temperature of the desuperheater. It is caused by the rising desuperheater working temperatures and pressures which lead to the increasing outlet temperature of the compressor. Under such operating condition, more power is consumed by the compressor while the heat transfer rate of the evaporator and the desuperheater is reduced. Finally, the energy performance of the studied system declined as shown in Figure 3.18.

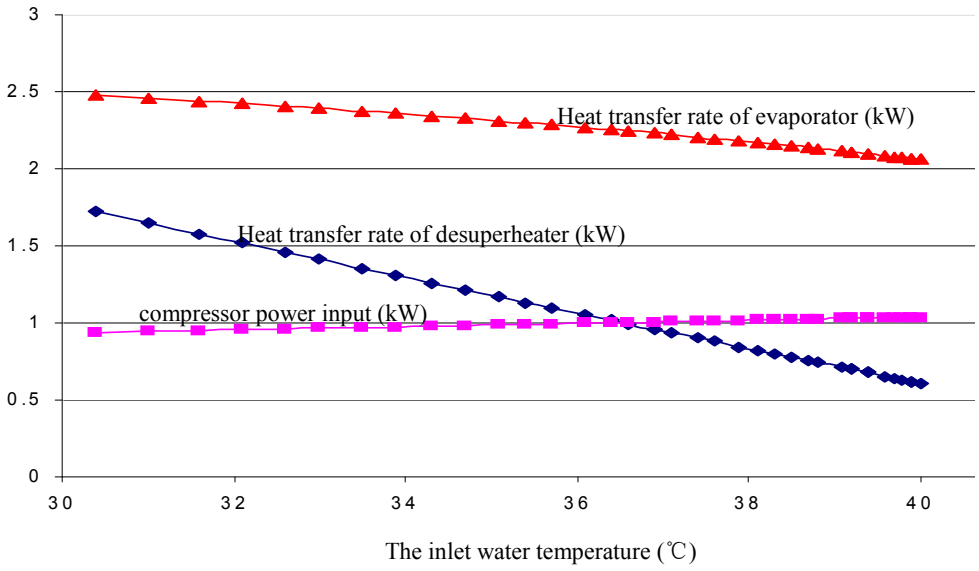

Figure 3.17 Effect of the inlet water temperature on system performance

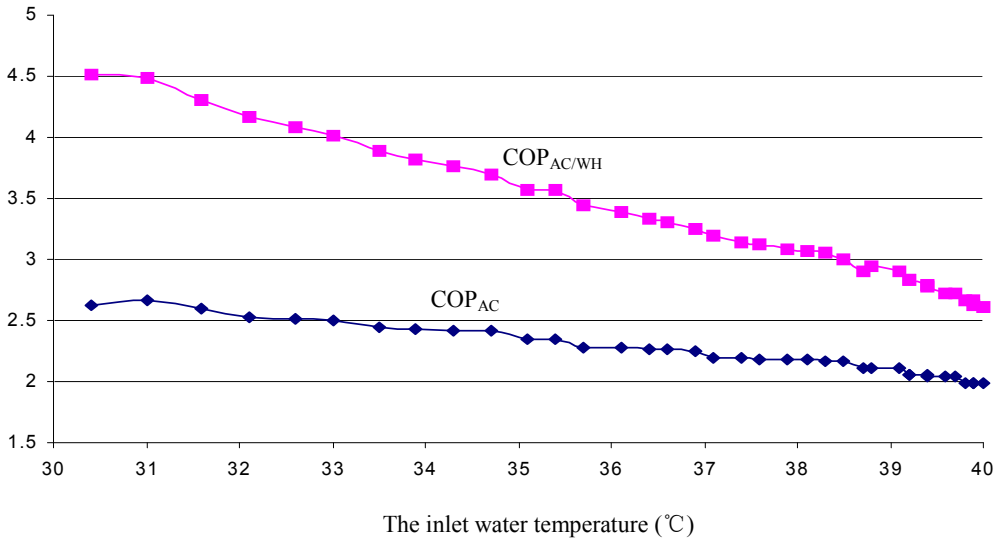

Figure 3.18 Effect of the inlet water temperature on energy performance

3.9.2.2 Performance in the only AC mode

When the proposed system works in the only AC mode, the operating principle is the same as a conventional air conditioner which is widely used in Hong Kong. Thus, a simple analysis of the operating performance is conducted here. When the ambient air temperature is around 27.6℃, the system performance is shown in Figure 3.19. It is clear that the COP value increases obviously during the early operating period. After a few minutes, the system operates with a relative steady COP (around 2.6) which is comparative with conventional air conditioners.

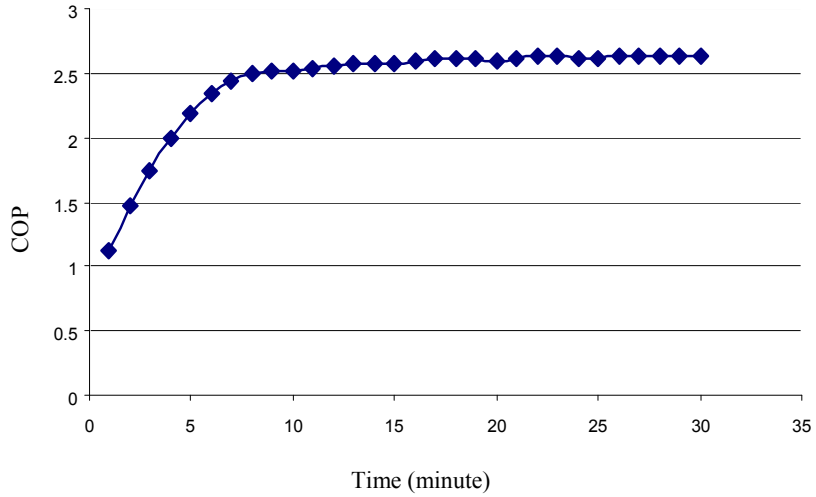

Figure 3.19 System performance in the only AC mode

3.9.2.3 Performance in the only WH mode

In moderate climatic conditions, the multi-functional ASHP system will operate in the only WH mode. Under this operating mode, it works in the same way as an air source heat pump water heater.

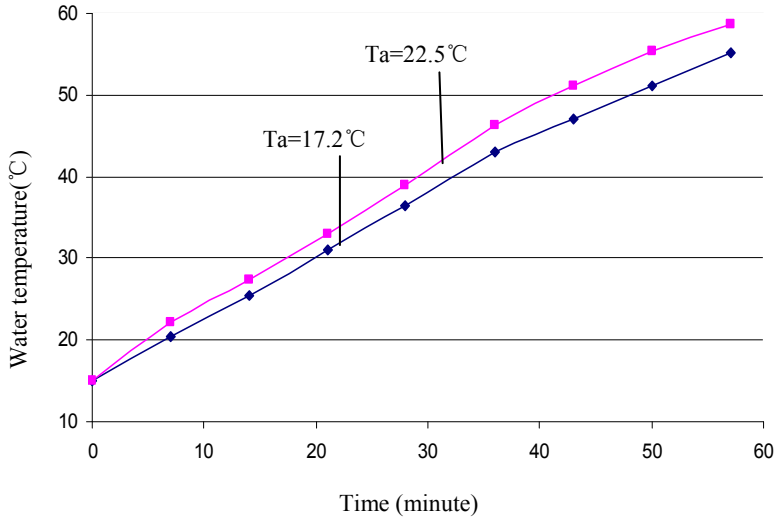

Figure 3.20 Outlet water temperature of condenser in only WH mode

From Figure 3.20, it can be found the same increasing trend of the outlet water temperature appears as that in the AC/WH mode. Also, the increasing rate decreases during the operating period. As mentioned above, when the system works in the only WH mode it has the same working principle with that of an ASHP water heater so that a relative high ambient air temperature can improve its water heating capacity. Moreover, the system performance COP_{WH} (see Figure 3.21) is also improved under the higher ambient air temperature.

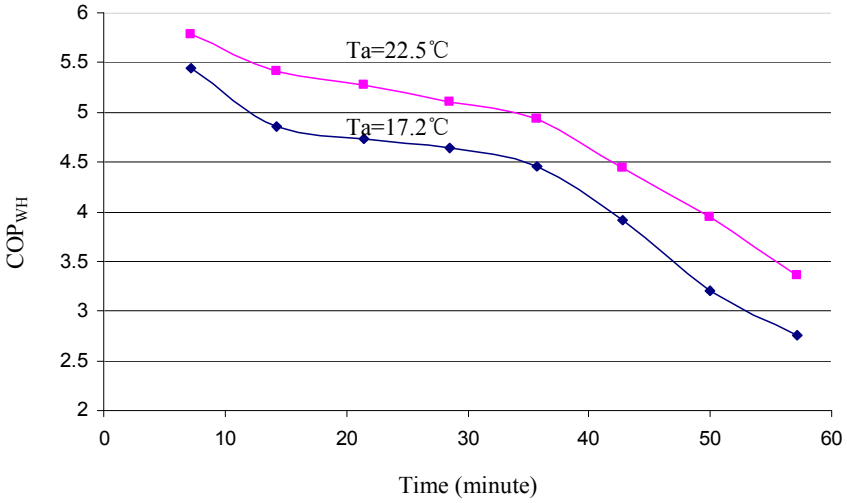

Figure 3.21 Effect of air temperature in only WH mode

3.10 Summary

The proposed novel MSA-ASHP system, which can operate in three modes, i.e. the AC/WH mode, the only AC mode and the only WH mode, is simulated in detail in this chapter. Firstly, The simulation model of each component is developed for both the solar collector loop and the multi-functional ASHP unit. Based on the basic principles of the energy balance, mass balance and pressure balance and the connection relationship

between two main circuits of the MSA-ASHP system, a comprehensive system model is obtained through coupling all the component models. And the corresponding program which is written in FORTRAN language is developed. Finally, the operating performance of the proposed system is analyzed and discussed in different working modes under weather conditions in Hong Kong.

The simulation results show that the water temperature in the preheating solar tank and the solar fraction are both heavily influenced by the solar radiation, and the volume of the storage tank. A larger volume of the preheating solar tank results in a relatively lower water temperature a smaller solar fraction, and longer heating time to obtain the required level.

Furthermore, it can be observed that this kind of SAHP system can provide a much better system performance than the traditional air conditioner and the ASHP water heater. The $COP_{AC/WH}$ of the multi-functional ASHP system ranges from 3.3 to 6.37, 36.2% larger than that when only air conditioning load is considered and 4.7% larger than that of the only WH mode. Under warmer ambient conditions, the water heating capacity of the multi-functional heat pump will be higher both in the AC/WH mode and in the only WH mode. With increase of the ambient air temperature, the COP_{WH} increases while $COP_{AC/WH}$ decreases. In addition, the analysis about the impact of the flow rate shows that a larger flow rate can not ensure a better system performance for the studied system, and an optimum flow rate should be found for a specific system.

It can be concluded that the developed systematic model of the MSA-ASHP system is useful and effective in analyzing its system performance in all kinds of operating

modes. Moreover, it can be used to design a MSA-ASHP system with high system performance by finding the appropriate match relationship among components.

CHAPTER 4 EXPERIMENTAL STUDY ON MSA-ASHP SYSTEM

4.1 Introduction

A prototype MSA-ASHP system was built to provide air conditioning service and domestic hot water on the campus of The Hong Kong Polytechnic University. The primary purposes of the sample system are to investigate the operating characteristics of the proposed system under subtropical weather conditions and to validate the developed simulation of the MSA-ASHP system.

In this chapter, firstly the test setup for the solar collector efficiency is described. The prototype multi-functional ASHP system is then presented, which is followed by describing the experimental device and data collection system. The uncertainty analysis is also investigated in terms of the measuring devices and the data acquisition system. The fitting curve of the solar collector efficiency is derived based on corresponding experimental data. Finally, a series of tests are conducted in order to find the appropriate control strategies for the MSA-ASHP system.

4.2 Test Setup for Solar Collector Efficiency

The solar collector is one of the most important components of the MSA-ASHP system and it plays a significant role in determining the system operating performance. In this research, the relatively cheap and commonly used flat plate solar collector is used in order to cut the initial cost of the proposed system. The detailed characteristic

parameters of the selected solar collector are shown in Table 7.3. In order to ensure the thermal performance of the proposed system, it is necessary to conduct an efficiency test of the selected solar collector. Accordingly, the efficiency curve of the solar collector can be obtained based on recorded experimental data.

A solar simulator with a 3-phase lamp array is employed to imitate necessary solar irradiation in the tests. The light source (2m×2m) is based on proven steady-state Halogen Dichroic system, which is made of 363×75 W lamps powered by 12VDC. The standard steady-state solar simulator can simulate the sunlight in a variety of conditions, with radiation from zero to approximately 1600 W/m^2. As the number of the lamps is large and the diffuse angle of the light is quite high, the solar radiation flux on the surface of solar collector is quite uniform.

Table 4.1 Equipment used in the efficiency test

1. Ambient air temperature sensor	10. Valves
2. Temperature sensors	11. Weighing vessel
3. Air vent	12. Balance
4. Anemometer	13. Flow control valve
5. Pyranometer	14. Flow meter
6. Solar collector	15. Sight glass
7. Artificial wind generator	16. Heat exchanger
8. Insulated pipe	17. Refrigerated Bath (Phoenix P1-C25P)
9. Pressure gauge	18. Solar simulator

In the solar simulator lab, the test setup for solar collector efficiency (as shown in Figure 4.1) is built based on the requirements of BS EN 12975-2:2006 (Thermal solar

systems and components – Solar collector – Part 2: Test methods). The measurement equipment used in the experiment is given in Table 4.1.

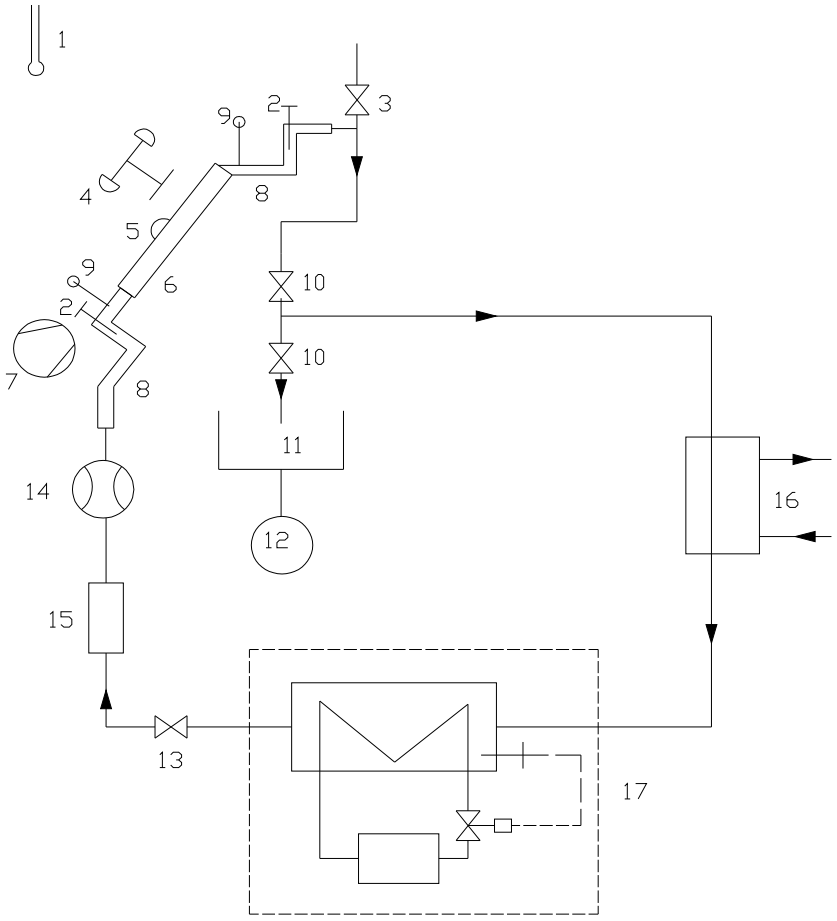

Figure 4.1 Schematic diagram for the efficiency test

The way in which a collector is mounted will influence the results of thermal performance tests. Therefore, the collector is mounted in accordance with the requirement of the standard. In this test, an open mounting structure is used which allows air to circulate freely around the front and back of the collector. Meanwhile, the collector shall be tested at tilt angles such that the incidence angle modifier for the collector varies by no more than ±2% from its value at normal incidence. For single

glazed flat plate collectors, this condition will usually be satisfied if the angle of incidence of direct solar radiation at the collector aperture is less than 20˚.

4.3 The Prototype Multi-functional ASHP System

The on-site photo of the prototype multi-functional ASHP system is shown in Figure 4.2. This system is mainly composed of an air-to-water heat pump unit with a desuperheater and a hot water storage tank for hot water supply. The specifications of each component and related parameters are summarized in Table 4.2.

Table 4.2 System parameters of the MSA-ASHP system

Location	Hong Kong
Solar collector	Flat plate with single cover, Ac=2 m^2
Storage tank	0.12m^3
Preheating solar tank	0.24m^3
Compressor	Displacement: 6.2m^3/h
Evaporator	Copper tube-in-tube heat exchanger; one outside tube with diameter of 42mm, length of 5.6m; five inner tubes with outer diameter of 10mm
Desuperheater	Copper tube-in-tube heat exchanger; one outside tube with diameter of 16mm, length of tube is 4.65m; one inner tube with outer diameter of 8mm
Condenser	Finned-tube heat exchanger; efficient tube length is 27.84m
Expansion valve	Thermostatic expansion valve

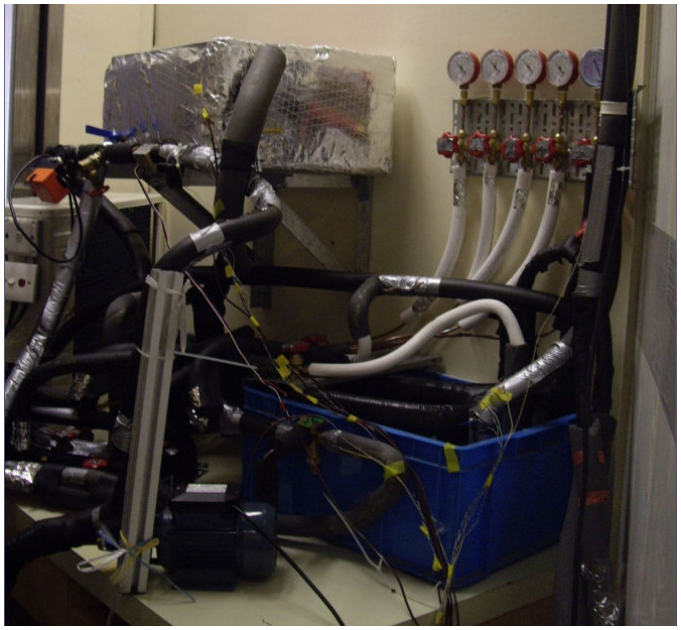

Figure 4.2 Sample system of the multi-functional ASHP unit

The multi-functional ASHP system consists of five basic components: a rolling piston compressor, a thermostatic expansion valve and three heat exchangers (i.e. evaporator, condenser and desuperheater). Both the evaporator and the desuperheater are copper tube-in-tube heat exchangers, where refrigerant flows through the inner tubes and water flows across the tubes. The outdoor condenser is a finned-tube heat exchanger. The other components are neglected in this study due to the comparatively little contribution to the thermodynamic analysis of the entire system. In this system, R22 is employed as refrigerant.

The desuperheater is installed between the compressor outlet and the reversing valve. The main function of the desuperheater is to absorb excess heat to produce or preheat domestic hot water. Therefore, the heat rejection into the ambient air is reduced and the heat pollution is alleviated. Consequently, the heat transfer deterioration of outdoor air-cooled condenser as described in Chapter 1 can be alleviated.

The prototype system can work in three different modes, which include the only AC mode, the only WH mode and the AC/WH mode. Besides, if space heating is required on special occasions, the system also can supply for the space heating load. Since space heating load is insignificant under Hong Kong weather conditions, the space heating with domestic water heating mode is not discussed in this research.

4.4 Test Device and Data Collection

In order to investigate the performance of the MSA-ASHP system, an experimental rig was established in the system. In the solar collector efficiency test, 3 thermocouples are needed for both the ambient air temperature and the inlet and outlet water temperatures of solar collector. As shown in Figure 4.3, there are 15 thermocouples located to measure the water and refrigerant temperatures at the inlet and outlet of the main components. The accuracy of all the thermocouples is calibrated to be within ±0.5 ℃. Three electromagnetic flow meters are used for the measurement of the water flow rates in the water loops. With the standard installation position, the accuracy of the flow meter is ±2% of full scale. Four pressure meters are installed to test the inlet and outlet pressure of the main components of the multifunctional ASHP unit. And the accuracy of the pressure meter has been calibrated by the manufacture to be ±1%. 2 PTX1400 pressure gauges are fixed besides the fluid temperature sensors of inlet and outlet of solar collector for the pressure drop measurement. This kind of pressure gauge has an accuracy of ±0.2% according to the specification of manufacturers. The relative humidity and temperature of the indoor and outdoor air are measured by the HOBO data

logger. The energy electricity consumed by the compressor is measured by a power monitor which has an accuracy of ±0.5% of its rated value.

The experimental data was collected using a 20 channels data collector GL-800. All thermocouples and the flow meters installed in the test rig are connected to this data logger. The power monitor and the HOBO data logger have the storage function for measurements. The same time interval of collecting data is set for the data logger, the power monitor and the HOBO data logger. Besides, it is set according to the actual operating conditions and research objectives.

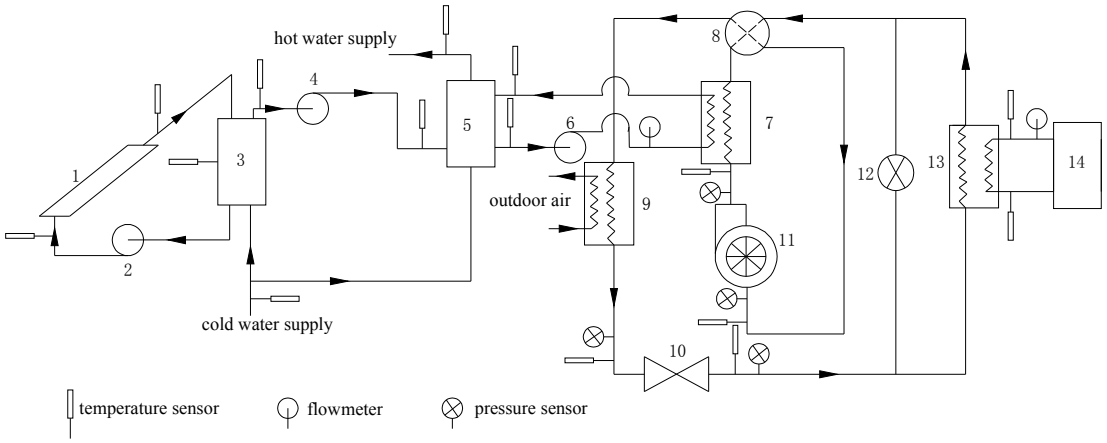

1-solar collector, 2-water pump, 3-preheating solar tank, 4-water pump, 5-storage tank, 6-water pump, 7-desuperheater, 8-four-way valve, 9-condenser, 10-expansion valve, 11-compressor, 12-electromagnetic valve, 13-evaporator, 14-air conditioning space.

Figure 4.3 Test sensors' distribution for the MSA-ASHP system

4.5 Uncertainty Analysis

Based on the method proposed by Holman (2001) and Treado and Snouffer (2001), the uncertainty analysis is conducted in this study to evaluate the errors of the indirectly

measured parameters using the classic root-sum-square formula. It is assumed that the calculated variable R is a function of the independent variables $x_1, x_2, \ldots, x_n$.

Based on the uncertainties of independently measured variables ($w_1, w_2, \ldots, w_n$), the relative uncertainty of the calculated variable can be estimated using the classic root-sum-square formula:

$$\sigma_R = \frac{\left[\left(\frac{\partial R}{\partial x_1} w_1\right)^2 + \left(\frac{\partial R}{\partial x_2} w_2\right)^2 + \ldots + \left(\frac{\partial R}{\partial x_n} w_n\right)^2\right]^{1/2}}{R} \tag{4.1}$$

where

w_i = the uncertainty of the independently measured variable x_i

$\frac{\partial R}{\partial x_i}$ = sensitivity coefficient, the partial derivative of the calculated variable R with respect to the measured variable x_i

Taking the heat transfer rate as an example, the cooling capacity of the MSA-ASHP system can be calculated by means of the measured values of water flow rate and water temperatures as follows:

$$Q = m_w c_p \left(t_{w,in} - t_{w,out}\right) \tag{4.2}$$

According to equation (4.1), the relative uncertainty of the cooling capacity can be calculated as:

$$\sigma_Q = \sqrt{\left(\frac{w_m}{m_w}\right)^2 + \left(\frac{w_t}{t_{w,in} - t_{w,out}}\right)^2 + \left(\frac{w_t}{t_{w,in} - t_{w,out}}\right)^2} \tag{4.3}$$

Thus, the relative uncertainty of the cooling capacity approximately ranges from 6.4% to 8% under the considered experimental conditions. This value may vary slightly with the variations of the actual flow rate and temperatures in practical operation.

4.6 Solar Collector Efficiency

For the solar collector efficiency test, two different testing conditions are adopted as shown in Table 4.3. Under each testing condition, a series of different water inlet temperatures are adopted. Correspondingly, four sets of independent data points are obtained as listed in Tables 4.4 ~ 4.11.

Table 4.3 Two different test conditions for the efficiency test

Test condition	Flow rate (kg/s)	Air temperature (°C)	Air speed (m/s)	Solar irradiance (W/m^2)
1	0.022	26.01	3.86	809.64
2	0.050	26.33	3.46	758.30

4.6.1 Solar collector efficiency calculation

The following equations are employed to calculate the solar collector efficiency on the basis of the recorded data.

$$\begin{aligned} \dot{Q} &= \dot{m} c_f \Delta T \\ &= \dot{m} c_f \left(t_{out} - t_{in}\right) \end{aligned} \tag{4.4}$$

$$\dot{Q} = AG\eta \tag{4.5}$$

Combining equations (4.4) and (4.5), the solar collector efficiency can be expressed as:

$$\eta = \frac{\dot{m} c_f \Delta T}{AG} \tag{4.6}$$

where,

$\dot{Q}$ - the actual useful heat absorbed by fluid, W;

$\dot{m}$ - mass flow rate of the fluid, kg/s;

c_f - fluid specific heat corresponding to the mean fluid temperature, J/(kg℃);

ΔT - fluid temperature difference between the inlet and the outlet, ℃;

t_{in} - inlet water temperature of solar collector, ℃;

t_{out} - outlet water temperature of solar collector, ℃;

A - absorber area of the solar collector, m^2;

G - solar radiation on the collector, W/m^2;

η - thermal efficiency of the solar collector.

4.6.2 Test results

Based on the above calculation method and the recorded data, the thermal efficiency of the solar collector is calculated and analyzed in this section.

When the water flow rate through the solar collector is set as 0.022 kg/s, the test results are presented as follows. Accordingly, the efficiencies are calculated to be 56.89%, 54.28%, 52.38% and 50.2% respectively.

Table 4.4 Test results when the fluid inlet temperature is set as 25.74℃

Test Time	11:32(AM)	11:36(AM)	11:40(AM)	11:44(AM)
Inlet temperature(℃)	25.72	25.7	25.75	25.78
Outlet temperature(℃)	34.21	34.81	35.29	34.61

Table 4.5 Test results when the fluid inlet temperature is set as 32.47℃

Test Time	12:24(PM)	12:28(PM)	12:32(PM)	12:36(PM)
Inlet temperature(℃)	32.29	32.45	32.49	32.7
Outlet temperature(℃)	40.65	41.01	41.13	41.21

Table 4.6 Test results when the fluid inlet temperature is set as 36.20℃

Test Time	13:26(PM)	13:30(PM)	13:34(PM)	13:38(PM)
Inlet temperature(℃)	35.97	36.27	36.17	36.37
Outlet temperature(℃)	44.37	44.57	44.42	44.48

Table 4.7 Test results when the fluid inlet temperature is set as 41.21℃

Test Time	13:49(PM)	13:53(PM)	13:57(PM)	14:01(PM)
Inlet temperature(℃)	41.06	41.13	41.3	41.36
Outlet temperature(℃)	49.05	49.56	49.59	49.77

As the water flow rate becomes 0.05 kg/s, the corresponding efficiencies are evaluated to be 74.3%, 72.35%, 68.91% and 64.86%, respectively.

Table 4.8 Test results when the fluid inlet temperature is set as 34.72℃

Test Time	13:09(PM)	13:13(PM)	13:17(PM)	13:21(PM)
Inlet temperature(℃)	34.85	34.75	34.63	34.65
Outlet temperature(℃)	39.73	39.67	39.71	39.61

Table 4.9 Test results when the fluid inlet temperature is set as 39.19℃

Test Time	13:48(PM)	13:52(PM)	13:56(PM)	14:00(PM)
Inlet temperature(℃)	39.16	39.12	39.31	39.15
Outlet temperature(℃)	44.06	44.03	44.11	44.02

Table 4.10 Test results when the fluid inlet temperature is set as 43.81℃

Test Time	14:35(PM)	14:39(PM)	14:43(PM)	14:47(PM)
Inlet temperature(℃)	43.88	43.85	43.8	43.69
Outlet temperature(℃)	48.48	48.44	48.29	48.41

Table 4.11 Test results when the fluid inlet temperature is set as 46.98℃

Test Time	15:20(PM)	15:24(PM)	15:28 (PM)	15:32(PM)
Inlet temperature(℃)	46.98	46.91	47.16	46.85
Outlet temperature(℃)	51.34	51.17	51.48	51.25

Judging from all the efficiencies calculated above, it is obvious that the efficiency of solar collector decreases as the inlet water temperature increases. That is because the larger temperature difference between the ambient air and the heat transfer fluid increases the heat convection loss between the ambient air and the absorber plate. In addition, a relatively higher efficiency can be obtained under the second testing

condition since the water flow rate is twice larger than that under the first testing conditions.

When the mean water temperature (t_m) at the inlet and outlet of solar collector is used, where

$$t_m = t_{in} + \frac{\Delta T}{2} \tag{4.7}$$

the corresponding relation between t_m and the efficiency of solar collector under the considered two kinds of testing conditions is summarized in Table 4.12. It can be observed that the efficiency decreases as the mean water temperature rises.

Table 4.12 Solar collector efficiency vs mean water temperature

1st	t_m (℃)	30.24	36.74	40.33	45.35
	η (%)	56.89	54.28	52.38	50.2
2nd	t_m (℃)	37.2	41.63	46.11	49.15
	η (%)	74.3	72.35	68.91	64.86

4.7 Experiments for different operation control strategies

In order to ensure an optimum operating performance of the proposed MSA-ASHP system, appropriate control strategies will be suggested based on the series of experimental results in this section.

4.7.1 The solar collector loop

Control parameters in solar energy collection systems are differentiated upon objective, complexity and way of operation. As presented in Chapter 1, in the MSA-ASHP system, the solar collector loop is mainly used for domestic hot water supply while the multi-functional ASHP unit works as its auxiliary heat source when solar radiation is not high enough. In this way, the multi-functional ASHP unit plays little impact on the thermal performance of the solar collector loop, especially when two water tanks are adopted in this system. Thus, the control strategy for the solar collector loop in this study is treated as same with that for a separate solar thermal hot water system.

Using the least square method, the instantaneous efficiency of the solar collector can be calculated by statistic curve fitting as shown in Figure 4.4. It shows the variation of the solar collector efficiency with changing temperature difference between the ambient air temperature (t_a) and the mean water temperature (t_m). It can be found that, the efficiency of the second testing conditions is significant larger than that of the first testing condition when the temperature difference is less than 35 ℃. With the growth of the temperature difference, the thermal efficiency of the solar collector with higher water flow rate (i.e. the second testing conditions) drops more quickly than that with lower water flow rate, say the first testing condition. As a result, the solar collector

efficiency of the second testing conditions becomes smaller than that under the first testing conditions. Therefore, control of the temperature difference and flow rate is an important factor to ensure thermal performance of the solar collector loop.

In literature (Kovarik and Lesse, 1976), an analysis of the optimal flow control problem in solar energy collection systems has shown that if the amount of energy collected is the only criterion of performance, maximum flow rate is to be applied whenever there is a positive gain from the collector. In most cases, the temperature difference of the flat plate solar collector will be in the range of 10-30℃. Thus, in order to absorb the most solar energy, in this study, the flow rate is suggested to be above 0.05 kg/s.

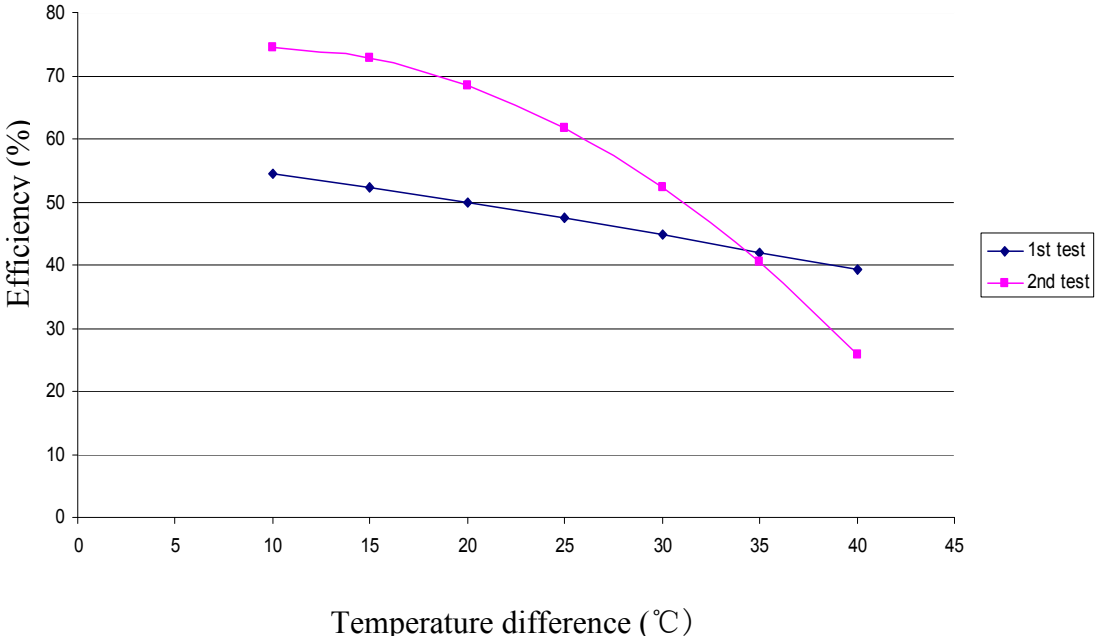

Figure 4.4 Solar collector efficiency vs temperature difference

4.7.2 The multi-functional ASHP unit

For the MSA-ASHP system, appropriate control strategy is important for its efficient operation. To find the optimal operation strategy, the system performance is measured and analyzed in different operation conditions. The main test thermal conditions are shown in Table 4.13. For these two tests, the water flow rates in the desuperheater and evaporator are set to be the same, i.e. 0.12kg/s.

Table 4.13 The test thermal environment

operation conditions	Dry bulb temperature (℃)	Relative humidity
A	27.6	74.6%
B	29.8	72.9%

Under the operating condition A, the system firstly operated in the only AC mode. In the following one hour, it was changed into the AC/WH mode. Finally, the outdoor air-to-refrigerant condenser was switched off and then the system still worked in the AC/WH mode but with all condensation heat absorbed by domestic hot water. While in operating condition B, the system also began in the only AC mode. Similarly, it was switched into the AC/WH mode later. A few minutes later, the outdoor condenser was bypassed and all the condensation heat was absorbed by domestic hot water. Half an hour later, the system operated in the only AC mode again.

The cooling capacities of the multi-functional ASHP unit under the described operating conditions are shown in Figure 4.5 and Figure 4.6, respectively. From Figure 4.5, it can be seen that, in operating condition A, the cooling capacity of the system almost keeps above 2kW in the first two operating modes (i.e. the only AC mode and

the AC/WH mode). When the system operates in the AC/WH mode with all condensation heat absorbed by hot water, the cooling capacity can still reach 1.5kW until the outlet temperature of hot water is 46.1℃. In order to improve the cooling performance, the outdoor air-to-refrigerant condenser should be turned on. In other words, the system should operate in the normal AC/WH mode.

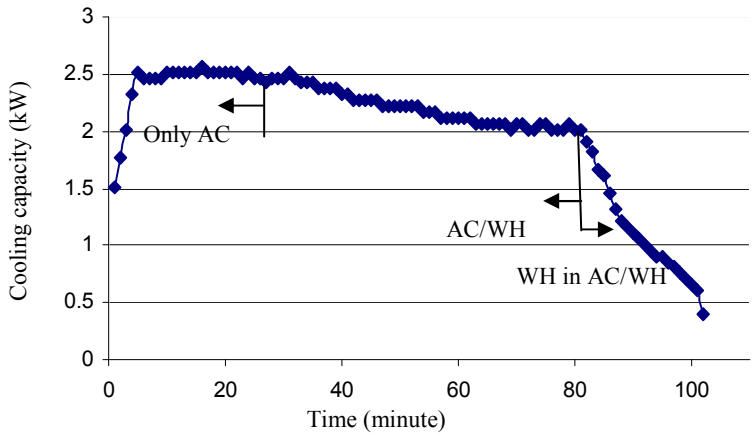

Figure 4.5 Cooling capacity under operation condition A

As shown in Figure 4.6, in the operation condition B, the cooling capacity of the system can also reach above 2kW during the initial operating process (i.e. the first only AC mode and the AC/WH mode). In the following half hour, the system works in the AC/WH mode with all condensation heat absorbed by the desuperheater. It can be found that the cooling capacity is above 1.5kW until the hot water is heated to 39℃. However, the corresponding COP is 3.4 (as shown in Figure 4.7) which is relatively higher compared with that of the only AC mode. If the required cooling capacity was 1.5kW, the system should turn into the normal AC/WH mode or the only AC mode to meet the required cooling load.

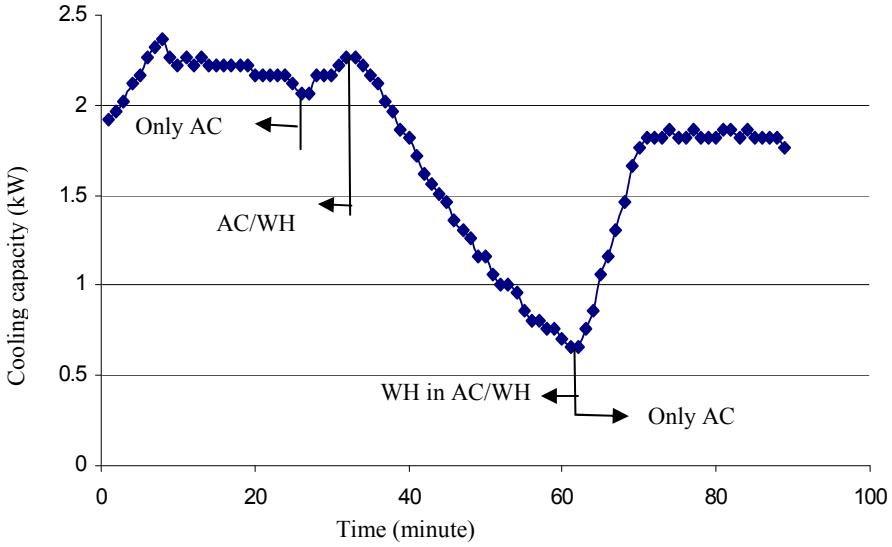

Figure 4.6 Cooling capacity under operation condition B

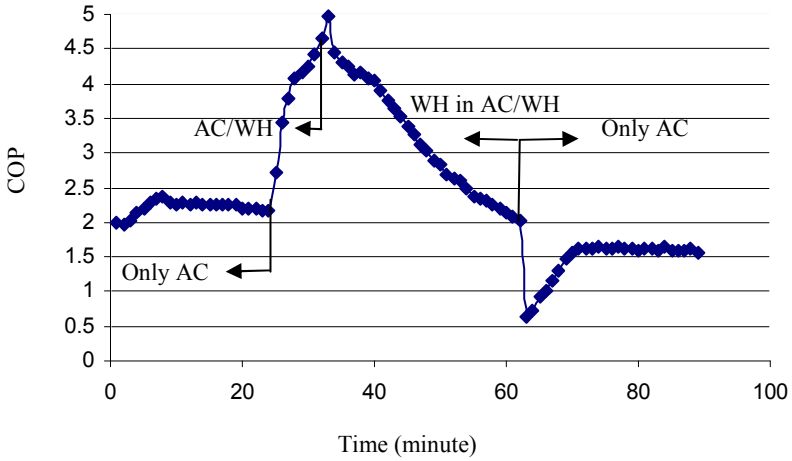

Figure 4.7 Variation of COP under operation condition B

The analysis above took the cooling capacity as the judgment parameter of switching operation modes. Actually, the COP of the system may affect the switching condition. Take the experiment under operation condition B for example. In order to obtain better energy performance in practice, the minimum COP of the system in the AC/WH mode is required to be 3.0. Thus, when the outlet water temperature reaches 41.4℃ the system

should be changed to the normal AC/WH mode. In other words, the outdoor air-to-refrigerant condenser should be turned on. Depending on different requirements of customers, similarly, the hot water heating capacity and the outlet water temperature of desuperheater can also act as the judgment parameters for determining the switching points.

As shown in Figure 4.8, under operation condition A, the average COP of the system is about 2.8 which is 13.4% higher than that under operation condition B (i.e. 2.47). Judging from Figure 4.9 and Figure 4.10, it can be found that, in order to obtain the same outlet water temperature, the operating time of operation condition A is twice as long as that under operation condition B even though the initial hot water temperature is a little higher. It is because the system mainly operates in the AC/WH mode with all condensation heat absorbed by hot water under operating condition B. Thus, more condensation heat is absorbed by hot water. Therefore, if hot water is required to be heated to a certain temperature in a relatively short time, the operation condition B is proposed. The operation condition A is preferred when most condensation heat is required to recover or when a higher energy performance is necessary.

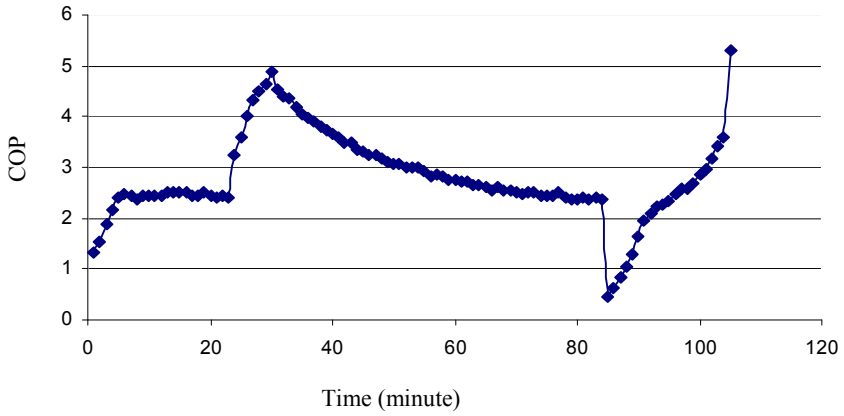

Figure 4.8 Variation of COP under operation condition A

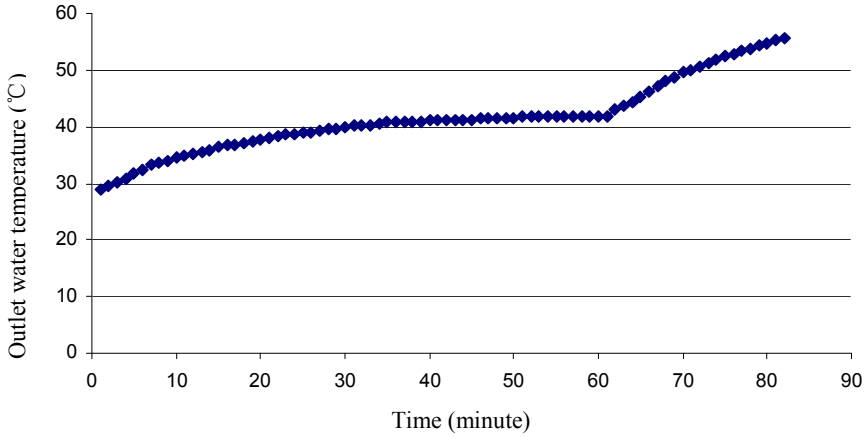

Figure 4.9 Outlet water temperature in operation condition A

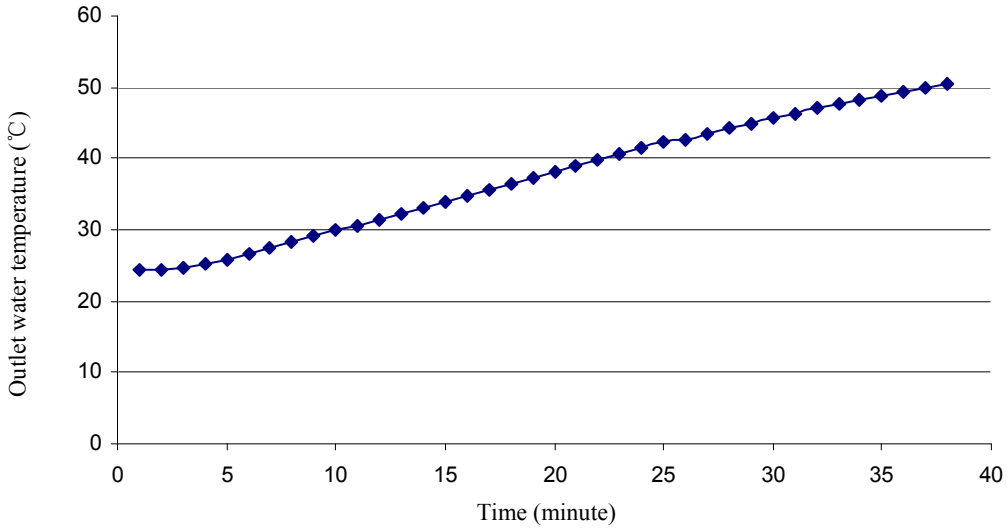

Figure 4.10 Outlet water temperature in operation condition B

4.8 Summary

This chapter mainly introduces a prototype system for experimental tests and simulation validation of the MSA-ASHP system. It is divided into two parts: one is the experimental setup for testing a solar collector's energy efficiency and the other is a

sample multi-functional ASHP unit. Accordingly, the used measurement apparatus and experimental methods are described. A more accurate method is adopted for the uncertainty analysis. The test results of solar collector efficiency show that the selected solar collector behaves well under the considered weather conditions. Averagely, the tested solar collector efficiency reaches 70.1%. The appropriate control strategies are found based on the experimental results. For the solar collector loop, the temperature difference and flow rate are selected as the control parameters. In order to maximize the absorbed solar energy, the flow rate is suggested to be above 0.05 kg/s. As for the multi-functional ASHP unit, different operation modes are suggested depending on different design purposes.

CHAPTER 5 SIMULATION VALIDATION

The simulation model of the MSA-ASHP system developed in Chapter 3 can be used to analyze the system operating performance and to identify any potential mismatches among all components. In addition, it can be employed to design and optimize the proposed system when some optimal algorithms are integrated into the simulation model. However, it is indispensable to validate the theoretical model using experimental methods before applying it either to engineering practice or other related research fields. In view of this point, the primary objective of this chapter is to experimentally verify the built mathematical model of the MSA-ASHP system in different operating conditions.

5.1 Description of Experiments

In order to validate the simulation model, a series of tests were conducted on the basis of the built sample system as described in Chapter 4. The total three operation modes (i.e. the only AC mode, the AC/WH mode and the only WH mode) and the AC/WH mode with all condensation heat absorbed by the desuperheater were investigated under different operating conditions. Table 5.1 summarizes the test thermal conditions and input data of the four sets of experiments.

Table 5.1 Test thermal conditions and input data

Operation mode	Dry bulb temperature (℃)	Relative humidity
The only AC mode	27.6	74.6%
The AC/WH mode	27.6	74.6%
The only WH mode	24.8	77.0%
The only WH in AC/WH mode	27.6	74.6%

Throughout the experiments, the data collection system presented in Chapter 4 was used to record the operating parameters including the inlet and outlet water temperatures of all water circuits, the water flow rates, the inlet and outlet refrigerant pressures and temperatures of each component in the multi-functional ASHP unit and the power consumption of the compressor.

On the basis of the uncertainties of the parameters directly measured, the uncertainties for the indirectly measured parameters can be calculated using the method described by Holman (2001), as presented in Chapter 4. According to the range of operating parameters during the experimental process, the relative uncertainty of the water temperature was found to be within 0.9%~3.9%. Whereas the relative uncertainty of the water flow rates was within 2.0%~5.2%. As for the power consumption of the compressor, the relative uncertainty was found to be 0.5%~1.4%. The heat transfer rates were found to have a large relative uncertainty of 2.1%~8.0% as it took the uncertainties of the temperature and flow rate into consideration and the relative uncertainty of the COP was within 10%.

Once the necessary parameters and the inlet water temperatures of the load sides and the domestic hot water side are assumed, the corresponding outlet parameters, heat transfer rates and the COP can be determined using the simulation model developed in Chapter 3.

5.2 The only AC Mode

When the MSA-ASHP system works in the only AC mode, it operates in the same principle with a conventional air conditioner. Figure 5.1 shows the system performance comparison between the tested COP and the simulated one. The greatest relative uncertainty is about 9.46% which is acceptable for engineering application. In addition, it demonstrates that the COP of the proposed MSA-ASHP system is comparative with that of the conventional air conditioners.

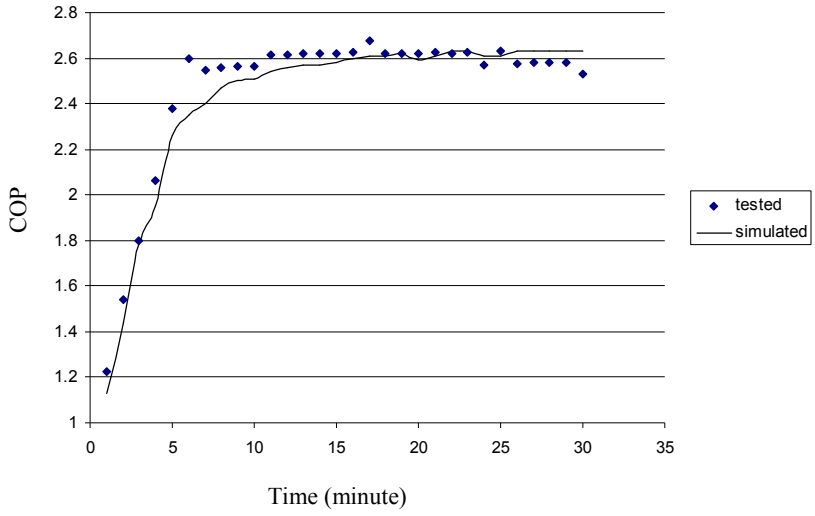

Figure 5.1 System performance in the only AC mode

5.3 The AC/WH Mode

In this section, the simulation model in terms of the AC/WH mode was validated using the corresponding experimental data. The operating performance of the system in the AC/WH mode was also discussed accordingly.

The comparisons between the experimental measurements and the model predictions were carried out in terms of the following parameters: the outlet water temperature of the desuperheater, heat transfer rates of all heat exchangers, the condensation pressure, the outlet refrigerant temperature of the compressor and the energy performance ($COP_{AC/WH}$ and COP_{AC}) of the system as well. The detailed results are shown in Figures from 5.2 to 5.8.

In general, the simulation model is accurate to within 10% of the experimental results. From Figure 5.2, it can be found that the deviation of the simulated outlet water temperature of desuperheater from the measured values was around ±0.5℃.For the outlet temperature of the compressor, the relative uncertainty ranged from 0.21% to 4.0% (as shown in Figure 5.3).

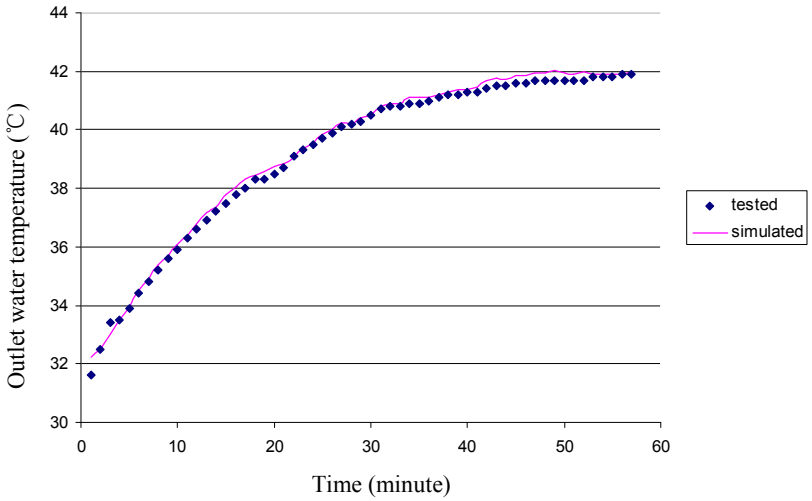

Figure 5.2 Outlet water temperature of desuperheater in the AC/WH mode

Figure 5.3 indicates the variation of the outlet refrigerant temperature of the compressor during the whole operating process. It is clear that the outlet refrigerant temperature rises quickly as the operation goes. However, the highest value of the outlet temperature is about 79℃ which is much lower than the upper safety limit.

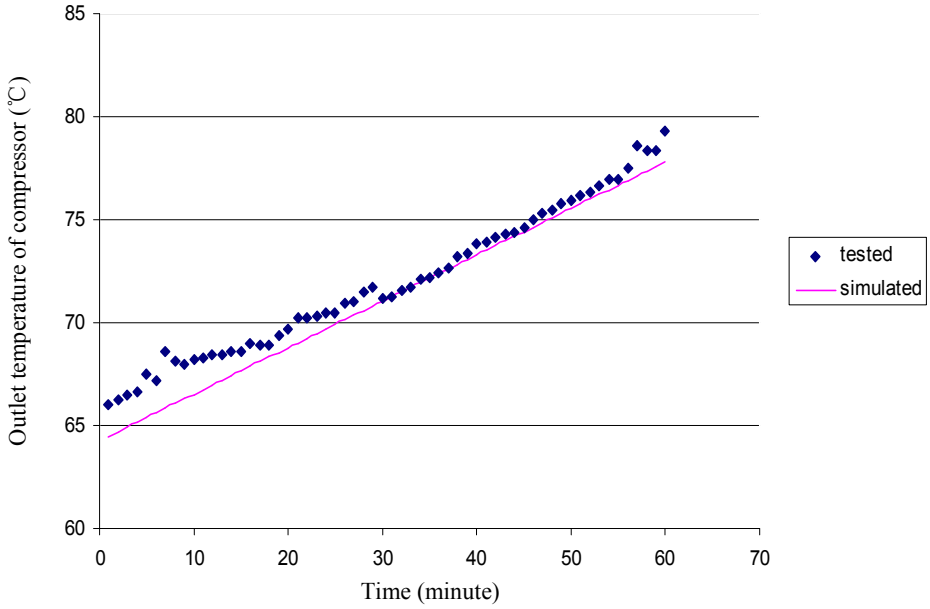

Figure 5.3 Outlet temperature of compressor in the AC/WH mode

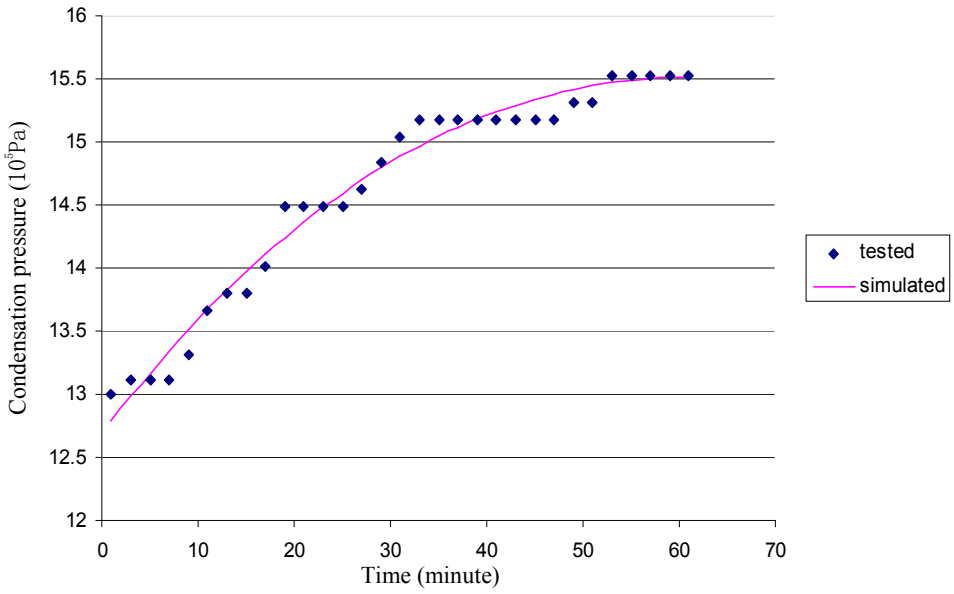

Figure 5.4 Condensation pressure in the AC/WH mode

As the outlet water temperature in the desuperheater rises, the condensation pressure is significantly increased. Figure 5.4 shows that the condensation pressure ranges from 1.3-1.55MPa throughout the whole operating process, and there is a good coherence between the simulation results and test data.

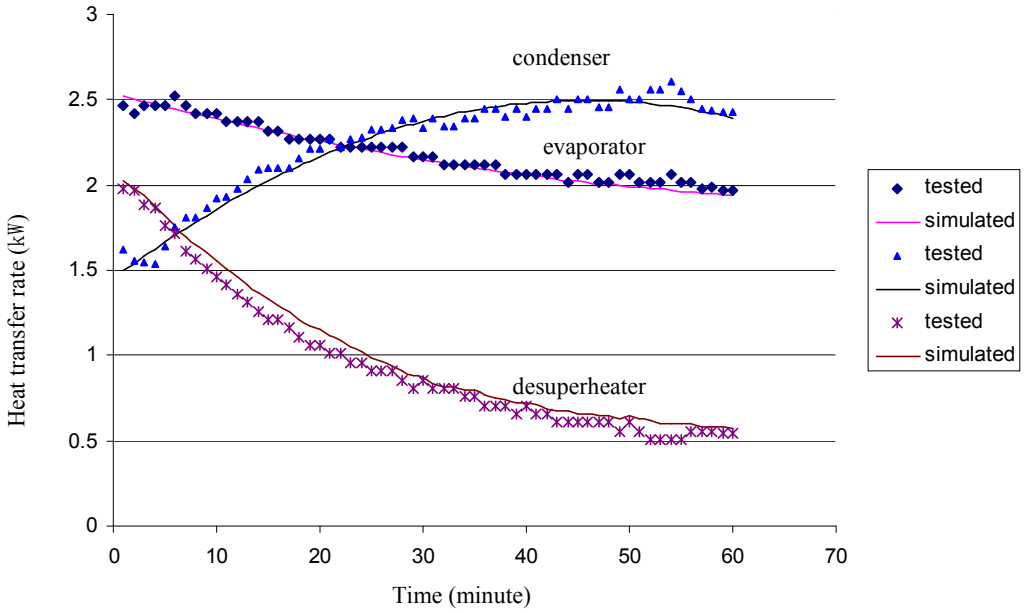

Figure 5.5 Heat transfer rates in the AC/WH mode

Figure 5.5 shows the changing characteristics of the heat transfer rates in all the three heat exchangers when the system operates in the AC/WH mode. There are two condensing devices in the MSA-ASHP system: the outdoor air-cooled condenser and the indoor water-cooled condenser, i.e. the desuperheater. In the AC/WH mode, the two condensers have complementary roles in condensation heat transfer. It is obvious that the heat transfer in the desuperheater deteriorates as the operation proceeds. Consequently, the percentage of heat exchange capacity of the water-cooled condenser is weakened as shown in Figure 5.6. The recovery rate of the condensation heat for heating hot water decreases from 55% to 16%. At the same time, the heating capacity of

the air-cooled condenser is enlarged. The function of the air-cooled condenser is very important for the MSA-ASHP system at elevated water temperature. It allows a reliable dissipation of the condensation heat. In this way, the cooling capacity of the system only reduces a little, say 0.5 kW during the whole operation process.

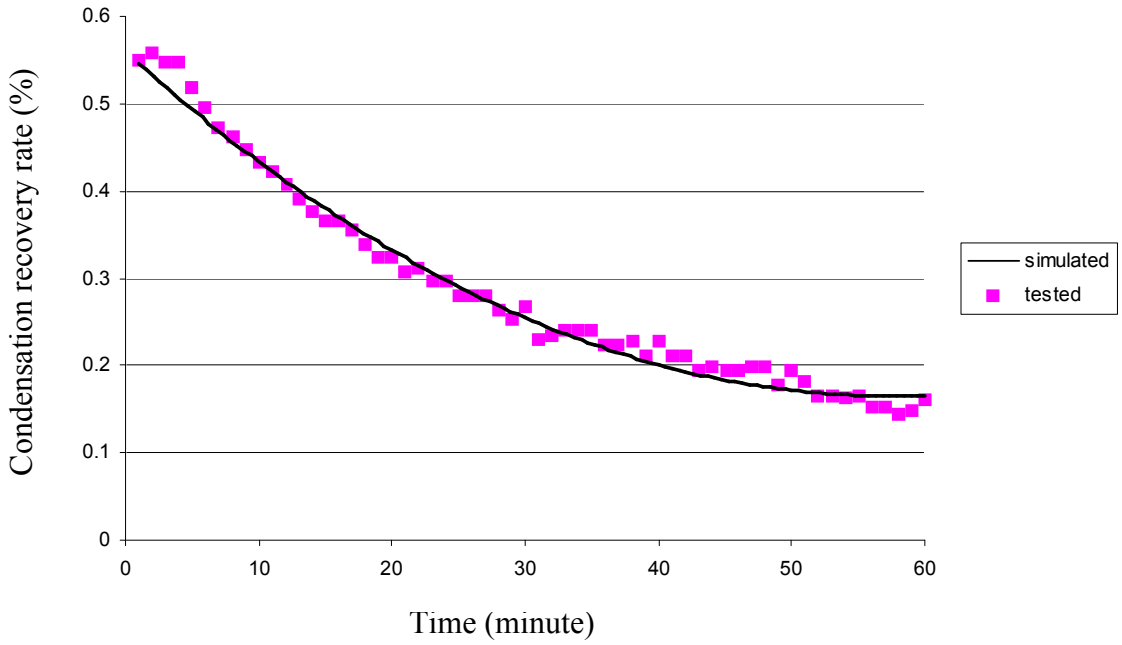

Figure 5.6 Condensation recovery rate vs time

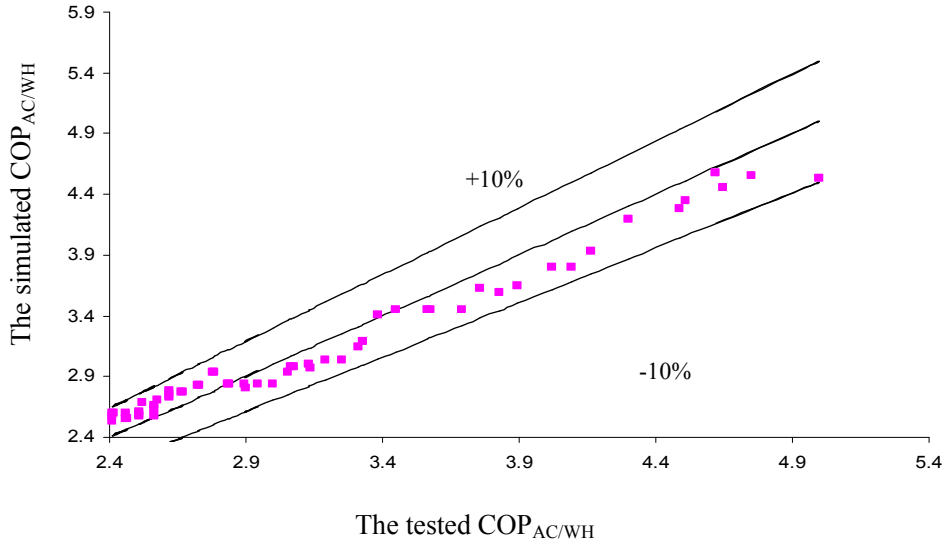

Figure 5.7 $COP_{AC/WH}$ in the AC/WH mode

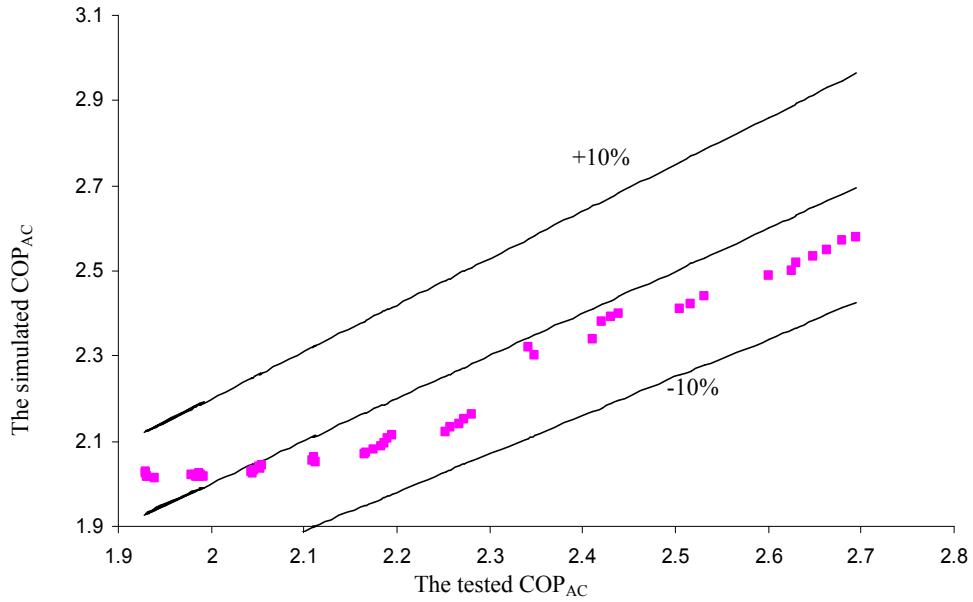

Figure 5.8 COP_{AC} in the AC/WH mode

Compared the results shown in Figure 5.7 and Figure 5.8, it is clear that the system performance is improved obviously when the condensation heat is recovered for hot water production. Under the test thermal conditions, the $COP_{AC/WH}$ ranges from 4.6 to 2.4. The COP_{AC}, which stands for the system performance coefficient when the cooling capacity of the system is only considered, changes from 2.7 to 1.9. These results further indicate that the proposed MSA-ASHP system can save energy considerably.

5.4 The only WH Mode

Figure 5.9 shows the outlet water temperature of condenser when the proposed system works in the only WH mode. It can be seen that the water can be heated from about ambient air temperature to the required value within an hour. If the water temperature is preheated by the solar collector loop, the required hot water temperature will be reached in a shorter heating period. Therefore, this system can meet the hot water

requirement timely in moderate climates even when the solar radiation is not high. Besides, as shown in Figure 5.10, the system performance in the only WH mode is about 2.0 on average which is much better than that of conventional water heaters.

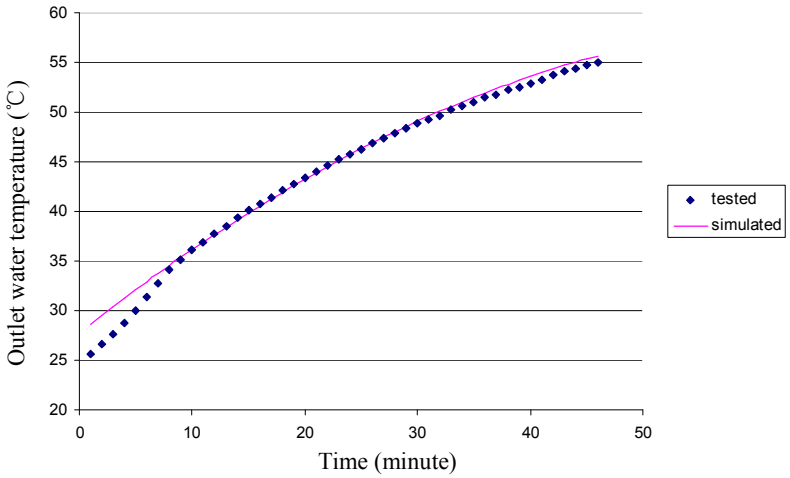

Figure 5.9 Outlet water temperature of condenser in the only WH mode

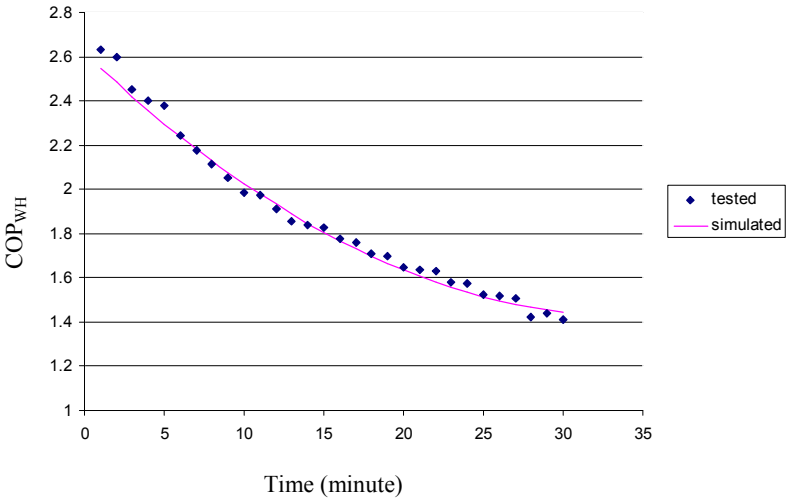

Figure 5.10 System performance in the only WH mode

5.5 The only WH in AC/WH Mode

For application of the MSA-ASHP system, the solar collector loop is firstly used to heat hot water. If the required temperature is not obtained, the multi-functional ASHP unit is then employed to continue heating the hot water to meet the heating requirement. In the only WH of AC/WH mode, the hot water is usually preheated by the solar collector to a certain degree. Then, the air-cooled condenser of the multi-functional ASHP unit is turned off and all condensation heat is absorbed by the hot water in the water-cooled condenser, say the desuperheater. From Figure 5.11, it is seen that the system COP in this operating mode reduces from 3.4 to 2.1, i.e. about 2.8 on an average basis, which is much higher than that of conventional water heaters and air conditioners. Figure 5.12 indicates that, about 20 minutes are needed to obtain the required water temperature from about 43℃. Compared with the heating time in only WH mode, shorter time is needed when the system operates in the only WH in AC/WH mode. The MSA-ASHP system can work in the only WH of AC/WH mode when allowed hot water heating time period is limited.

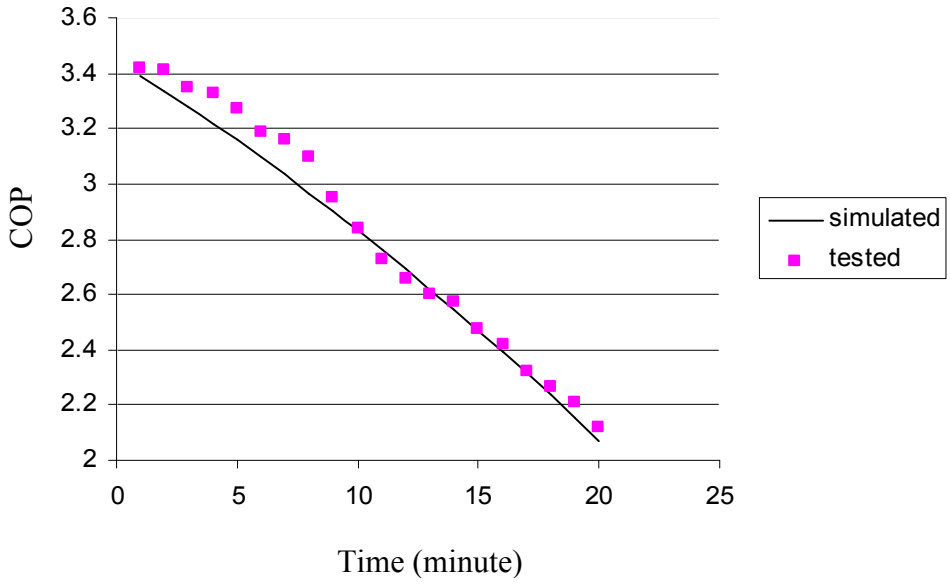

Figure 5.11 System performance of the only WH in AC/WH mode

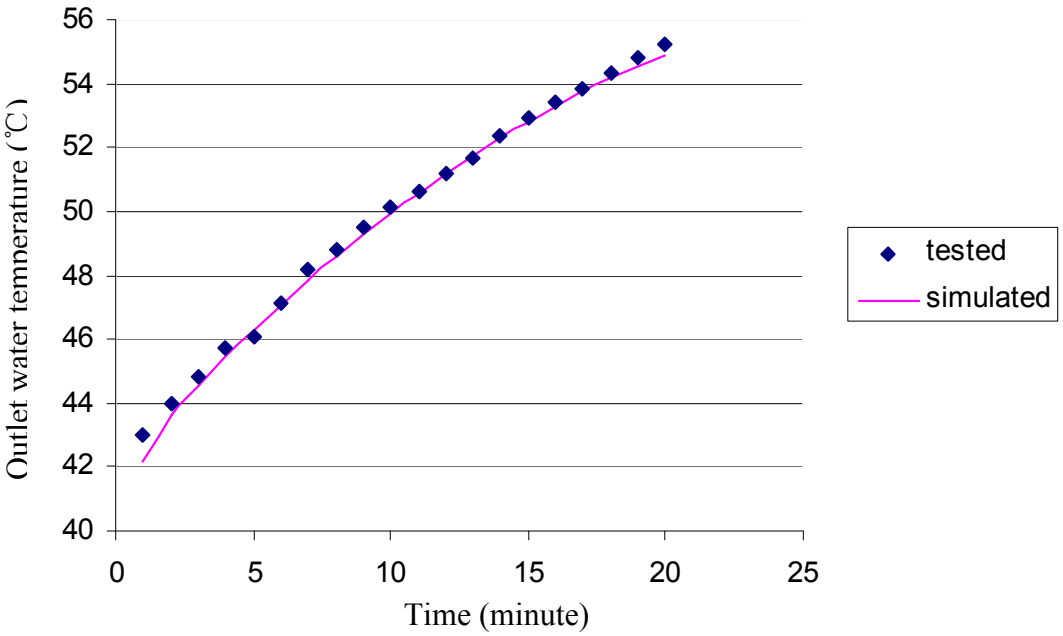

Figure 5.12 Outlet water temperature of desuperheater

5.6 Summary

In this chapter, the simulation model developed in this study is validated through a series of experiments. Comparisons between the simulation results and the test data are conducted in terms of four possible operating modes: the only AC mode, the AC/WH mode, the only WH mode and the only WH in AC/WH mode. The investigation results show that the relative uncertainty of the simulation models is within 10% which is acceptable for engineering applications. In addition, in the only AC mode, the proposed system behaves better than conventional air conditioners. In the AC/WH mode, the system performance is improved significantly when the condensation heat recovery is considered for free hot water supply. As for the only WH mode, the system performs better as compared with the conventional water heaters. When the system operates in the

only WH of the AC/WH mode, the system performance is very good and required hot water temperature can be obtained quickly.

As a whole, the investigation analysis obtained from four different operating modes indicate that simulation results agrees well with experimental data and the MSA-ASHP system can save a lot of energy compared with conventional systems for air conditioning and water heating purposes.

CHAPTER 6 ENERGY AND EXERGY ANALYSIS OF THE MSA-ASHP SYSTEM

6.1 Introduction

Exergetic analysis has become an integral part of thermodynamic assessment of any solar assisted heat pump system. The conventional energy analysis (based on the first law analysis) does not give the qualitative assessment of the various losses occurring in the components. The major indicator – the coefficient of performance (COP) of the heat pump system, which is directly derived from the first law of energy conservation principle, can only compare the desired energy output to the required energy input. In other words, it cannot represent the quality of energy and indicate the irreversibility or the energy losses in the components of a thermal system (Wark, 1995). That is why the exergy analysis (based on the second law analysis) is used to get a clear picture of the various losses quantitatively as well as qualitatively (Singh, et al., 2000).

In recent years, experimental studies and theoretical analysis based on the exergy concept with heat pump systems have been reported. Ding et al. (2004) studied an improved air source heat pump (ASHP) and presented a new subcooling system employing a scroll compressor with supplementary injections that can effectively solve the problems. The prototype of an ASHP was validated and relevant dynamic performance was tested in this study. Ozgener and Hepbasli (2005), investigated performance analysis of a solar-assisted-ground source heat pump (SAGSHP)

greenhouse system and researched the performance characteristics with a 50 m vertical u-bend group heat exchanger. Kaygusuz and Ayhan (1993), studied a solar-assisted heat pump (SAHP) system experimentally and analyzed the data using exergy concept method. Pei et al. (2005), presented the performance of multi-functional domestic heat pump system and discussed the working principles and the basic features of this system. Pei et al. (2005), also reported that a multi-functional domestic heat pump system that can provide much better energy performance and higher equipment utilization, causes less thermal pollution than the heat pump water heater and the conventional air conditioner. Torres Reyes et al. (1998), studied exergy analysis and optimization of a SAHP system and discussed the optimum evaporation temperature as a function of a parameter that involves ambient conditions and the overall heat transfer coefficient. Badescu (2002), studied first and second law analysis of a SAHP system and found that most of exergy losses occur during compression and condensation. He reported that the photovoltaic array can provide all the energy, required to drive the heat pump compressor. Li et al. (2007), studied the thermal performance of a direct expansion solar-assisted heat pump water heater (DX-SAHPWH) experimental setup. They evaluated through energy and exergy analysis and also calculated the exergy loss coefficient of each component and the exergy efficiency of the whole DX-SAHPWH system. Hepbasli (2007), deal with the exergetic modeling and performance evaluation of solar-assisted domestic hot water tank integrated GSHP systems and applied the model to a system. Li et al. (2007), studied on the experimental performance analysis and optimization of a DX-SAHPWH. They reported that the highest exergy loss occurs in the compressor and collector/evaporator, followed by the condenser and expansion

valve, respectively. Ozgener and Hepbasli (2007) have reviewed comprehensively energy and exergy analysis of SAHP systems. They summarized the studies conducted on the energy and the exergy analysis of SAHP systems in Turkey and around the world. Kara et al. (2008) have reviewed exergetic assessment studies about direct-expansion SAHP (DX-SAHP) systems. Cervantes de Gortari and Torres-Reyes (2002) conducted experiments on a DX-SAHP system and determined the maximum exergy efficiency. They (2001) also found that the exergetic efficiencies of the system are in the range of 0.067-0.13 and 0.083-0.14, which were calculated for two different equations, while the COP values for the heat pump varied from 2.56 to 4.36.

The literature review shows that exergy investigation has become an essential part for analyzing heat pump systems including the SAHP systems and the multi-functional heat pump systems. However, very limited review studies have been done for analyzing the operating performance of the MSA-ASHP system on the basis of the exergy concept. Therefore, this chapter aims to evaluate the energy and exergy efficiencies of the MSA-ASHP system for supplying both air conditioning load and hot water heating load under subtropical weather conditions.

6.2 Energy Analysis of the MSA-ASHP System

The energy analysis of the MSA-ASHP system has been conducted in detail in Chapter 3. It mainly involves the energy balance and energy performance definition as follows:

The energy balance:

$$Q_{des} + Q_{con} = W + Q_{evp} \tag{6.1}$$

The definition of COP in different operation modes:

$$\mathrm{COP_{AC}} = \frac{\mathrm{Q_{evp}}}{\mathrm{W}} \tag{6.2}$$

$$\mathrm{COP_{AC/WH}} = \frac{\mathrm{Q_{evp}} + \mathrm{Q_{des}}}{\mathrm{W}} \tag{6.3}$$

$$\mathrm{COP_{WH}} = \frac{\mathrm{Q_{con}}}{\mathrm{W}} \tag{6.4}$$

The above equations for energy analysis show that the COP only relates to the energy transferred between the different components in the system. It gives equal weighting to both the electric energy supplied to the compressor and the low-grade thermal energy in the heat exchangers. No consideration on the quality changes of the different energy resources is found in the energy analysis. Hence, it is necessary to further investigate the exergy performance of the MSA-ASHP system on the basis of the second law of thermodynamics.

6.3 Exergy Analysis of the MSA-ASHP System

An exergy analysis (or second law analysis) has proven to be a powerful tool in the simulation thermodynamic analyses of energy systems. In other words, it has been widely used in the design, simulation and performance evaluation of energy systems. Exergy analysis method is employed to detect and to evaluate quantitatively the causes

of the thermodynamic imperfection of the process under consideration. It can, therefore, indicate the possibilities of thermodynamic improvement of the process under consideration (Hepbasli, 2008).

6.3.1 General relations of exergy analysis

Exergy is the measurement of maximum useful work that can be produced by the system interacting with an environment having constant pressure (P_0) and temperature (T_0) (Ozgener and Hepbasli, 2005). When a system and its environment are in equilibrium with each other, the system can be assumed to be in its dead state (Li et al., 2007; Hepbasli, 2007). In this study, the dead state is taken as the average state of the local atmospheric air during the experimental test.

For a general steady-flow process, the four balance equations (mass, energy, entropy and exergy) are applied to the work and heat interactions, the rate of exergy decrease, the rate of irreversibility, the energy and exergy efficiencies (Li et al., 2007; Ozgener and Hepbasli, 2007; Balkan et al., 2005; Cornelissen, 1997; Wall, 2003).

The mass balance equation can be expressed in the rate form as

$$\sum \dot{m}_{in} = \sum \dot{m}_{out} \tag{6.5}$$

The general exergy balance for a control region can be written as follows

$$\sum \dot{E}x_{in} - \sum \dot{E}x_{out} = \sum \dot{E}x_{dest} \tag{6.6}$$

or

$$\dot{E}x_{heat} - \dot{E}x_{work} + \dot{E}x_{mass,in} - \dot{E}x_{mass,out} = \dot{E}x_{dest} \tag{6.7}$$

with

$$\dot{E}x_{work} = \dot{W} \tag{6.8}$$

$$\dot{E}x_{mass,in} = \sum \dot{m}_{in}\psi_{in} \tag{6.9}$$

$$\dot{E}x_{mass,out} = \sum \dot{m}_{out}\psi_{out} \tag{6.10}$$

where $\dot{W}$ is the power consumption rate. The exergy associated with the heat transfer on the control surface is determined by the maximum work that could be obtained using the environment as a reservoir of thermal energy (Kotas, 1985). For a heat transfer rate $\dot{Q}$ through the boundary at temperature T the heat exergy is:

$$\dot{E}x_{heat} = \sum \left(1 - \frac{T_0}{T}\right)\dot{Q} \tag{6.11}$$

The specific stream exergy of a fluid in a steady-flow process with kinetic and potential-energy changes neglected can be calculated as:

$$\varphi = (h - h_0) - T_0(s - s_0) \tag{6.12}$$

where h is enthalpy, s is entropy, and the subscript zero indicates properties at the restricted dead state of P_0 and temperature T_0.

Then, the exergy change of a fluid with mass flow rate $\dot{m}$ between the two states is:

$$\psi_2 - \psi_1 = \dot{m}\left(h_2 - h_1 - T_0\left(s_2 - s_1\right)\right) \tag{6.13}$$

Numerous ways of formulating exergetic (or exergy or second-law) efficiency for various energy systems are given in Ref. (Cornelissen, 1997). It is very useful to define efficiencies based on exergy. Whereas there is no standard set of definitions in the literature, two different approaches are generally used – one is called "brute-force", the other is called "functional" (Dipippo, 2004).

The "brute-force" exergy efficiency is defined as the ratio of the sum of all output exergy terms to the sum of all input exergy terms. While a "functional" exergy efficiency for any system is defined as the ratio of the exergy associated with the desired energy output to the exergy associated with the energy expended to achieve the desired output.

Here, in a similar way, exergy efficiency is defined as the ratio of total exergy output to total exergy input, i.e.

$$\varepsilon = \frac{\dot{E}x_{output}}{\dot{E}x_{input}} = 1 - \frac{\dot{E}x_{dest}}{\dot{E}x_{input}} \tag{6.14}$$

where “output or out” stands for “net output” or “product” or “desired value” or “benefit”, and “input or in” stands for “given” or “used” or “fuel”. It is clear that the brute-force definition can be applied in a straightforward manner, irrespective of the nature of the component, once all exergy flows have been determined. The functional definition, however, requires judgment and a clear understanding of the purpose of the system under consideration before the working equation for the efficiency can be formulated (Dipippo, 2004).

On the basis of the aforementioned formulations about exergy analysis and the operating characteristics of the system, it is convenient to deduce the exergy decreases and gains for each of the multi-functional SAHP system components, which is illustrated in Table 6.1.

Table 6.1 Exergy analysis for the system components

Component	Exergy input $\dot{E}x_{in}$ (kW)	Exergy output $\dot{E}x_{out}$ (kW)	Irreversibility $\dot{E}x_{dest}$ (kW)
Solar collector	$\dot{E}x_{scol}$	$m_{w2}\psi_{w2} - m_{w1}\psi_{w1}$	$\dot{E}x_{scol} - m_{2w}\psi_{2w} + m_{1w}\psi_{1w}$
Compressor	$\dot{W}_{com}$	$m_r\left(\psi_{r13} - \psi_{r12}\right)$	$\dot{W}_{com} - m_r\left(\psi_{r13} - \psi_{r12}\right)$
Evaporator	$m_r\left(\psi_{r10} - \psi_{r11}\right)$	$m_{15w}\left(\psi_{16w} - \psi_{15w}\right)$	$m_r\left(\psi_{r10} - \psi_{r11}\right) - m_{15w}\left(\psi_{16w} - \psi_{15w}\right)$
Desuperheater	$m_r\left(\psi_{r13} - \psi_{r14}\right)$	$m_{6w}\left(\psi_{7w} - \psi_{6w}\right)$	$m_r\left(\psi_{r13} - \psi_{r14}\right) - m_{6w}\left(\psi_{7w} - \psi_{6w}\right)$
Condenser	$m_r\left(\psi_{r8} - \psi_{r9}\right)$	$Q_a\left(1 - \frac{T_0}{\bar{T}_a}\right)$	$m_r\left(\psi_{r8} - \psi_{r9}\right) - Q_a\left(1 - \frac{T_0}{\bar{T}_a}\right)$
Expansion valve	$m_r\psi_{r9}$	$m_r\psi_{r10}$	$m_r\left(\psi_{r9} - \psi_{r10}\right)$

Van Gool (1997) has also proposed that maximum improvement in the exergy efficiency for a process or system is obviously achieved when the exergy loss or irreversibility is minimized. Consequently, he suggested that it is useful to employ the concept of an exergetic "improvement potential" when analyzing different processes. In this thesis, except for the exergy and energy efficiencies, the Van Gool's improvement potential (*IP*) is evaluated as:

$$IP = (1-\varepsilon)\left(\dot{E}x_{in} - \dot{E}x_{out}\right) \tag{6.15}$$

6.3.2 Calculation methods of related thermodynamic properties

Three kinds of substances are involved during the operation of the MSA-ASHP system. Some basic thermodynamic properties (i.e. enthalpy and entropy) of these substances are necessary for the exergy analysis as shown in the above section. The corresponding calculation methods for the related thermodynamic properties are described in the following sections.

6.3.2.1 The thermodynamic properties of water

The enthalpy of water is obtained based on the following equation:

$$
\begin{aligned}
h_w \Big/ 70120.4 &= A_0\theta - \sum_{n=1}^{10}(n-2)A_n\theta^{n-1} \\
&+ A_{11}\left\{Z\left[17\left(\frac{Z}{29}-\frac{Y}{12}\right)+5\theta\frac{Y'}{12}\right]+a_4\theta-(a_3-1)\theta YY'\right\}Z^{-5/17} \\
&+\left[A_{12}-A_{14}\theta^2+A_{15}(9\theta+a_6)(a_6-\theta)^9+A_{16}\left(20\theta^{19}+a_7\right)\left(a_7+\theta^{19}\right)^{-2}\right]\beta \\
&-\left(12\theta^{11}+a_8\right)\left(a_8+\theta^{11}\right)^{-2}\left(A_{17}\beta+A_{18}\beta^2+A_{19}\beta^3\right)+A_{20}\beta^{18}\left(17a_9+19\theta^2\right) \\
&\times\left[(a_{10}+\beta)^{-3}+a_{11}\beta\right]+A_{21}a_{12}\beta^3+21A_{22}\theta^{-20}\beta^4
\end{aligned}
\tag{6.16}
$$

where,

$Y = 1 - a_1\theta^2 - a_2\theta^{-6}$,

$Y' = -2a_1\theta + 6a_2\theta^{-7}$,

$Z = Y + \left(a_3Y^2 - 2a_4\theta + 2a_5\beta\right)^{1/2}$

h_w = the water enthalpy under temperature T_w, J/kg;

θ = reduced temperature, $\theta = T_w/T_{w,cr}$, $T_{w,cr}$ is the critical temperature (647.3K);

β = reduced pressure, $\beta = P_w/P_{w,cr}$, $P_{w,cr}$ is the critical pressure (22.12Mpa).

As for the entropy of water, it is calculated as:

$$
\begin{aligned}
s_w \Big/ 108.32 &= A_0\ln\theta - \sum_{n=2}^{10}(n-1)A_n\theta^{n-2} + A_{11}\left\{\left[\frac{5}{12}Z-(a_3-1)Y\right]Y'+a_4\right\}Z^{5/17} \\
&+\left[-A_{13}-2A_{14}\theta+10A_{15}(a_6-\theta)^9+19A_{16}\left(a_7+\theta^{19}\right)^{-2}\theta^{18}\right]\beta \\
&-11\left(a_8+\theta^{11}\right)^{-2}\theta^{10}\left(A_{17}\beta+A_{18}\beta^2+A_{19}\beta^3\right)+A_{20}\theta^{17}\left(18a_9+20\theta^2\right) \\
&\times\left[(a_{10}+\beta)^{-3}+a_{11}\beta\right]+A_{21}\beta^3+20A_{22}\theta^{-21}\beta^4
\end{aligned}
\tag{6.17}
$$

where S_w is the entropy of water at temperature T_w, J/kg. The related coefficients involved in the calculation are shown in Table 6.2.

Table 6.2 Related coefficients for water thermodynamic properties

Item	Value	Item	Value	Item	Value
A_0	$6.824787741 \times 10^{3}$	A_{12}	$-2.616571843 \times 10^{-2}$	a_1	$8.438375405 \times 10^{-1}$
A_1	$-5.422063673 \times 10^{2}$	A_{13}	$1.522411790 \times 10^{-3}$	a_2	$5.362162162 \times 10^{-4}$
A_2	$-2.0966666205 \times 10^{4}$	A_{14}	$2.284279054 \times 10^{-2}$	a_3	1.72
A_3	$3.941286787 \times 10^{4}$	A_{15}	$2.421647003 \times 10^{2}$	a_4	$7.342278489 \times 10^{-2}$
A_4	$-6.733277739 \times 10^{4}$	A_{16}	$1.269716088 \times 10^{-10}$	a_5	$4.97585887 \times 10^{-2}$
A_5	$9.902381028 \times 10^{4}$	A_{17}	$2.074838328 \times 10^{-7}$	a_6	6.5371543×10^{-1}
A_6	$-1.093911774 \times 10^{5}$	A_{18}	$2.17402035 \times 10^{-8}$	a_7	1.15×10^{-6}
A_7	$8.590841667 \times 10^{4}$	A_{19}	$1.105711498 \times 10^{-9}$	a_8	1.5108×10^{-5}
A_8	$-4.511168742 \times 10^{4}$	A_{20}	$1.293441934 \times 10^{1}$	a_9	1.4188×10^{-1}
A_9	$1.418138926 \times 10^{4}$	A_{21}	$1.308119072 \times 10^{-5}$	a_{10}	7.002753165
A_{10}	$-2.017271113 \times 10^{3}$	A_{22}	$6.047626338 \times 10^{-14}$	a_{11}	$2.995284926 \times 10^{-4}$
A_{11}	7.982692717			a_{12}	2.04×10^{-1}

6.3.2.2 The thermodynamic properties of air

The enthalpy of air can be evaluated using the following equation:

$$h(T) = 1000 \sum_{n=1}^{4} a(n) T^{n} \tag{6.18}$$

where $h(T)$ stands for the enthalpy of air at temperature T, J/kg; $a(n)$ are the related coefficients, and the detailed values are:

$a(1)=0.12074\times10^{2}$, $a(2)=0.924502$, $a(3)=0.115984\times10^{-3}$,

$a(4)=-0.563568\times10^{-8}$

The air entropy is calculated as:

$$s(T)=1000\left[\sum_{n=1}^{2}b(n)T^{n}+b(3)\ln(T)\right] \tag{6.19}$$

where $s(T)$ is the air entropy at temperature T, J/kg; $b(n)$ are related coefficients, and the following specific values are adopted:

$b(1)=1.386989$, $b(2)=0.18493\times10^{-3}$, $b(3)=0.95$

6.3.2.3 The thermodynamic properties of refrigerant

As mentioned in Chapter 3, the enthalpy of the refrigerant is calculated using the simplified model proposed by Cleland (1986). For the entropy calculation, the following equations are adopted.

For the saturated vapor, the entropy is expressed as:

$$s_g=-T_c^{-1}\int\left(\frac{\partial p}{\partial T_r}\right)_p\rho^{-2}d\rho+s_0+s_c \tag{6.20}$$

where s_g is the entropy of the saturated refrigerant vapor, J/(kg.K); T_c is the critical temperature of refrigerant; T_r is the reduced temperature of refrigerant; P is refrigerant pressure; ρ is the density of refrigerant vapor; s_0 is the constant-volume entropy; s_c is a related constant (Rankhesh et al., 2003).

For the saturated liquid refrigerant, the entropy is calculated as:

$$s_l = s_g - \frac{1}{10}\left(\frac{1}{\rho_g} - \frac{1}{\rho_l}\right)\frac{dp_s}{dT} \tag{6.21}$$

where s_l is the entropy of the saturated liquid refrigerant; ρ is the density of refrigerant; p_s is the saturated vapor pressure; the subscripts g and l stand for vapor and liquid respectively.

6.3.3 Exergy analysis in the AC/WH mode

As illustrated in Figure 6.1, the multi-functional SAHP system can be divided into two sections, i.e. the solar collector circuit and the multifunctional ASHP unit, which are coupled by the storage tank for hot water supply. The former part includes the solar collector, the preheating tank and two water pumps, while the latter consists of a rolling piston compressor, a thermostatic expansion valve, three heat exchangers (desuperheater, condenser and evaporator) and one water pump.

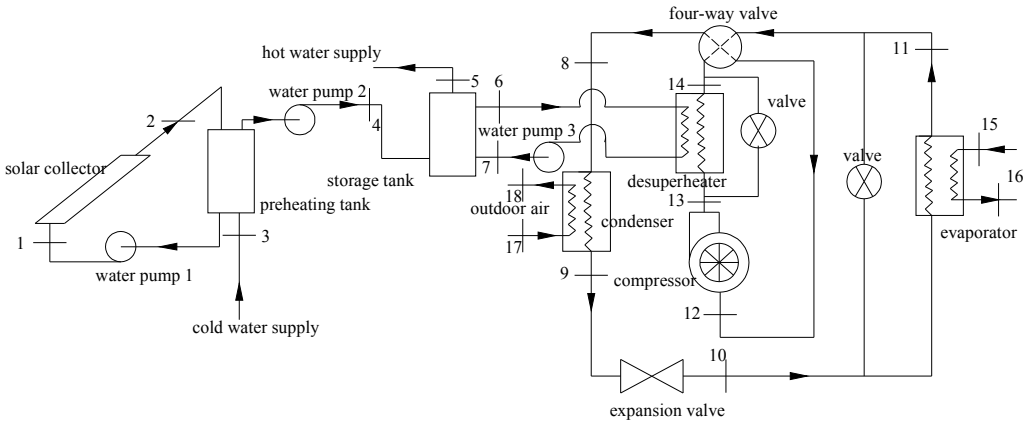

Figure 6.1 MSA-ASHP system in the AC/WH mode for Exergy Analysis

6.3.3.1 Exergy equations in the AC/WH mode

Taking the AC/WH mode as an example, the exergy efficiencies of two major circuits of the MSA-ASHP system are evaluates as follows:

- The solar collector circuit

$$\dot{E}x_{in,scol} = \dot{E}x_{scol} + \dot{E}x_{3w} + \dot{W}_{pump,1} + \dot{W}_{pump,2} \tag{6.22}$$

The Petela expression (Petela, 2003; Petela, 2005) is used in calculating the exergy of solar radiation ($\dot{E}x_{scol}$) as the exergy input to the solar collector.

$$\dot{E}x_{scol} = AI_t\left[1+\frac{1}{3}\left(\frac{T_0}{T_{sr}}\right)^4 - \frac{4}{3}\left(\frac{T_0}{T_{sr}}\right)\right] \tag{6.23}$$

where T_{sr} is the solar radiation temperature and taken to be 6000K; A is the solar collector area, m^2; I_t is the total solar radiation on the tilt surface, W/m^2.

$$\dot{E}x_{out,scol} = \dot{E}x_{4w} \tag{6.24}$$

$$\varepsilon_{scol} = \frac{\dot{E}x_{4w}}{\dot{E}x_{scol} + \dot{E}x_{3w} + \dot{W}_{pump,1+}\dot{W}_{pump,2}} \tag{6.25}$$

- The multifunctional ASHP unit

$$\dot{E}x_{in,unit} = \dot{W}_{comp} + Q_{evp}\left(\frac{T_0}{\bar{T}_{wc}} - 1\right) + \dot{W}_{pump,3} \tag{6.26}$$

where $\bar{T}_{wc}$ means the average chilled water temperature in the evaporator.

The exergy output of the unit is the sum of the exergy gains in the desuperheater and condenser:

$$\dot{E}x_{out,unit} = Q_{des}\left(1 - \frac{T_0}{\bar{T}_w}\right) + Q_{con}\left(1 - \frac{T_0}{\bar{T}_{air}}\right) \tag{6.27}$$

where $\bar{T}_w$ means the average hot water temperature in the desuperheater and $\bar{T}_{air}$ is the average air temperature throughout the condenser.

Therefore, the exergy efficiency of the multifunctional ASHP unit is calculated as follows:

$$\varepsilon_{unit} = \frac{Q_{des}\left(1-\frac{T_0}{\bar{T}_w}\right)+Q_{con}\left(1-\frac{T_0}{\bar{T}_{air}}\right)}{\dot{W}_{com}+Q_{evp}\left(\frac{T_0}{\bar{T}_{wc}}-1\right)+\dot{W}_{pump,3}} \tag{6.28}$$

6.3.3.2 Discussion on exergy results in the AC/WH mode

For exergy analysis in the AC/WH mode, based on the recorded experimental data, the dead state is taken as the average state of the local atmospheric air during the experimental test, which are P_0=1 atm and T_0=26.94℃.

In the present study, a more precise method (Holman, 2001) of estimating uncertainty in experimental results is employed as introduced in Chapter 4. Based on the measured data and their uncertainties, the relative uncertainty of the COP was found to be within 9.6% and the relative uncertainty of the exergy efficiency varied from 7.8 % to 10% in the concerned experiments.

Based on these calculation methods together with the recorded data of the selected operating point, the detailed property data is calculated and shown in Table 6.3.

The exergy analysis results are listed in Table 6.4. It can be found that the greatest irreversibility occurs in the solar collector, followed by the evaporator, the compressor, the desuperheater, the condenser and the thermostatic expansion valve.

As seen in Table 6.4, the exergy efficiency of the solar collector is the lowest of all components since the highest exergy destruction occurs in this part. Solar energy is highly inefficient from the standpoint of avoiding the one-way destruction of exergy.

Therefore, solar energy should be first used in high temperature applications. The thermal energy from those first applications can be then cascaded to applications at lower temperatures, eventually.

Irreversibility in three heat exchangers (i.e. evaporator, desuperheater and condenser) is mainly caused by the temperature differences between the two heat exchanger fluids, pressure losses and heat transfer with the environment. In the present system, the experimental data show that the greatest pressure loss (0.56MPa) occurs in the evaporator, which may be the main cause that the evaporator has the greatest exergy loss among three heat exchangers.

It is known that the input work consumed by the compressor depends heavily on the inlet and outlet pressures. Hence, any heat exchanger improvement that reduces the temperature difference will decrease the compressor power consumption by bringing the condensing and evaporating temperatures closer. In this way, the compressor irreversibility can be reduced and its exergy efficiency is increased accordingly. In this study, the exergy efficiency of the compressor is 61.2%.

The exergy efficiencies of the solar collector loop and the multi-functional ASHP unit are calculated based on equations (6.25) and (6.27). The exergy efficiency of the solar collector loop (10.48%) is a little lower than that (14.53%) of the similar solar collector circuit in Hepbasli's study (Hepbasli, 2007). That may be because the work input consumed by water pumps in the solar collector loop is considered in the present study. The exergy efficiency of the multi-functional ASHP unit is about 13.4%, while its

COP reaches 2.98. Compared with a conventional air conditioner, which has a COP around 2.4, the proposed system shows 24.2% higher system performance.

Van Gool's improvement potential (*IP*) is calculated for each component of the system as shown in Table 6.4. It is indicated that the solar collector has the largest *IP* value with 0.97kW, followed by the evaporator, the compressor, the desuperheater and the condenser with 0.61, 0.16 and 0.12kW, respectively.

Table 6.3 Property data of the system

State no.	Fluid	Temperature T(℃)	Enthalpy h(kJ/kg)	Entropy s(kJ/kg K)	flow rate m(kg/s)
0	Air	26.94	0.999	0.0406	----
1	Water	35	146.63	0.5051	0.18
2	Water	39.5	165.44	0.5657	0.18
3	Water	25	104.83	0.3672	0.18
4	Water	37	156.24	0.5361	0.18
6	Water	39.5	165.44	0.5657	0.18
7	Water	40.8	185.09	0.628	0.18
8	R22	35.1	243.1	1.146	0.043
9	R22	32	239.2	1.133	0.043
10	R22	11.6	239.2	1.134	0.043
11	R22	14.8	414.9	1.777	0.043
12	R22	11.9	411	1.725	0.043
13	R22	62.6	437.2	1.763	0.043
14	R22	35.1	243.1	1.146	0.043
15	Water	18	75.54	0.2677	0.12
16	Water	13.8	57.95	0.2069	0.12
17	Air	26.94	0.999	0.041	0.65
18	Air	30.4	1.225	0.046	0.65

Table 6.4 Exergy analysis results of the system

Component	Exergy input $\dot{E}x_{in}$ (kW) (kW)	Exergy output $\dot{E}x_{out}$ (kW)	Irreversibility $\dot{E}x_{dest}$ (kW)	Exergy efficiency ε (%)	IP
Solar collector	1.18	0.11	1.07	9.5	0.97
Compressor	1.04	0.64	0.4	61.2	0.16
Evaporator	0.76	0.08	0.68	10.53	0.61
Desuperheater	0.38	0.17	0.21	44.74	0.12
Condenser	0.16	0.02	0.14	12.5	0.12
Expansion valve	2.83	2.77	0.06	97.88	0.001
Solar collector loop	1.24	0.13	1.11	10.48	0.99
ASHP unit	2.54	0.34	2.2	13.4	1.91

6.4 Case Study

As described in Chapter 5, three different experiments which are corresponding to different operating modes have been conducted based on the built sample system. In order to further investigate the exergy and energy performance of the MSA-ASHP system, the actual exergy efficiencies of the three experiments together with the COP values are calculated according to the experimental data. The detailed experimental conditions have been presented in Chapter 5.

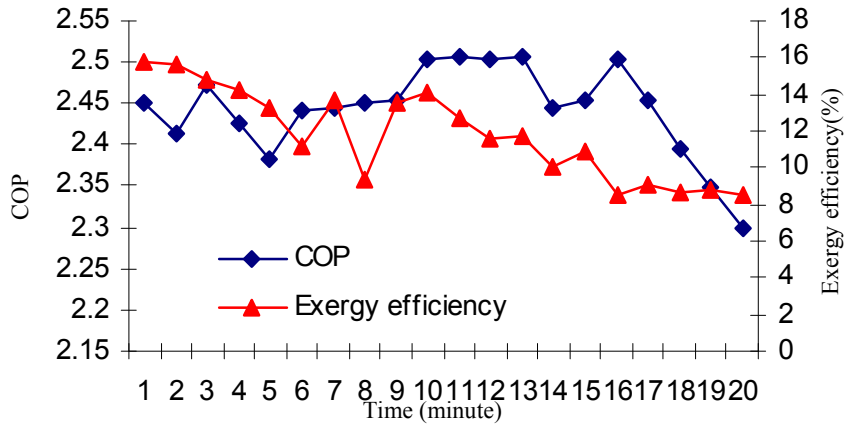

Figure 6.2 Exergy efficiency and COP in only AC mode

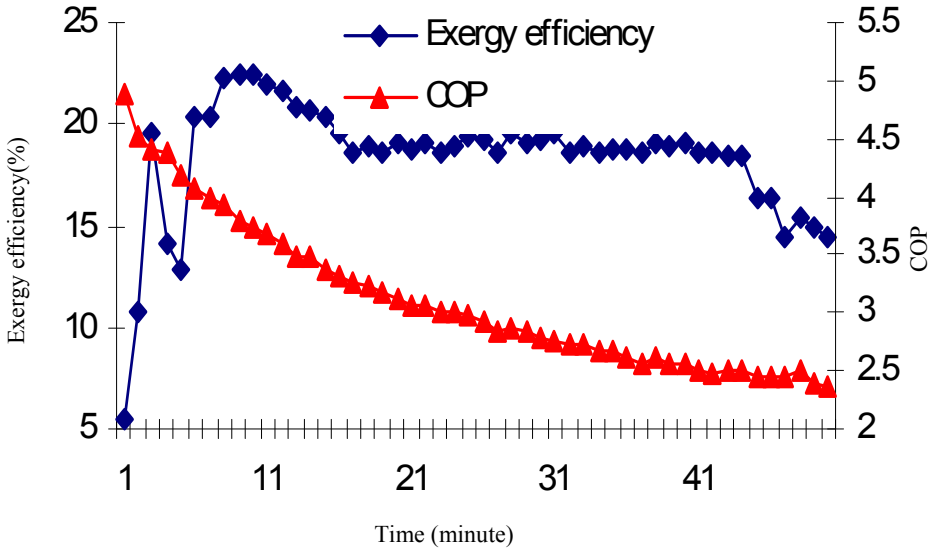

Figure 6.3 Exergy efficiency and COP in AC/WH mode

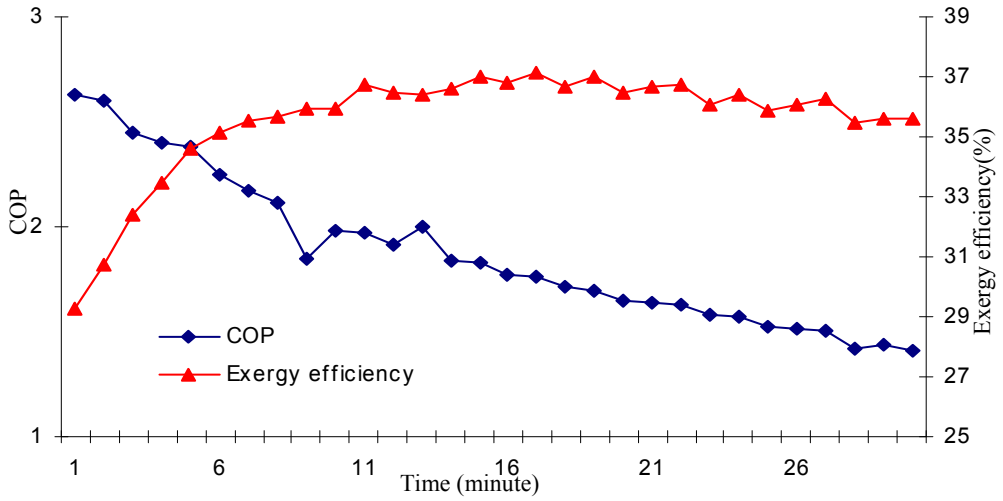

Figure 6.4 Exergy efficiency and COP in only WH mode

The variations of energy and exergy efficiencies in the two cases of the only AC and AC/WH modes are illustrated in Figure 6.2 and Figure 6.3 respectively. In general, compared with the only AC mode, the AC/WH mode behaved a distinctly higher operating performance associated with the energy and exergy efficiencies due to the useful energy gain of the domestic hot water. As shown in Figure 6.2, the exergy efficiency of the only AC mode was decreased from 16% to 9% with operating time. For the AC/WH mode, whereas, its exergy efficiency was found to be firstly increased to a high value of about 22% during several minutes and then decreased as the operation processed. This is due to the fact that the increase rate in the exergy gain of the domestic hot water was larger than that relative increase rate of power consumption at the beginning of the experiment and, after several minutes, the power input played a dominant role in determining the exergy efficiency.

Figure 6.4 shows the variation of the COP and the exergy efficiency of the proposed system in the only WH mode. It can be found that the average value of COP was around

2.0 during the considered experimental period, which is greatly higher than that of the conventional hot water heaters. The COP was obviously reduced with the operating time. That is because the increased domestic hot water temperature resulted in the continual growth of the compressor power consumption. However, the corresponding exergy efficiency was increased from 29% to 36%. The contrary changing trends between the COP and the exergy efficiency reveal that higher COP of a MSA-ASHP system may not represent a higher exergy efficiency which should be further investigated by co-analysis of exergy and energy.

6.5 Comparisons with Commonly Used Hot Water Heating Systems

In order to further analyze the operating performance of the MSA-ASHP system, a meaningful comparison of energy and exergy efficiencies has been conducted between the proposed system and the other three kinds of commonly used systems with respect to domestic hot water supply. The considered systems include the electric water heater, the gas-fired water heater and the conventional ASHP system. Based on a series of experimental data, the energy performance of the MSA-ASHP system can be expressed as a function of the average domestic hot water (DHW) temperature ($\overline{T}_{DHW}$). A second-order polynomial regression is employed to fit the correlation of energy performance (i.e. COP). The fitted equation is given as follows:

$$COP_{MSA-ASHP} = 0.0049\overline{T}_{DHW}^{\,2} - 0.519\overline{T}_{DHW} + 15.71 \tag{6.29}$$

When the comprehensive performance data of a heat pump unit from manufacturers are available, the relationship between its energy performance (i.e. COP_{ASHP}) and the

average DHW temperature can be obtained through a linear regression of the catalog data. In this case, an ASHP unit with the same nominal capacity as the designed system is selected for comparison. Similarly, a second-order polynomial equation is given as:

$$COP_{MSA-ASHP} = 0.0015\overline{T}_{DHW}^{\,2} - 0.1893\overline{T}_{DHW} + 7.5826 \tag{6.30}$$

Based on the second law of thermodynamics, the exergy efficiency of an electric water heater can be expressed as:

$$\varepsilon_{elec} = \frac{Q_{DHW}\left(1-\frac{T_{env}}{\overline{T}_{DHW}}\right)}{Q_{DHW}/\eta_{elec}} = \left(1-\frac{T_{env}}{\overline{T}_{DHW}}\right)\cdot\eta_{elec} \tag{6.31}$$

The exergy efficiency of the gas-fired water heater is evaluated as:

$$\varepsilon_{gas} = \frac{Q_{DHW}\left(1-\frac{T_{env}}{\overline{T}_{DHW}}\right)}{\left(Q_{DHW}/\eta_{gas}\right)\cdot\varphi} = \left(1-\frac{T_{env}}{\overline{T}_{DHW}}\right)\cdot\eta_{gas}\Big/\varphi \tag{6.32}$$

where Q_{DHW} is the heat gain by the DHW; T_{env} is the environmental temperature which equals the outdoor air temperature; η_{elec} means the energy efficiency of the electric water heater which is assumed to be 95%; η_{gas} is the energy efficiency of the gas-fired water heater which is proposed to be 85% and φ is the ratio of specific chemical exergy of the gas to its net calorific value (1.04) (Kotas, 1985).

The exergy efficiency of the ASHP system can also be deduced based on the second law of thermodynamics:

$$\varepsilon_{ASHP} = \left(1 - \frac{T_{env}}{\overline{T}_{DHW}}\right) \cdot COP_{ASHP} \tag{6.33}$$

Based on the aforementioned assumptions and equations (6.29) through (6.33), the energy and exergy efficiency of four different DHW supply systems were calculated under the specific operating conditions of $T_{env} = 25$℃ and $\overline{T}_{DHW}$ in the wide range of 30-50℃. The investigation results are shown in Figures 6.5 and 6.6.

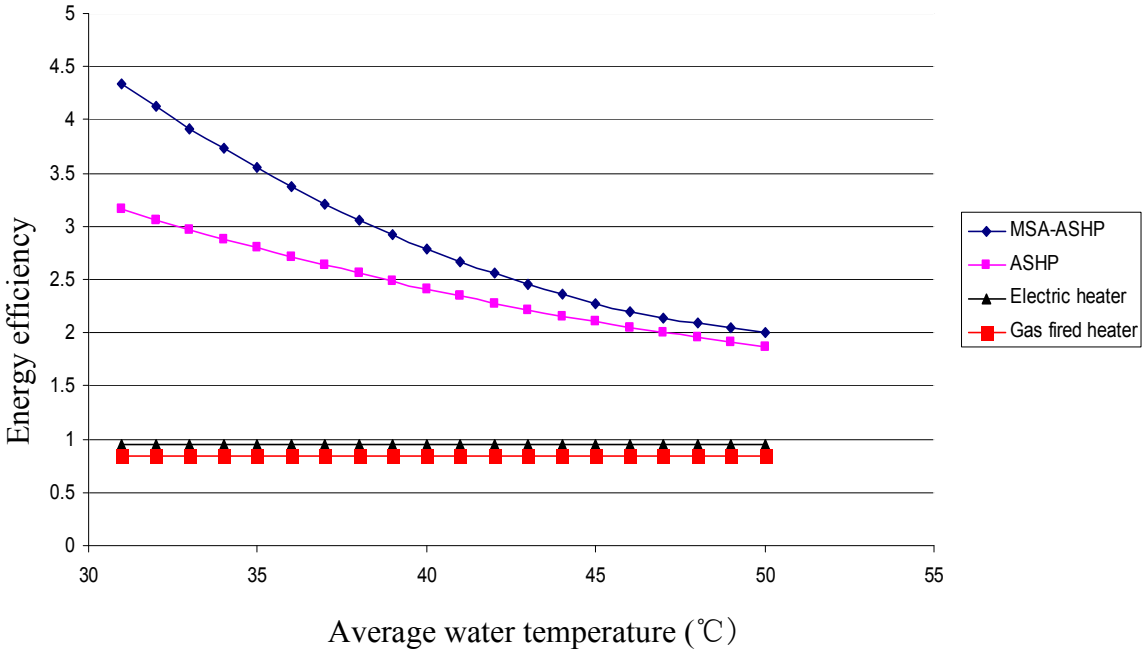

Figure 6.5 Comparison of energy performance

It can be observed from Figure 6.5 that the MSA-ASHP system resulted in the highest energy performance which ranges from 4.3 to 2.0. It is followed by the ASHP system (3.2-1.9), the electric water heater (0.95) and the gas-fired water heater (0.85). Consequently, the energy performance of the MSA-ASHP system is 18.9% higher

compared with that of the conventional ASHP system and significantly more energy can be saved as compared with the electric water heater and the gas-fired water heater.

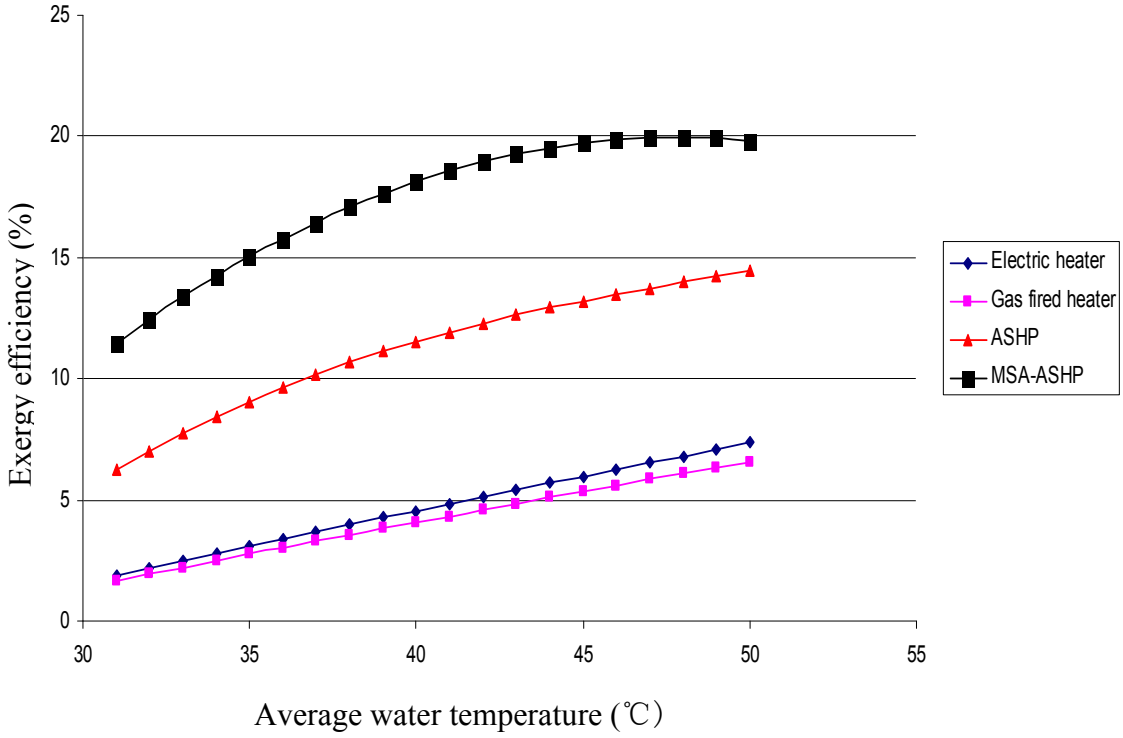

Figure 6.6 Comparison of exergy efficiencies

As shown in Figure 6.6, similarly, the MSA-ASHP system offered the highest exergy efficiency of about 20%, followed by the ASHP system which has a relatively higher value of 14.4%. When it comes to the electric water heater and gas-fired water heater, the maximum efficiencies are only 7.3% and 6.6% respectively.

From Figure 6.6, it can also be found that the increasing rate of exergy efficiencies of the MSA-ASHP and ASHP systems decreases as the average water temperature increases. The reduction can be explained through the fact that the growth of the power consumption becomes a major role in the exergy efficiencies rather than the increase of

the exergy gain in the case of the high temperature of $\overline{T}_{DHW}$. On the other hand, the exergy efficiencies of the electric water heater and gas-fired water heater are always increases with the rise of $\overline{T}_{DHW}$ owing to the gradually reduced difference of energy quality between the energy supplied to the system and system output, say the hot water. Unfortunately, their exergy efficiencies were still much lower than those of the MSA-ASHP and ASHP systems, even at the highest DHW temperature. The low exergy efficiencies of the electric water heater and gas-fired water heater indicate a poor match between the quality of energy supplied to the system and the quality of output produced by the system. This mismatch obviously results in considerable irreversible losses because of the large irreversible heat transfer. Therefore, it is not economical to supply DHW using the commonly used water heaters, say electric water heater and gas-fired water heater.

6.6 Summary

The exergetic modeling and performance evaluation of the MSA-ASHP system were conducted in this chapter. Appropriate exergy equations are derived for the considered system and its each component. Based on experimental data, the energy and exergy performances of the MSA-ASHP system in three different operation modes have been analyzed. Some specific conclusions of this investigation can be drawn as follows.

The greatest irreversibility on the whole system occurs in the solar collector, followed by the evaporator, the compressor, the desuperheater, the condenser and the thermostatic expansion valve according to the detailed exergy analysis for each component of the proposed system in the AC/WH mode. Solar energy is highly

inefficient from the standpoint of avoiding the one-way destruction of exergy. For the multi-functional ASHP unit, more attention should be paid to the evaporator to reduce its exergy loss. The exergy destruction in the compressor in this study was also significant. The external exergy loss in the compressor due to the electrical and mechanical efficiencies can be significantly reduced by improving the performance of the motors, valves or lubrication systems. The internal exergy loss due to the fluid friction and the pressure difference in the compressor can be progressively reduced by decreasing the condensing and evaporation pressure difference.

The exergy efficiencies of the solar collector loop and the multi-functional air source heat pump unit are 10.48% and 13.4% respectively. The COP of the studied system reaches 2.89 which is 24.2% larger than that of the conventional air conditioner. In addition, the solar collector has the highest improvement potential value, followed by the evaporator, the compressor, the desuperheater and the condenser.

The case study shows that a higher COP of the MSA-ASHP system may not represent a higher exergy efficiency. The optimal operating condition may be obtained for the MSA-ASHP system to achieve high energy efficiency and simultaneously to keep high exergy efficiency through the co-analysis of the first and second laws of thermodynamics.

The comparison analysis among the four different DHW heating systems shows that the MSA-ASHP system has the highest energy and exergy efficiencies. The significantly low exergy efficiencies of the conventional water heaters are caused by the mismatch of the high quality energy supply and low quality energy demand. All investigation above

demonstrates that this novel MSA-ASHP system is a good choice for buildings with heating and cooling loads throughout a year, e.g. residential buildings, hotels, hospitals and other commercial/industrial buildings in subtropical areas.

CHAPTER 7 ANNUAL ENERGY PERFORMANCE PREDICTION AND ECONOMIC ANALYSIS

7.1 Introduction

In order to find the annual energy saving of the MSA-ASHP system, the accurate typical meteorological year (TMY) data for simulations is needed. In this chapter, the TMY is firstly developed using a relatively simple procedure (i.e. Weather Year for Solar Systems, WYSS). The simulation model developed in Chapter 3 and the synthetically generated weather data are incorporated in the annual performance prediction program. For the solar collector loop, the monthly performance is also analyzed based on the basic mathematical correlations adopted in the F-chart method (Haberl, 2004). The investigation results indicate that the generated typical weather year data gives better accuracy than that of other available weather data. The annual simulation results show that the monthly solar fraction of the system can reach 61.8% on an average. The monthly average system COP value is 3.0 throughout a year. The annual energy saving of 54.9% can be achieved when the MSA-ASHP system is adopted instead of an electric water heater plus a conventional air conditioner. The life cycle saving (LCS) analysis for using the MSA-ASHP system in Hong Kong is conducted as compared to the conventional ASHP system with an electric water heater.

7.2 Development of Typical Meteorological Year

Predicting the performance of a solar system by using simulation methods requires weather data input from the location where the system is being installed. These sets of data should depict the weather pattern of the location, examples of which are widely known as Typical Meteorological Year (TMY), Weather Year for Energy Calculations (WYEC) and Test Reference Year (TRY). In Hong Kong, TMY and TRY are generally used. The example weather year of Hong Kong which is deemed as TRY data was developed by Wong and Ngan (1993), using 13 years real hourly weather data (from 1979-1991).The selection criterion of TRY is based on the smallest deviation from the long term historical years' values and the year 1989 was selected as the example year. The TRY selected tends to be rather mild, extremely high or low mean temperatures were progressively eliminated, thus not necessarily reflecting the prevailing ''average'' weather conditions. To address the shortcomings of the TRY, more sophisticated TMY was developed by Chow and Chan (2006) using the hourly measured weather data of a 25 year period (1979-2003) in Hong Kong. Unlike the TRY, the TMY is not an actual past year. It is composed of 12 typical meteorological months (TMMs) that selected by comparing their cumulative distribution function (CDF) with the long-term CDF. By considering the weighting factor of the annual and monthly mean values of major weather indices, the month with the smallest deviation from the mean value is taken as 'standard' month and used for formulation of a TMY. The selection of TMY is highly relays on the weighting factors of the different metrological variables.

For strict statistical significance, different energy systems will have different TMYs. The aforementioned studies are mostly for building energy simulation and may not be appropriate to address the renewable energy application systems such as wind and solar

energy applications. Yang and Lu (2002) studied the impact of different TMYs and EWYs according to their different weather parameters and weighting factors and concluded that the right weighting factors of meteorological parameters play an important role in the process of generating TMYs for renewable energy application systems and the persistent structure of meteorological parameters is also important in affecting the reliability and initial cost of these kind of renewable energy system with energy storage. Argiriou et al. (1999) presented more detailed examination of 17 major TMY selection methodologies reported in literature and those obtained TRYs were evaluated according to their impact on performance simulations for flat plate solar collector, photovoltaic, large scale solar heating system with seasonal storage and the annual heating and cooling loads of a typical building. They found that the optimal TRY differs from system to system. These differences may lead to erroneous conclusions on the performance, the sizing and feasibility assessment of a certain energy system.

The earlier studies reveal that the selection of the TMY or TRY greatly depend on the weighting factors and for different energy system the TMY or TRY may not be the same for best performance evaluation and prediction. Further more, none of the aforementioned methods for deriving TMY take the sensitivity of the system into account. Thus, in this research, a new method – Weather Year for Solar Systems (WYSS) proposed by Gazela and Mathioulakis (2000) is adopted for determining a set of typical weather data in order to evaluate the long-term performance of the MSA-ASHP system.

7.2.1 Development of methodology

Several methods for TMY generation have been reported in the literature. Procedures have been reported by Klein et al. (1976), Crow (1981), ASHRAE Fundamentals (1997), Bahadori and Chamberlain (1985), Pissimanis et al. (1988), Festa and Ratto (1993), Marion and Urban (1995). The primary objective of these methods is to select single years or single months from a multi-year database, preserving a statistical correspondence. This means that the occurrence and the persistence of the weather should be as similar as possible in the TMY to all available years. In addition, the aforementioned methods often seem rather complicated when put into use. Moreover, these methods significantly change the final selected 'typical' months or years in the same way as the results of the long term prediction of the system performance. This could lead to dubious results for the behavior of the system and may give rise to confusion, especially when the system is being tested.

In this research, the WYSS procedure is adopted to generate the TMY data. This method is quite straightforward, easily applicable and can be reliably applied in predicting the long term performance of a solar hot water heating system, minimizing the error in the estimation. The optimum selection of each individual month, considering this error, relies on the observation that the solar sensitivity of the solar system to weather pattern affects the accuracy of the prediction. Thus the primary difference of the WYSS procedure from the existing ones is that it is system oriented. On the one hand, this solves the problems which derive from the subjectivity of the criteria for generating TMY data and on the other hand makes the WYSS procedure more suitable for testing solar hot water heating systems.

7.2.2 The WYSS procedure

All the aforementioned methods for TMY data generation aim to represent the weather pattern at a particular location. Special care is given to choosing months (or years in the US National Oceanic and Atmospheric Administration Method, i.e. NOAA method) where weather sequences and persistence maintain correspondence to long-term data. However, through the literature review, typicality appears subjective. This is due to the fact that the selection criteria for typical months or year are based mostly on mathematical and statistical methods rather than the natural operation of the system. Besides, a remarkable fluctuation is noted among the typical months selected according to these existing procedures. Moreover, the final results such as the monthly delivered power of the system when long term performance is estimated, are significantly different (Argiriou et al., 1999). This could be a serious problem, especially when a solar system is tested and the final conclusions for the system should be reliable and accurate.

The most important criterion for selecting typical months is the use to which the data is being put since typicality inevitably remains subjective. The WYSS procedure is directed towards the prediction of long term behavior of a solar hot water heating system. In this case, the performance indicator is characterized by the delivered power of the studied system. In this research, the selection is based on the monthly solar gain of the solar collector loop. In this way, the TMY data receive a specified orientation, a bit different from the one it already has. This is due to the combination of climatological conditions, weather sequences and system characteristics which affect its behavior.

The typical weather data selected by the WYSS procedure consist of 8760 hourly values of the two meteorological parameters: global solar radiation and the ambient air dry bulb temperature. For generating this set of typical weather data, the real hourly weather conditions of a long period (from 1993 to 2007) have been used (Hong Kong Observatory). During the selection procedure, the monthly solar gain of the solar collector loop is calculated through the basic mathematical equations adopted in the F-chart method (Haberl, 2004) as presented in Chapter 2.

7.2.3 Description of the WYSS procedure

The selection of the typical meteorological values using the WYSS procedure mainly consists of three stages as shown in Figure 7.1. In the first stage, the monthly solar gain of the solar water heating systems is calculated using the equations introduced above for all the 15 years (i.e. SG_{ym} for m=1,2, … , 12 and y=1, 2, … , 15). In the second stage, the typical months are selected for the WYSS according to the following procedure.

- Calculation of the mean value of the solar gains of all the 15 years

$$\overline{SG}_m = \frac{\left(\sum_{y=1}^{15} SG_{ym} \right)}{15} \tag{7.1}$$

- Calculation of the 15 values

$$\tau_{ym} = \left[SG_{ym} - \overline{SG}_m \right]^2 \tag{7.2}$$

- Designation of the month m of year y in which τ_{ym} is minimum. This month m is considered typical and is selected for the WYSS.

In the third and final stage, cubic spline is applied for elimination of abrupt changes at the interfaces of the months.

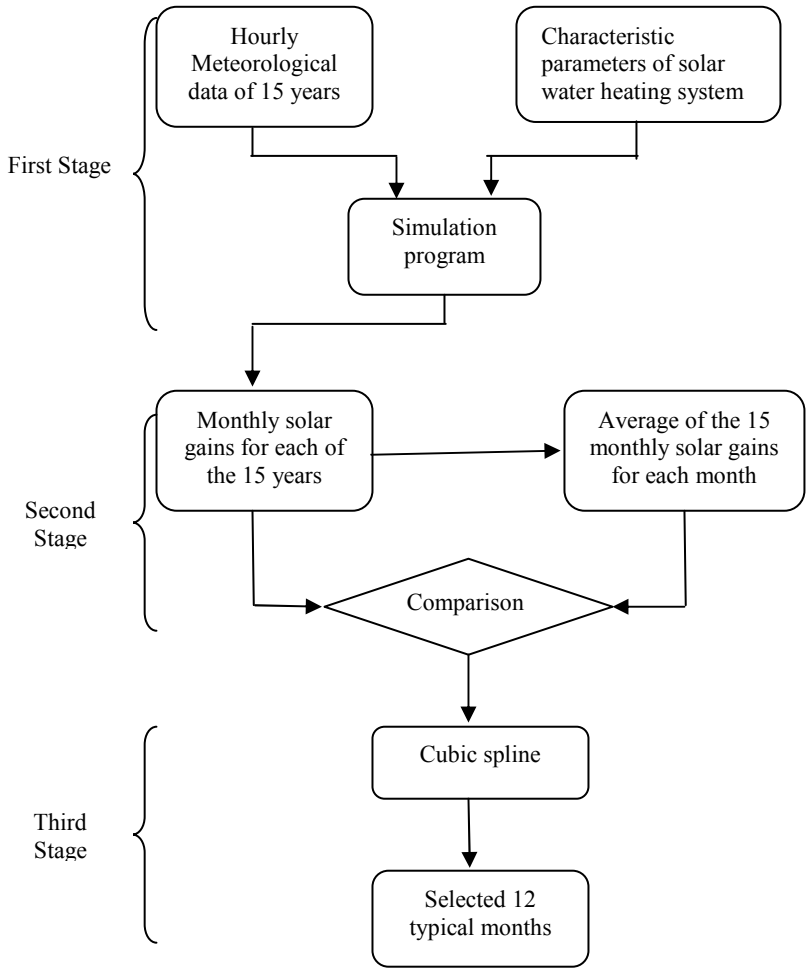

Figure 7.1 Flow chart for selecting typical months

7.2.4 Results and validation

Based on the proposed method (WYSS), one year of hourly total solar radiation and ambient air temperature were created. The selected typical months of the TMY is listed in Table 7.1. The selected typical weather data have been compared qualitatively and quantitatively with those of the observed values. Figure 7.2 shows the selected hourly weather data throughout a year. The statistical characteristics of the generated typical weather data are compared with the long-term average value of the real weather data, the TMY data and the TRY data. As shown in Table 7.2, the comparison includes annual average, standard deviation, yearly maximum and minimum values. The comparison results reveal that the generated weather data well preserved the characteristics of the real weather data and the relative errors are all within 5% magnitude. The largest relative error happens to the minimum value of air dry-bulb temperature which is 4.91%. Compared with TMY and TRY, the simulated weather data are also satisfactory. On the whole, the relative errors of generated weather data are within the same magnitude as those of TMY and TRYs'. Actually, the generated weather data are relatively better than TMY and TRY. The largest relative error of the TMY is the minimum value of air temperature, which is calculated to be 13.02%, and for the TRY, the largest relative error is 5.08% which are a little larger than that of the generated weather data.

Table 7.1 The years in which the selected typical months belong to

Month	1	2	3	4	5	6	7	8	9	10	11	12
Year	2003	1995	1999	1993	2007	2002	2005	2001	2007	2004	1993	2003

Table 7.2 Comparison between the real weather data and generated weather data

Parameters	Observed real data (1993-2007)			
	Global solar radiation [W/m^2]		Air dry-bulb temperature [℃]	
Average	331.10		23.71	
Standard deviation	256.19		5.12	
Maximum	1014.07		33.97	
Minimum	0.00		8.14	
Parameters	WYSS			
	Value [W/m^2]	Relative error [%]	Value [℃]	Relative error [%]
Average	338.23	2.15	22.86	3.58
Standard deviation	257.80	0.63	5.28	3.13
Maximum	1019.45	0.53	35	3.03
Minimum	0.00	0.00	7.74	4.91
Parameters	TMY			
	Value [W/m^2]	Relative error [%]	Value [℃]	Relative error [%]
Average	344.88	4.16	23.85	0.59
Standard deviation	246.34	3.84	5.35	4.49
Maximum	972.00	4.15	32.80	3.44
Minimum	0.00	0.00	9.20	13.02
Parameters	TRY89			
	Value [W/m^2]	Relative error [%]	Value [℃]	Relative error [%]
Average	337.23	1.85	23.81	0.42
Standard deviation	251.17	1.96	5.38	5.08
Maximum	1015.00	0.09	33.90	0.21
Minimum	0.00	0.00	7.80	4.55

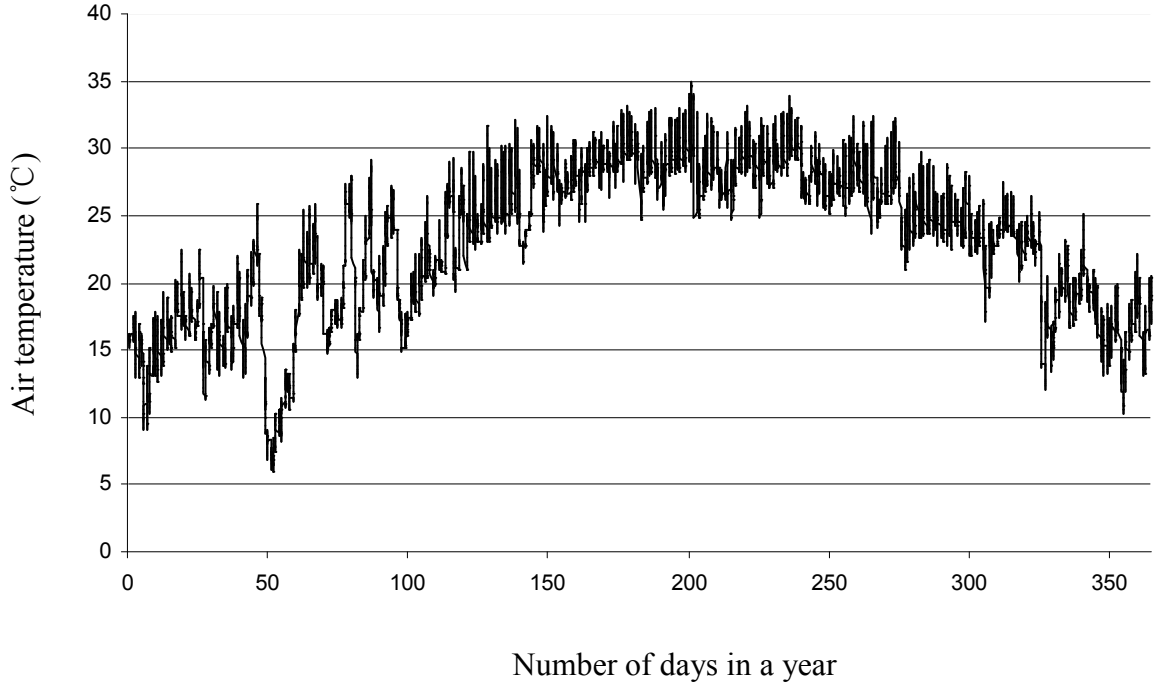

(a) The ambient air temperature

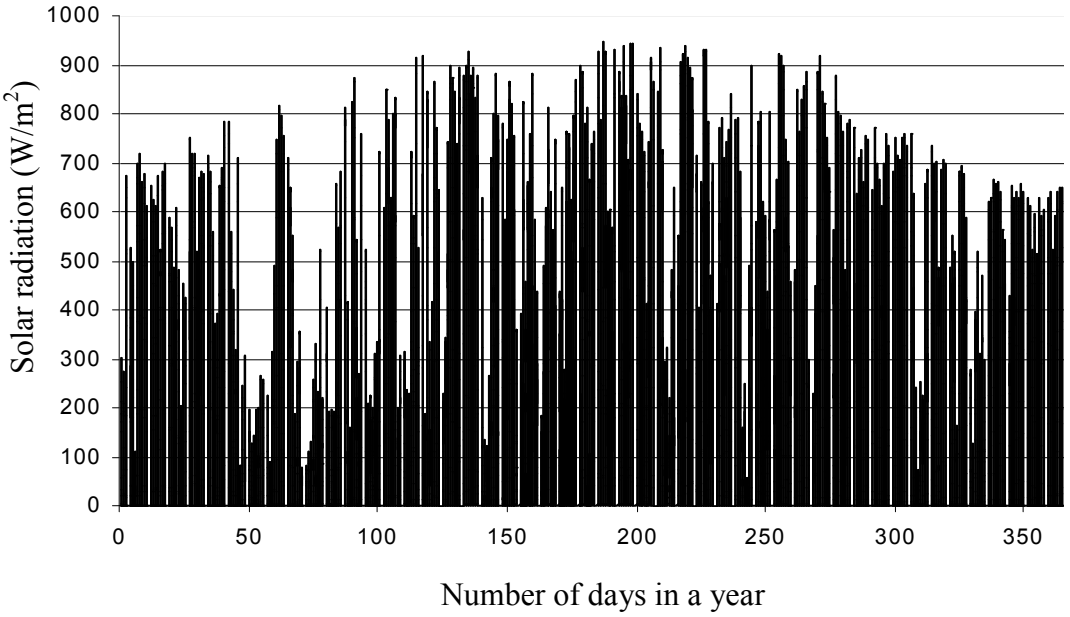

(b) The hourly total solar radiation

Figure 7.2 Generated hourly weather data through WYSS method

7.3 Annual Energy Performance of the MSA-ASHP System

The use of comprehensive computer programs, which is able to simulate building-plant system behavior in dynamic conditions, permits one to obtain a correct evaluation of the long-term performance of a heat pump. This analysis is particularly important when the solar assisted air source heat pump is considered. One reason is that the discontinuity of the solar radiation and the other is about the variability of the ambient air conditions. Besides, a great number of factors affect the performance of the proposed MSA-ASHP system, such as the system capacity, various load profiles and the changing environmental conditions. Therefore, a long-term performance analysis is very important for the studied system for a given building under given weather conditions.

7.3.1 Monthly performance analysis of the solar collector loop

As introduced in Chapter 2, the theoretical evaluation of the long-term performance of solar thermal systems is possible through different approaches. When the solar systems started to appear, the estimation of long-term performance was done through the simplified calculation methods. The F-chart method is available to calculate the system's monthly solar fraction (ratio of useful solar energy to the required thermal load) through correlations with system parameters, including collector area, collector efficiency and thermal load. Considering the acceptable accuracy and the specific advantages in system design process, the F-chart method is adopted for the monthly performance evaluation of the solar collector loop. The specification of the designed MSA-ASHP system and relative parameters are summarized in Table 4.2.

On the basis of the aforementioned method and assumptions, the long-term performance of the solar collector loop was analyzed under the generated TMY data of Hong Kong. The characteristic parameters of the solar collector used in the F-chart method are listed in Table 7.3. The system is designed to supply hot water and air condition for a family of two persons. According to ASHRAE handbooks and the local domestic hot water usage profile, the average daily domestic hot water demand per person for a typical residential apartment is about 60 liters. Hence, this system is required to produce 120 liters hot water to meet the designed hot water heating load. Figure 7.3 shows the monthly hot water heating load under the generated TMY weather conditions. It can be found that there is a decrease of hot water demand during summer months. This is attributed to the fact that during the summer months the air dry-bulb temperature is higher (as indicated in Figure 7.4) which results in higher inlet water temperature of the solar collector. Consequently, the hot water heating load during these months is reduced.

Table 7.3 Characteristic parameters of the solar collector

Parameter	A_c	$\tau\alpha$	F_R	U_L	Tilt angle
Value	2 m^2	0.835	0.934	3.39 W/(m^2℃)	19.4°

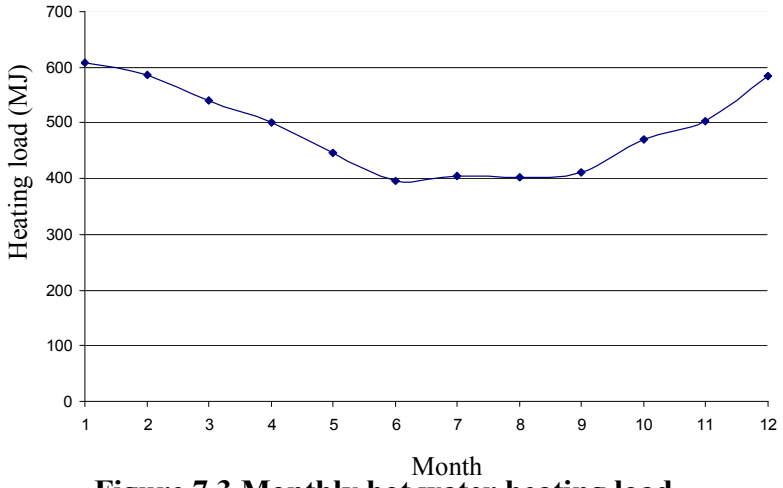

Figure 7.3 Monthly hot water heating load

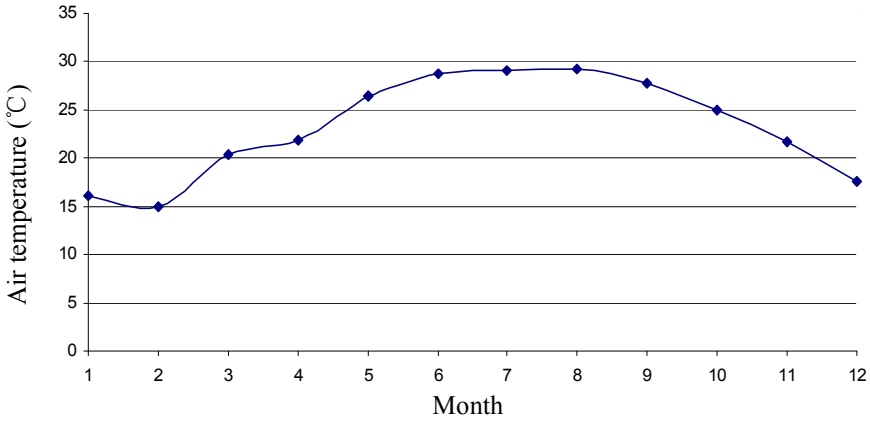

Figure 7.4 Monthly average air dry-bulb temperature

As shown in Figure 7.5, the monthly average solar fraction of the system rises gradually from January until July. It then decreases as the time goes. Averagely, the solar fraction of the designed system reaches 61.8%. The highest solar fraction appears in summer. That is because, in these months, solar radiation is relative higher and it plays a significant impact in determining the thermal performance of the solar collector loop. Also, the temperature difference between the solar collector and ambient air is smaller which results in less heat loss of the solar collector.

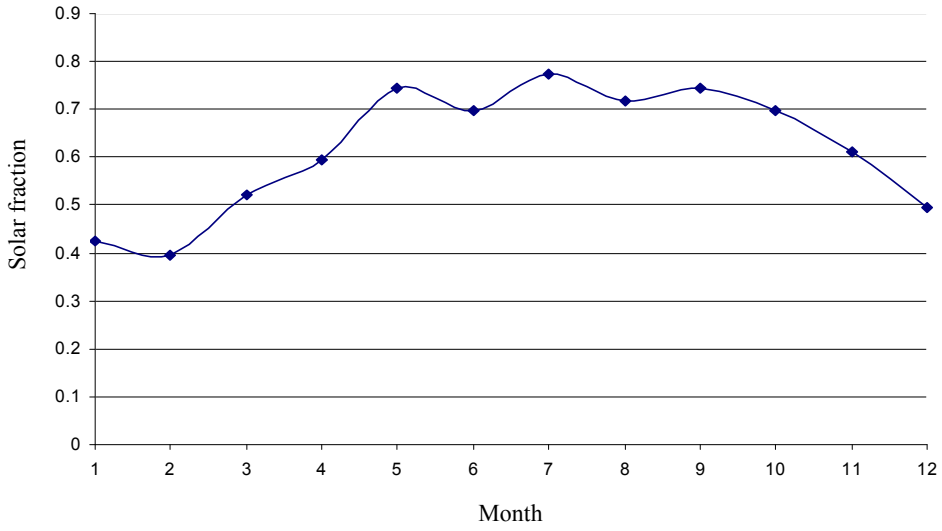

Figure 7.5 Monthly solar fraction in the generated TMY

7.3.2 Monthly performance analysis of the multi-functional ASHP system

Usually, the long-term performance is evaluated by carrying out the transient system analysis that determines the thermal performance of the system at some chosen time interval, representing a reasonable compromise between computational effort and accuracy. In this study, simulations were carried out with the created TMY data of Hong Kong. The annual hourly cooling load of the sample building in the selected TMY, as shown in Figure 7.6, was calculated using the Residential Load Factor (RLF) method (ASHRAE, 2005).

According to the mathematical model built in Chapter 3 and the generated TMY data above, a simulation program is written in FORTRAN language for the long-term performance of the considered system. The predicted variations in the monthly average COP and the energy consumption for a year round performance are shown in Figure 7.7 and 7.8, respectively. From Figure 7.7, it can be found that, during the summer months,

the system performance is better compared with the rest months in the year. The reason is that the multi-functional ASHP unit operates in all three operating modes (i.e. the only AC mode, the AC/WH mode and the only WH mode) during these months. In addition, the system COP is obviously higher when it operates in the AC/WH mode as presented in Chapter 3. Furthermore, the COP of the only WH mode is higher since the ambient air temperature obtains relatively higher under summer weather conditions. On average, the annual average COP of the MSA-ASHP system is around 3.0 which is much better than that of the conventional air conditioner and the conventional water heater under the similar weather conditions.

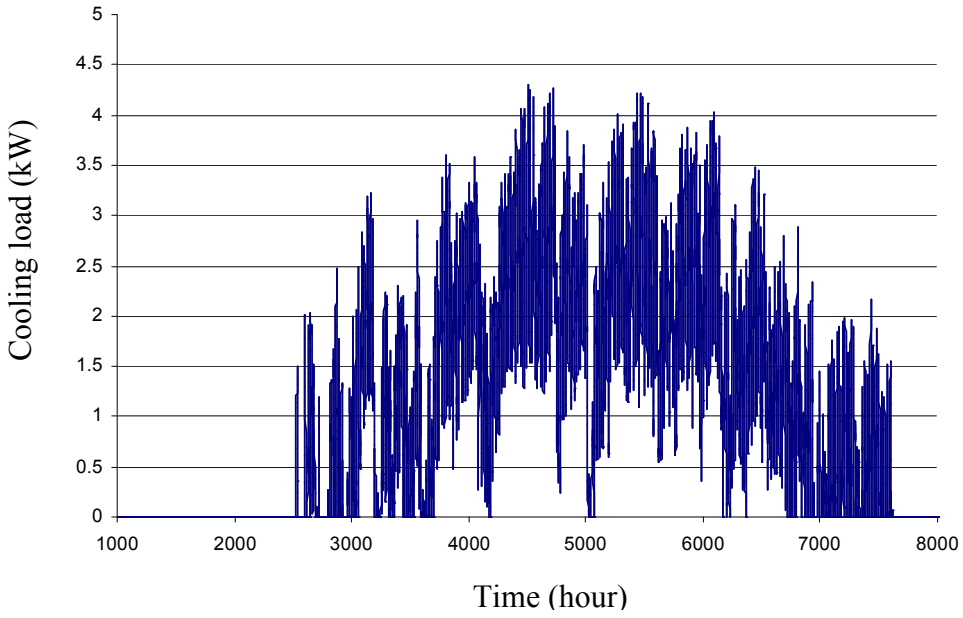

Figure 7.6 Annual hourly cooling loads

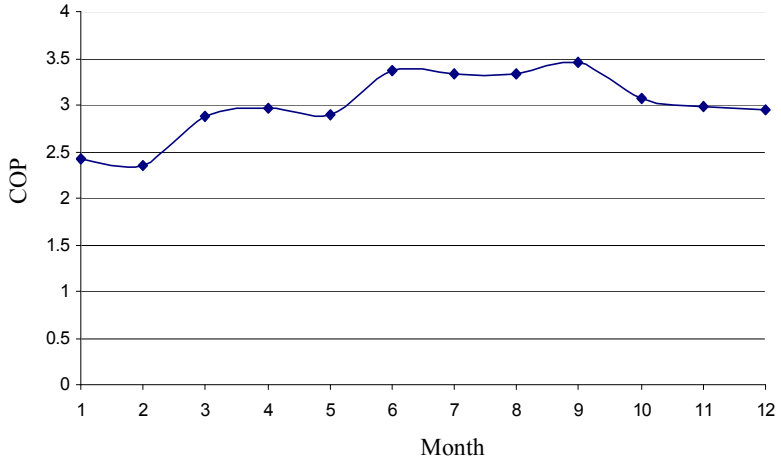

Figure 7.7 Variation of the monthly average COP

In order to further investigate the system performance of the proposed system, an energy consumption comparison during the TMY was conducted between the MSA-ASHP system and a base case system (i.e. the conventional air conditioner plus the electric water heater system). As shown in Figure 7.8, the energy consumption of the MSA-ASHP system is obviously lower than that of the base case, especially in cooling seasons. As a whole, the annual energy consumption of the proposed system for air-conditioning and hot water heating can reduce 54.9% of the energy consumption of a conventional air-conditioning unit combined with a conventional electric water heater system. If only the multi-functional ASHP unit is considered, about 32% of the total energy can be saved based on the present calculation method.

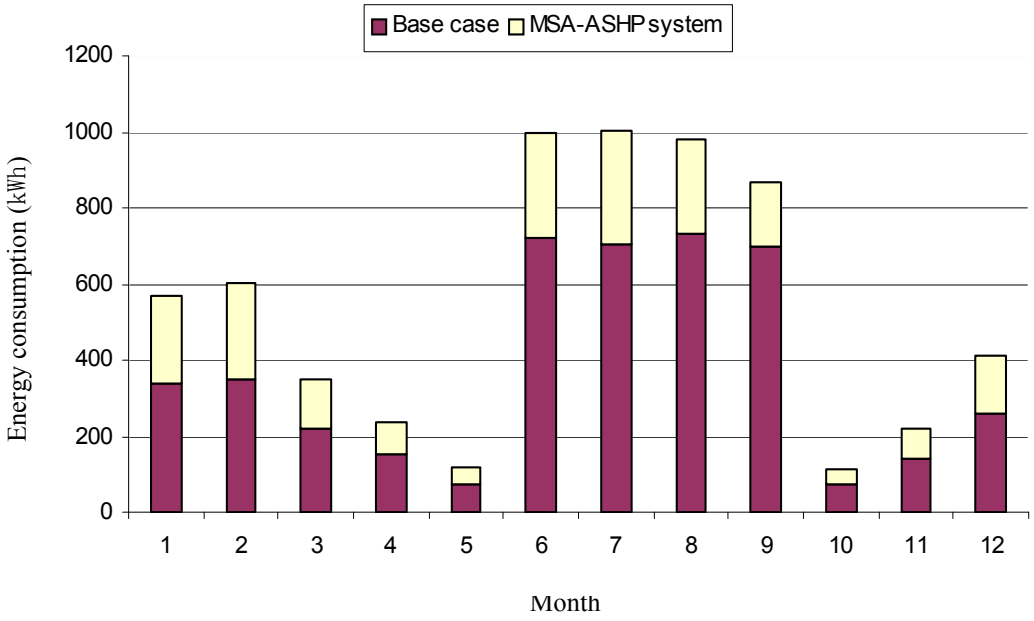

Figure 7.8 Energy consumption of the MSA-ASHP system and base case

7.4 Economic Analysis

It is important to perform an economic feasibility analysis of the MSA-ASHP system as compared with conventional air-conditioning systems plus electric water heating systems. In this section, firstly, the economic analysis is conducted based on the real cost of the experimental system which represents the relative small scale project. In order to further investigate the economic feasibility of the MSA-ASHP system, secondly, a case study based on a hypothetical hotel building is carried out.

7.4.1 Economic analysis of the experimental system

The initial cost of the experimental system is estimated based on the real cost of the experimental setup as shown in Table 7.4.

Table 7.4 Initial cost of the MSA-ASHP system

Solar collector [HK$]	Water tanks [HK$]	Water pumps [HK$]	Heat pump unit [HK$]	Installation & maintenances [HK$]	Sum [HK$]
4000	1000	700	8000	4500	18200

The life cycle savings (LCS) is the difference between the present value of the life cycle energy saving and the extra initial expenditure. If this quantity is positive, the proposed system is worth the extra expenditure, otherwise it is not. In this study, the LCS analysis is conducted for the MSA-ASHP system to show its economic feasibility. During this analysis, the life cycle of the system is assumed to be 20 years. The conventional air conditioner plus the electric water heater is selected as the base system. Thus, the extra expenditure of the MSA-ASHP system covers the costs of the solar collector, one water tank and two heat exchangers. Therefore, an initial extra expenditure C (i.e. HK$ 6850) for the experimental system was invested at a market discount rate d equal to 0.08, in order to make a saving S in the yearly energy bill that is inflating at a rate e equal to 0.1 over a period N of 20 years. The system is assumed to have no resale value. The life cycle savings is then given by Duffie and Beckman (1980):

$$LCS = -C + PWF(N, e, d)S \tag{7.3}$$

where

$$PWF(N, e, d) = \frac{1}{d - e}\left(1 - \left(\frac{1+e}{1+d}\right)^{N}\right) \quad if \quad e \neq d \tag{7.4}$$

$$PWF(N,e,d) = \frac{N}{1+d} \quad if \quad e = d \tag{7.5}$$

Based on the assumed parameters and aforementioned correlations, the LCS of the experimental system is calculated to be around HK$ 20605. For a set of specified economic parameters, the return on investment (ROI) can be determined. ROI is defined as the market discount rate that results in zero life cycle savings. A positive LCS implies an ROI greater than the market discount rate; the reverse occurs if the LCS is negative.

The payback period is defined in many ways. In this research, the payback period is defined as the time needed for the cumulative fuel savings to equal the total initial investment, that is, how long it takes to get an investment back by savings in fuel. The common way to calculate this payback time is without discounting the fuel savings. In this way, the payback period can be evaluated as (Duffie and Beckman, 1991):

$$N_p = \frac{\ln\left[\frac{C_s \cdot e}{S} + 1\right]}{\ln(1+e)} \tag{7.6}$$

where C_s is the initial cost of the MSA-ASHP system as shown in Table 7.4. Based on the aforementioned assumptions and equation (7.6), the payback period of the experimental MSA-ASHP system is calculated to be about 9.4 years. When the conventional air conditioner plus the electric water heater system is considered, its payback period is evaluated to be 10.3 years. Therefore, the proposed system has a little shorter payback period as compared with the commonly used system.

7.4.2 Case study

In order to further investigate the economic characteristics of the MSA-ASHP system, a case study based on a hypothetical hotel building is carried out according to the generated TMY weather conditions of Hong Kong. The total floor area of this building is 5100 m^2. The air conditioning area is 3400 m^2. In this hotel, there are 40 guest rooms and each room is designed for two persons. Accordingly, there are 80 servers and the canteen can accommodate 100 people at one time. There also exists a laundry room. Using the Cooling Load Factor method, the monthly cooling load of the considered building is calculated as shown in Figure 7.9. The amount of the required hot water is presented in Table 7.5.

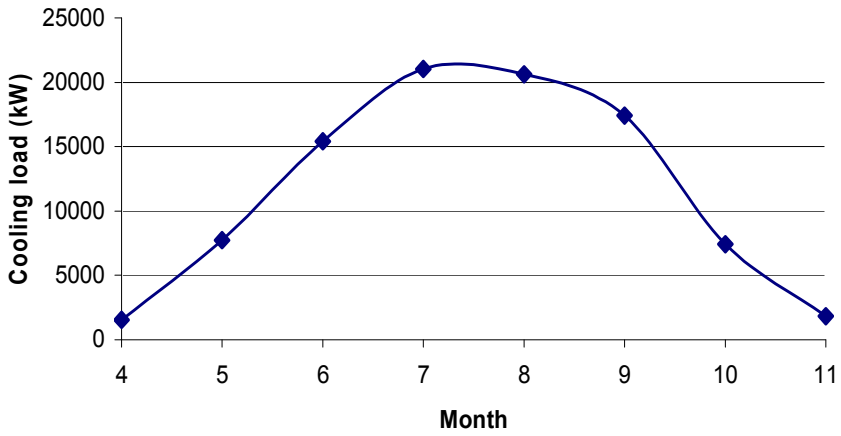

Figure 7.9 The monthly cooling load of the hotel

Table 7.5 The required hot water of the hotel building

Item	Guest	Server	Canteen	Laundry
Standard (L/(day.person))	140	80	8	5
Sum (L/day)	11200	6400	800	400

The designed MSA-ASHP system is applied to supply both cooling load and hot water heating load for the hotel, as shown in Figure 7.10. In this case study, the cooling capacity of the MSA-ASHP system is assumed to be 600 kW which can satisfy the cooling load of the hotel during summer months. The solar fraction of the system is designed to be 50%. The hot water heating load is supplied by the solar collector loop, the recovery of condensation heat and the multi-functional ASHP unit. The multi-functional ASHP unit is not a market available product at present. As the multi-functional ASHP unit is designed based on commonly used ASHP unit, the cost of the multi-functional ASHP unit can be evaluated according to the price of conventional ASHP unit. In this study, it is assumed to be 850 HK$/kW for the multi-functional ASHP unit. Based on the designed MSA-ASHP system for the hotel building, the initial cost is estimated as shown in Table 7.6.

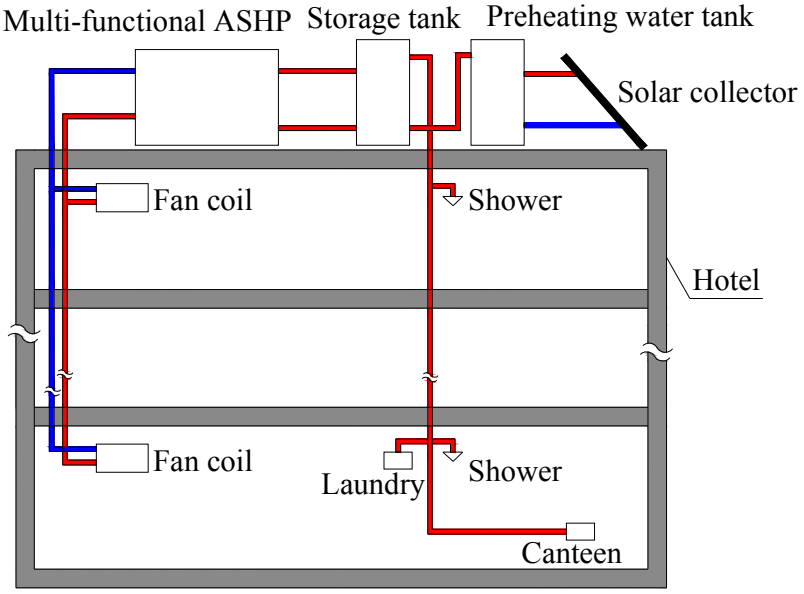

Figure 7.10 The system schematic diagram

Table 7.6 The initial cost of the designed system

Solar collector		Water pump	Heat pump unit	Water tank	Installation & maintenances	Sum
Area [m^2]	price [HK$/$m^2$]	100 [HK$/kW]	850 [HK$/kW]	18000	159100	954600
130	1600	59500	510000	[HK$]	[HK$]	[HK$]

Based on the aforementioned calculation method and assumptions, the LCS of the designed MSA-ASHP system is calculated to be about HK$ 3.8 million. Compared with the LCS of the MSA-ASHP system, the extra cost, i.e. HK$ 216233, is much lower. Consequently, the payback period is decreased to be 4.5 years. If the monthly average solar fraction, i.e. 61.8%, is adopted in this case study, the LCS would be increased to HK$ 4.45 million and the corresponding payback period will be shortened to be 4.0 years. It can be found that the payback period of the case study is much shorter than that of the sample system for experimental tests. One reason is that each component of the experimental system is specially designed and manufactured. In this way, the initial cost would be much higher, especially the multi-functional ASHP unit. Another reason is that the structure of the proposed MSA-ASHP system is relative complicated for a small scale residential house. Therefore, the studied MSA-ASHP system is suggested to be applied for relatively large scale buildings considering the economic feasibility. Besides, the economic feasibility of the MSA-ASHP system can be further improved by considering the space heating function and optimizing its structure and operating parameters through some optimal algorithms.

7.5 Summary

In this chapter, the generated weather data and the mathematical model are incorporated into a comprehensive simulation program to evaluate the long-term performance of the MSA-ASHP system. The results show that the energy saving potential of the MSA-ASHP system is significant under Hong Kong weather conditions due to the improvement of the system performance resulted from the integration of the solar collector with heat pump technology and the combination of the condensation heat recovery. Annually, 54.9% energy will be saved compared with the conventional air conditioner with electric heater. Considering the substantial annual energy savings and reasonable payback period, the extra cost is acceptable. In addition, the payback period of the MSA-ASHP system is shorter than that of the conventional air conditioner plus electric water heater system, especially when the proposed is used in relative large scale buildings. When the space heating function of the system is considered, the corresponding payback period will be further shortened.

CHAPTER 8 CONCLUSIONS AND RECOMMENDATIONS FOR FUTURE WORK

8.1 Summary of the Research Results

A novel multi-functional SAHP (i.e. MSA-ASHP) system integrated with a desuperheater has been proposed to supply DHW and air conditioning for buildings in subtropical areas. The objective of this thesis is to develop the simulation model of the MSA-ASHP system and to investigate the operating performance of the system with respect to the energy and exergy efficiencies in different operation modes. In this chapter, the main conclusions of this research are highlighted as follows:

A detailed steady-state simulation model has been developed for the MSA-ASHP system based on the basic principles of the energy balance, mass balance and pressure balance and connection relationships between the two main circuits. Accordingly, the operating performance of the MSA-ASHP system is analyzed and discussed in different operation modes under Hong Kong's weather conditions. The investigation results reveal that both solar radiation and volume of storage tank play significant impacts on the thermal performance of the solar collector circuit. A larger volume of the preheating solar tank results in a relatively lower water temperature, a smaller solar fraction, and longer heating time to obtain the required temperature level. In addition, the simulation results show that the MSA-ASHP system performs much better than a traditional air conditioner and the ASHP water heater. The system's COP in the AC/WH mode ranges

from 3.3 to 6.37, which is 36.2% larger than that when only air conditioning load is considered and 4.7% larger than that of the only WH mode. The effects of different operating parameters are identified. The water heating capacity will be increased under warmer ambient conditions. With increase of the ambient air temperature, the COP_{WH} increases while $COP_{AC/WH}$ decreases. The analysis about the impact of the flow rate indicates that a larger flow rate can not ensure a better system performance for the studied system.

The sample system is built and tested in order to analyze the thermal performance of the MSA-ASHP system and to validate the simulation results. The experimental tests for solar collector efficiency show that the selected solar collector behaves well and the tested solar collector efficiency reaches 70.1% on average. Appropriate control strategies are suggested based on series of experimental results. The flow rate of the solar collector loop is suggested to be above 0.05 kg/s. For the multi-functional ASHP unit, the specific operation mode should be determined on the basis of different design requirements.

The simulation model of the MSA-ASHP system is validated through experiments covering all possible operating modes: the only AC mode, the AC/WH mode, the only WH mode and the only WH in the AC/WH mode. The comparison results show that, on the whole, the simulation model is generally accurate to be within 10% of the experimental data.

The experimental results also indicate that the MSA-ASHP system can achieve a relatively high performance in all possible operation modes, for example, an average

COP of 3.2 in the AC/WH mode. According to the experimental data, in the AC/WH mode, the desuperheater can capture a significantly large percentage of the total condensation heat, ranging from 16%~55%. Therefore, the heat pollution may be reduced obviously and the insufficient cooling problem of air-cooled condensers can be improved.

To sum up, the developed simulation model for the MSA-ASHP system can be a useful and effective tool to analyze the system performance in different operation modes. It is also suitable for research study and engineering applications with an acceptable accuracy.

Based on experimental data and the simulation results, the exergetic modeling and performance evaluation of the MSA-ASHP system are carried out for different operation modes. The investigation results show that the greatest irreversibility on the whole system occurs in the solar collector, followed by the evaporator, the compressor, the desuperheater, the condenser and the thermostatic expansion valve. In addition, the solar collector has the highest improvement potential value, followed by the evaporator, the compressor, the desuperheater and the condenser.

The energy and exergy efficiencies of the experimental MSA-ASHP system in three different operation modes show that a higher COP of the MSA-ASHP system may not represent a higher exergy efficiency. The optimal operating condition may be obtained for the MSA-ASHP system to achieve high energy efficiency and simultaneously to keep high exergy efficiency through the co-analysis of the first and second laws of thermodynamics.

The comparison analysis between the MSA-ASHP system and the other three kinds of commonly used systems show that the MSA-ASHP system has the highest energy and exergy efficiencies. The energy efficiency of the MSA-ASHP system is 18.9% higher than that of the conventional ASHP system. Much more energy can be saved as compared with electric water heaters or gas-fired water heaters. The largest exergy efficiency of the MSA-ASHP system reaches about 20%.

Finally, the annual monthly energy performance of the MSA-ASHP system is evaluated by the simulation model using the generated TMY data through WYSS method. The results indicate that the monthly average solar fraction of the designed system is 61.8% and the monthly average COP of the system is about 3.0. Annually, 54.9% energy will be saved compared with the conventional air conditioner with electric water heater. The MSA-ASHP system has significant energy saving potential under Hong Kong weather conditions. In addition, the economic feasibility analysis shows that the extra cost of the MSA-ASHP system is acceptable and a shorter payback period is obtained. The payback period of the MSA-ASHP system is further shortened when this kind of system is applied in relative large scale buildings.

In summary, all investigation results demonstrate that it is feasible and desirable to apply the MSA-ASHP system to cooling-dominated buildings in subtropical areas.

8.2 Recommendations for Future Work

Although, in this thesis, the MSA-ASHP system has been proven to be a promising technology, there are still some aspects that are not included or just briefly discussed in

this study. Therefore, it is worthwhile and necessary to make further investigation on the MSA-ASHP system.

In this study, refrigerant R22 is adopted for the heat pump unit in the MSA-ASHP system. Even though the ozone depleting potential of R22 is not as high as that of CFCs, it still contains ozone depleting chlorine and hence the parties to the Montreal protocol (1987) decided to phase out R22 eventually and the regulation for the HCFC production has begun from 1996 in developed countries. Under such conditions, the use of more environmentally friendly working fluids as refrigerants for the MSA-ASHP system should be considered.

To a certain extent, the system performance of the MSA-ASHP system depends on the ratio of the heating load to the air conditioning load in a building. Generally, it is proposed to apply the MSA-ASHP system in subtropical areas where the heating load and the air conditioning load are similar. A suitable range for the ratio of the heating load to the air conditioning load for application of the MSA-ASHP system should be identified.

In order to further improve the performance of the MSA-ASHP system, it is essential to optimize the combination of the system components and control strategy, which can be realized to incorporate a specific optimum method into the simulation program, such as the artificial neural networks.

REFERENCES

Ajona, JI, Gordon, JM. 1987. An analytic model for the long-term performance of solar air heating systems. Solar Energy, 38(1): 45-53.

Allen JJ, and Hamilton JF. 1983. Steady-state reciprocating water chiller models. ASHRAE Transactions 89(2A): 398-407.

Ammar, A, Okaz, AM, Ghoneim, AA. 1989. Investigation of optimum parameters for solar domestic hot water system in Alexandria, Egypt. Solar & Wind Technology, 5:627-632.

Argiriou A, Lykoudis S, Kontoyiannidis S, Balaras CA, Asimakopoulos D, Petrakis M and Kassomenos P, 1999. Comparison of methodologies for TMY generation using 20 years data for Athens, Greece. Solar Energy , 66(1):33-45.

ASHRAE. 2000 ASHRAE Handbook, HVAC Systems and Equipment. Atlanta: American Society of Heating, Refrigerating, and Air-Conditioning Engineering, Inc., Atlanta.

ASHRAE, 2005. Handbook: Fundamentals. American Society of Heating, Refrigerating and Air-conditioning Engineers, Inc., Atlanta.

Aye Lu, Charters WWS, Chaichana C. 2002. Solar heat pump systems for domestic hot water. Solar Energy;73(3):169-75.

Badescu V. 2002. First and second law analysis of a solar assisted heat pump based heating system. Energy Conversion and Management;43:2539-2552.

Balkan F, Colak N, Hepbasli A. 2005. Performance evaluation of a triple effect evaporator with forward feed using exergy analysis. International Journal of Energy Research; 29:455-470.

Brinkworth D, 2001. Solar DHW system performance correlation revisited. Solar Energy 71 (6): 377-387.

Barley, D, Winn, CB. 1978. Optimal sizing of solar collectors by the method of relative areas. Solar Energy, 21(4):279-289.

Bensafi, A, S. Borg DP. 1997. CYRANO: a computational model for the detailed design of plate-fin-and-tube heat exchangers using pure and mixed refrigerant. International Journal of Refrigeration, 20(3): 218-228.

Cervantes JG, Torres-Reyes E, 2002. Experimental on a solar-assisted heat pump and an exergy analysis of the system. Applied Thermal Engineering; 22:1289-1297.

Chan ALS, Chow TT, Fong SKF and Lin JZ. 2006. Generation of a typical meteorological year for Hong Kong. Energy Conversion and Management, 47:87-96.

Chandrasekar, B, Kandpal TC, 2004. Techno-economic evaluation of domestic solar water heating systems in India. Renewable Energy 29:319-332.

Chan WW, Lam JC, 2003. Energy-saving supporting tourism sustainability: a case study of hotel swimming pool heat pump, Journal of sustainable tourism;11(1):74-83.

Charters WWS and Taylor LE, 1976. Some performance characteristics of a solar boosted heat pump. In Proceedings of I.I.R Conference, pp. 641-648, Melbourne, Australia.

Charters WWS, de Forest L, Dixon CWS, Taylor LE, 1980. Design and performance of some solar boosted heat pumps. In ANZ Solar Energy Society Annual Conference, Melbourne, Australia.

Charters WWS, LuAye, 1999. Electrical and engine driven heat pumps for effective utilisation of renewable energy resources. In World Renewable Energy Congress'99, February 10-13, 1999, Murdoch University, Perth, Australia.

Chi J, Didion D. 1982. A simulation model of the transient performance of a heat pump. International Journal of Refrigeration, 5(3): 176-184.

Chow TT, Fong KF, Chan ALS, Lin Z. 2006. Potential application of a centralized solar water-heating system for a high-rise residential building in Hong Kong Applied Energy; 83:42-54.

Chow TT, He W, Ji J. 2007. An experimental study of façade-integrated photovoltaic/water-heating system Applied Thermal Engineering;27:37-45.

CIBSE GUIDE, 1986. vol. B: 4 – 8. 5th ed. London: Staples Printers St Albans Ltd.

Cleland AC. 1986. Computer subroutines for rapid evaluation of refrigerant thermodynamic properties. International Journal of Refrigeration, 9(8):346-351.

Colle, S, Vidal, H, 2004. Upper bounds for thermally driven cooling cycles optimization derived from the f- ϕ chart method. Solar Energy;76 (1-3):125-133.

Cook RE, 1990. Water storage tank size requirement for residential heat pump/air-conditioner desuperheater recovery. ASHRAE Transactions;96(Part 2):715–719.

Cornelissen RL, 1997. Thermodynamics and sustainable development: the use of exergy analysis and the reduction of irreversibility. PhD thesis, University of Twente, The Netherlands.

Ding GL, Zhang CL, 2001. Simulation and optimization for refrigeration and air conditioning system. Science press, Beijing China.

Ding Y, Chai Q, Guoyuan M, Jiang Y, 2004. Experimental study of an improved air source heat pump. Energy Conversion and Management;45:2393–2403.

DiPippo R, 2004. Second Law assessment of binary plants generating power from low-temperature geothermal fluids. Geothermics;33:565-586.

Domanski P, Didion D. Computer modeling of the vapor compression cycle with constant flow area expansion device. NBS Building Science Series 155.

Drew, MS, Selvage, RBG, 1979. Correspondence between solar load ratio method for passive water wall systems and F-Chart performance estimates. Solar Energy,23(4):327-331.

Duffie, J.A., Beckman, W.A., 1991. Solar Engineering of Thermal Processes, second ed. Wiley, New York, pp. 686-732.

Electrical and Mechanical Services Department (EMSD), 2007. Hong Kong energy end-use data. http://www.emsd.gov.hk/emsd/e_download/pee/HKEEUD280907.pdf.

Environmental Protection Department (EPD), Hong Kong greenhouse gas emission inventory, 2007.http://www.epd.gov.hk/epd/english/environmentinhk/air /data/files/table_ghg_wtc.pdf.

Evans BL, Beckman WA, Duffie JA, 1985. F-Chart in European climates. Proceedings of the First European Conference Solar Heating, Amsterdam. pp. 161-165.

Fisher SK, Rice CK, 1983. The Oak Ridge heat pump models: 1. A steady-state computer design model for air-to-air heat pumps. Report No. ORNL/CON-80/R1. Oak Ridge, Tenn.: Oak Ridge National Laboratory.

Florides GA, Kalogirou SA, Tassou SA, Wrobel LC, 2002. Modelling, simulation and warming impact assessment of a domestic-size absorption solar cooling system. Applied thermal engineering;22:1313-1325.

Fung YY, Yang HX, 2005. Study on optimum inclination angle of solar collecting surface in Hong Kong. HKIE transactions;12(1):44-48.

Fung WY, Lam KS, Hung WT, Pang SW, Lee YL, 2006. Impact of urban temperature on energy consumption of Hong Kong. Energy;31:2623-2637.

Gazela M and Mathioulakis E. A new method for typical weather data selection to evaluate long-term performance of solar energy systems. Solar Energy, 70(4):339-348.

Goldschmidt VW, 1990. Desuperheater water-heater and air-to-air heat pump system: representative performance data. ASHRAE Transactions;96(Part 2):417–421.

Hamilton JF, Miller JL, 1990. A simulation program for modeling an air-conditioning system. ASHRAE Transactions 96(1): 213-221.

Healy CT, Wetherington Jr TI, 1965. Water heating by recovery of rejected heat from heat pump. ASHRAE Journal;(4):68–74.

Hepbasli A, 2007. Exergetic modeling and assessment of solar assisted domestic hot water tank integrated ground-source heat pump systems for residences. Energy and Buildings;39:1211–1217.

Hepbasli A, Kalinci Y, 2009. A review of heat pump water heating systems. Renewable and Sustainable Energy Reviews; 13(6-7):1211-1229.

Hepbasli A, 2008. A key review on exergetic analysis and assessment of renewable energy resources for a sustainable future, Renewable and Sustainable Energy Reviews;12:593-661.

Holman JP, 2001. Experimental methods for engineers, 7th ed. New York: McGraw-Hill.

Hong Kong and China Gas Company Limited, Sustainability report 2005/2006, 2007. http://www.towngas.com/files/TGS021_C4.pdf.

Incropera FP, DeWitt DP, 1990. Fundamentals of heat and mass transfer. New York: Wiley, pp.508.

Jeff S. Haberl, Literature review of uncertainty of analysis methods, Report to the Texas Commission on Environmental Quality. Texas Engineering Experiment Station Texas A&M University System.

Jiang HM, Jiang YQ, Wang Y, Ma ZL, Yao Y, 2006. An experimental study on a modified air conditioner with a domestic hot water supply (ACDHWS). Energy 31:1789-1803.

Ji J, Chow TT, He W, 2003. Dynamic performance of hybrid photovoltaic/thermal collector wall in Hong Kong. Building and Environment;38:1327-1334.

Ji J, Chow TT, Pei G, Dong J, He W, 2003. Domestic air-conditioner and integrated water heater for subtropical climate. Appllied Thermal Engineering;23(5):581–592.

Jin H and Spitler JD, 2002. A Parameter Estimation Based Model of Water-To-Water Heat Pumps for use in Energy Calculation Programs. ASHRAE Transactions 108(1): 3-17.

Joudi KA, Abdul-Ghafour KJ, 2003a. Development of design charts for solar cooling systems – part I. Energy Conversion and Management;44 (2):313-339.

Joudi KA, Abdul-Ghafour KJ, 2003b. Development of design charts for solar cooling systems – part II. Energy Conversion and Management;44 (2):341-355.

Jordan RC, Priester GB, 1948. Refrigeration and Air Conditioning. Prentic-Hall, Inc.: New York.

Kandlikar SG, 1990. A general correlation for saturated two-phase flow boiling heat transfer inside horizontal and vertical tubes. Journal of Heat Transfer, 112(2): 219-228.

Kara O, Ulgen K, Hepbasli A, 2008. Exergetic assessment of direct-expansion solar-assisted heat pump systems: Review and modeling. Renewable and Sustainalbe Energy Reviews, 12:1383-1401.

Kaygusuz K, Ayhan T, 1993. Exergy analysis of solar assisted heat pump systems for domestic heating. Energy;18:1077–1085.

Klein, SA, Beckman, WA, Duffie, JA, 1976. A design procedure for solar heating systems. Solar Energy 18:113-127.

Klein, SA, Beckman, WA, 1979. A general design method for closed loop solar energy systems. Solar Energy 22:269-282.

Klein SA, Cooper PI, Freeman TL, Beekman DL, Beckman WA, Duffie JA, 1975. A method of simulation of solar processes and its application. Solar Energy 17:29 – 37.

Kotas TJ, 1985. The exergy method of thermal plant analysis. Tiptree, Essex: Anchor Brendon Ltd.

Kovarik M, Lesse PF, 1976. Optimal control of flow in low temperature solar heat collectors.Solar Energy, 18: 431-435.

Krakow KL, Lin S, 1987. A numerical model of heat pumps having various means of refrigerant flow control and capacity control. ASHRAE Transactions, 93(1):491-510.

Kuang YH, Sumathy K, Wang RZ, 2003. Study on a direct-expansion solar-assisted heat pump water heating system. International Journal of Energy Research;27:531-548.

Lancaster, Richard, 2007. Making emission reduction happen – CLP's experience in Hong Kong. http://www.hkie.org.hk/iccc2007/docs/PDF/Oral%20Papers/L0 3.PDF.

Li W, TaoWQ, Kang HJ et al., 1997. Experimental study on heat transfer and resistance property for unitary finned-tube heat exchanger. Chinese Journal of Mechanical Engineering, 33(1):81-86.

Li YW, Wang RZ, Wu JY, Xu YX, 2007. Experimental performance analysis on a direct-expansion solar-assisted heat pump water heater. Applied Thermal Engineering;27:2858–2868.

Li YW, Wang RZ, Wu JY, Xu YX, 2007. Experimental performance analysis and optimization of a direct expansion solar-assisted heat pump water heater. Energy;32:1361–1374.

Li H and Yang HX, 2009. Potential application of solar thermal systems for hot water production in Hong Kong. Applied Energy 86:175-180.

Lund PD, 1989. General design methodology for seasonal storage solar systems. Solar Energy 42:235-251.

Lund PD, Peltola SS, 1992. SOLCHIPS – A fast pre-design and optimization tool for solar heating with seasonal storage. Solar Energy;48:291-300.

Lockhar RW, Martinelli RC, 1949. Proposed correlation data for isothermal two-phase two-component flow in pipes. chemical Engineering Progress, 45 (1):39-48.

Meyer J, 1999. Domestic hot water consumption of the developed and developing communities in South Africa. ASHRAE Transactions;105(Part 1):173-178.

Minnerly BVV, Klein SA, Beckman WA, 1991. A rating procedure for solar domestic hot water systems based on ASHRAE-95 test results. Solar Energy, 47(6):405-411.

Olszeweki M, 1984. Economic viability of heat pump desuperheater for supplying domestic hot water. ASHRAE Transactions;90(Part 1B):169–177.

Ozgener O, Hepbasli A, 2005. Experimental performance of a solar assisted ground-source heat pump greenhouse heating system. Energy and Buildings;37:101–110.

Ozgener O, Hepbasli A, 2007. A review on the energy and exergy analysis of solar assisted heat pump systems. Renewable and Sustainable Energy Reviews;11:482–496.

Pei G, Chow TT, He W, Zhang A, Dong J, Yi H, 2005. Performance of multi-functional domestic heat-pump system. Applied Energy;80:307–326.

Petela R, 2003. Exergy of undiluted thermal radiation. Solar Energy;74:469-488.

Petela R, 2005. Exergy analysis of the solar cylindrical-parabolic cooker. Solar Energy;79:221-233.

Pillai Indu R, Banerjee Rangan, 2007. Methodology for estimation of potential for solar water heating in a target area. Solar Energy, 81:162-172.

Rankhesh B, Venkatarathnam G, Srinivasa Murthy S, 2003. Experimental studies on a heat pump operating with R22, R407C and R407A: Comparison from an exergy point of view. Journal of energy resources technology, 125:101-112.

Rylatt, M, Gadsden, S, Lomas, K, 2001. GIS-based decision support for solar energy planning in urban environment. Computers, Environment and Urban Systems, 25:579-603.

Sen, Z, Sahin, AD, 2001. Spatial interpolation and estimation of solar irradiation by cumulative semivariograms. Solar Energy 71(11):11-21.

Sfeir A, 1980. A stochastic model for predicting solar system performance. Solar Energy,25(2):149-154.

Shi WX, Shao SQ, Wang BL, Ma J, Li XT, Yan QS, 2002. Thermodynamics analysis and thermoeconomics evaluation on heat recovery inverter air-cooling heat pump with domestic hot water. In: Proceedings of the seventh International Energy Agency conference on heat pump technologies, 2: 889–894.

Singh N, Kaushik SC, Misra RD, 2000. Exergetic analysis of solar thermal power system. Renewable Energy; 19(1-2): 135-143.

Sozen A, Arcaklioglu E, Ozalp M, Kanit, EG, 2005. Solar energy potential in turkey. Applied Energy, 80(4):367-381.

Sporn P, Ambrose ER, 1955. The heat pump and solar energy. In: Proceedings of the World Symposium on Applied Solar Energy, Phoenix, Ariz, November 1-5.

Tan KX, Deng SM, 2002. A simulation study on a water chiller complete with a desuperheater and a reversibly used water cooling tower (RUWCT) for service hot water generation. Build Environ;37(7):741–751.

Toh KC, Chan SK, 1993. Thermosiphon heat recovery from an air-conditioner for a domestic hot water system. ASHRAE Transactions;99(Part 1):259–264.

Torres Reyes E, Picon Nunes M, Cervantes J, 1998. Exergy analysis and optimization of a solar assisted heat pump. Energy;23: 337–344.

Torres-Reyes E, Cervantes JG, 2001. Optimal performance of an irreversible solar-assisted heat pump. Exergy; 1:107-111.

Treado SJ, Snouffer T, 2001. Measurement considerations for the determination of central plant efficiency. ASHRAE Transactions, 107(1): 401–406.

Tsilingiris PT, 1996. Solar water-heating design--A new simplified dynamic approach. Solar Energy, 57(1):19-28.

Van Gool W, 1997. Energy policy: fairly tales and factualities, in: O.D.D. Soares, Martins da Cruz A., Costa Pereira G., I.M.R.T. Soares, A.J.P.S. Reis (Eds.), Innovation and Technology-Strategies and Policies, Kluwer, Dordrecht, pp. 93-105.

Voinvontas, D, Tsiligiridis G, Assimacopoulos D,1998. Solar potential for water heatin g explored by GIS. Solar Energy, 62(6):419-427.

Wallis GB. One-dimensional two-phase flow: McGrwa-Hill, pp.51-54.

Wall G. Exergy tools, 2003. Proc Inst Mech Eng 2003:125-136.

Wark, K, 1995. Advanced thermodynamics for engineers, New York: McGraw-Hill.

Wong WL, Ngan KH, 1993. Selection of an 'example weather year' for Hong Kong. Energy and Buildings, 19(44):313-316.

Wu YZ, 1997. Design guideline for the small refrigeration equipment. Mechanical industry press, Beijing, China.

Xu GY, Zhang XS, Deng SM, 2006. A simulation study on the operating performance of a solar-air source heat pump water heater. Applied Thermal Engineering 26:

1257-1265.

Yang H, Lu L, 2004. The development and comparisons of typical meteorological years for building energy simulation and renewable energy applications. ASHRAE Transactions.110 (2):424-431.

Yang JC, 2007. Study on a novel type IESA-MDHP system. PhD thesis, University of Science and Technology of China, Hefei, China.

Yang HX, Lu L, 2004. Study on typical meteorological years and their effect on building energy and renewable energy simulations. ASHRAE Transactions;100(2).

Ying WM, 1989. Performance of room air conditioner used for cooling and hot water heating. ASHRAE Transactions;95(Part 2):441–444.

Yik, Francis W H, Chung TM, Chan KT, 1995. A method to estimate direct and diffuse radiation in Hong Kong and its accuracy, HKIE Transactions, 2 (1):23-29.

You Y, Harmon S, Sidney P, 2002. A new heat pump system for year-round water heating and seasonal space cooling. In:Proceedings of the seventh International Energy Agency conference on heat pump technologies, 2002:780–784.